Coordination Chemistry of Gold(I) Metalloligands with Mixed Sulfur-containing Amino Acid and Mono-, Di-, or Triphosphine

（含硫アミノ酸とモノホスフィン、ジホスフィン、またはトリホスフィンを併せもつ金(I)錯体配位子の配位化学）

Yuji Hashimoto

Department of Chemistry, Graduate School of Science
Osaka University

2014

Index

General Introduction.

Multinuclear metal complexes, in particular heterometallic multinuclear complexes, have attracted attention for many years because of their fascinating properties based on cooperative effects between metal ions, which arise from artful combination of inherent natures of metal ions or electronic communication between them.[1] However, it is not easy to control the coordination structure consisting of many components. Thus, the way to construct heterometallic multinuclear compounds, in which different metal ions and ligands are placed at proper positions in the structure in order to exhibit a desired functionality, has been explored, and it still remains a challenging issue today.[2] One of the way for the rational construction of heterometallic complexes is a stepwise reaction of different metal ions; first, a homometallic complex with coordination donors as a "metalloligand" is prepared, and second, a heterometallic complex is synthesized by the coordination of the metalloligand to another metal ion.[2c,3]

For the stepwise-synthetic strategy using a metalloligand, employing organic thiolate ligands is one of useful ways to introduce available coordination donors to complexes. While a thiolate group can easily bridge two or three metal ions due to its strong electron-donating ability and expanded valence orbital of a sulfur atom, it is possible to synthesize a metal complex with coordinating but non-bridging thiolato groups under appropriate conditions.[4] Thus, non-bridging thiolato groups can make further coordination bonds to another metal ion with retaining the first coordination bond, to form a sulfur-bridged multinuclear structure, which may bring strong metal-metal interactions through a single sulfur atom. Therefore, the complexes with non-bridging thiolato groups are good candidates of the metalloligands for the rational construction of heterometallic multinuclear complexes, and many kinds of thiolato metalloligands have been developed to build heterometallic structures.[5]

In this context, chiral sulfur-containing amino acids (SAAs) are particularly appealing, because their amino and carboxylate groups are available for coordination as relatively hard Lewis bases in addition to the soft thiolate group to provide a versatility of metalloligand. Moreover, the amino and carboxylate groups can form hydrogen bonds, which are commonly observed in higher-order structures of proteins, to be available for the control of molecular structures, conformations, arrangements, and functionalities.[6] Among many homo- and hetero-metallic complexes with SAAs synthesized until now,[5b,7-9] multinuclear complexes based on monogold(I) metalloligand with two D-penicillaminate ligands, $[Au^{I}(D\text{-pen-}\kappa S)_2]^{3-}$ (D-H_2pen = D-penicillamine), are especially interesting.[8] Gold(I) ion, which is a very soft Lewis acid, exclusively binds to the sulfur atom despite three different donors in the D-pen, and preferably adopts a two-coordinate linear geometry. As a result, $[Au^{I}(D\text{-pen})_2]^{3-}$ has two sets of N,O,S coordinating donors in opposite sides, and exhibits various coordination modes as a bridging metalloligand to produce interesting heterometallic coordination structures

(Chart 1).[8a,b,f,9] Thus, gold(I)-SAAs complexes are potentially very useful metalloligands which allow rational design of heterometallic multinuclear complexes by their high-directional characteristics and coordination versatility, as well as aurophilic interactions that are weak attractive interaction to be available for structural control and often involve luminescent properties.[10] On the other hand, this simple structure consisting of only one gold(I) ion and two penicillaminate ligands has limitations to utilize.

As an attempt to overcome the limitations, a new digold(I) complex composed of two $\{Au^{I}(D\text{-pen})\}^{-}$ units linked through a diphosphine ligand, $[Au^{I}_{2}(dppe)(D\text{-pen})_2]^{2-}$ (dppe = 1,2-bis(diphenylphosphino)ethane), was recently developed by Lee *et al.* (Chart 1).[11] In that study, the following features of the coordination system constructed with the "longer" D-penicillaminato gold(I) metalloligand have been demonstrated: (i) coordination behavior of $[Au^{I}_{2}(dppe)(D\text{-pen})_2]^{2-}$ as a bis(tridentate-N,O,S) bridging metalloligand to produce heterometallic hexanuclear complexes, $[M_2\{Au^{I}_{2}(dppe)(D\text{-pen})_2\}_2]^{n+}$ (M = Cr^{III}, Co^{III}, or Ni^{II}; n = 2, 2, or 0, respectively), by reactions with octahedral metal ions (Chart 2), (ii) anomalous separate aggregations of cations and anions in the crystal structure of $[M_2\{Au^{I}_{2}(dppe)(D\text{-pen})_2\}]X$ (M = Cr^{III} or Co^{III}; X = $(ClO_4)_2$, Cl_2, Br_2, $(NO_3)_2$, $(BF_4)_2$, $(N_3)_2$, SO_4, SiF_6, or mixture of them) triggered by hydrophobic interactions of dppe ($\pi\cdots\pi$ and $CH\cdots\pi$ interactions) in addition to hydrogen bonds of D-pen, (iii) rearrangement of Au–P and/or Au–S coordination bonds in the system, which was observed as scrambling of a pair of homochiral enantiomers, $[Au^{I}_{2}(dppe)(D\text{-pen})_2]^{2-}$ and $[Au^{I}_{2}(dppe)(L\text{-pen})_2]^{2-}$, to form a heterochiral isomer, $[Au^{I}_{2}(dppe)(D\text{-pen})(L\text{-pen})]^{2-}$. The successful development of the D-penicillaminato digold(I) metalloligand with dppe implies potentially great utilities of gold(I) metalloligands with mixed SAAs and multidentate phosphines, because it is expected that the number, positions, and orientations of Au^{I}-SAA units in this class of metalloligands can be controlled by designing phosphines. In other words, the derivatives of this metalloligand which have different ligand properties can be obtained just by employing a variety of commercially available phosphines, and they should lead to the heterometallic multinuclear complexes showing fascinating properties. However, the fundamental coordination chemistry of this system has scarcely been uncovered, because the previous work employed only dppe as phosphines and mainly focused on the aggregation behavior of complex cations and anions on crystallization and its relationship with the chirality of the metalloligands.

Thus, studies presented in this thesis are aimed at creating a series of heterometallic Au^{I}-M-SAAs-phosphines coordination systems derived from the gold(I) metalloligands with mixed SAAs and a variety of phosphines. In this system, gold(I)-phosphine backbones can control the coordination ability of the multi-functional SAA donors toward the secondary metal ions (M) exerting various properties and reactivity, leading to the functionalities that have not been achieved in traditional thiolato-bridged systems (Chart 3). In this thesis, the

fundamental and essential coordination chemistry and potential applications of thiolato-bridged heterometallic multinuclear complexes controlled by gold(I)-phosphine backbone are presented through the syntheses, structures, properties, and reactivity of the heterometallic complexes derived from gold(I) metalloligands with mixed D-pen and mono-, di-, or triphosphine, together with the comparison with the traditional non-phosphine system.

In Chapter I, the coordination behavior of the simplest gold(I) metalloligand with a monophosphine (PPh_3 = triphenylphosphine) was investigated in order to reveal the general nature of the gold(I) metalloligands and heterometallic complexes with mixed D-pen and phosphines (Chart 4). The monogold(I) metalloligand was reacted with 3d transition metal ions (Co^{II}, Ni^{II}, Zn^{II}) to give heterometallic complexes, whose structures, properties and reactivity were discussed by the UV-vis absorption, circular dichroism (CD), luminescence, and NMR spectroscopy, together with the X-ray crystallography. In Chapter II, the coordination behaviors of gold(I) metalloligands with a diphosphine (dppm = bis(diphenylphosphino)methane) were investigated (Chart 4). Two phosphorus atoms bridged by one methylene group in dppm often put the binding gold(I) ions closer to each other to promote the formation of intramolecular aurophilic interactions, which have not been observed in the previous system with dppe. In addition to the control of coordination mode of the metalloligands by the effective intramolecular aurophilic interactions, structural interconversion reactions linking with property changes between digold(I) and trigold(I) structures are discussed on the basis of the absorption, CD, NMR spectra in the solution state, and luminescence spectra and crystal structures in the solid state. In Chapter III, the coordination behavior of trigold(I) metalloligands with a triphosphine (tdme = 1,1,1-tris(diphenylphosphinomethyl)ethane) toward cobalt ion was investigated (Chart 4). The tripodal structure of tdme allows the metalloligand to have a flexible but partially restricted backbone and three D-pen functional arms, leading to versatility on coordination. As a result, two Au^{I}-Co^{III} complexes with quite different structures were made up from a tripodal metalloligand depending on the reaction routes and characterized on the basis of the absorption, CD, and NMR spectra, as well as the crystal structures. Moreover, since a rare complex with octahedral cobalt(II) centers coordinated by aliphatic thiolates was unexpectedly found in this system, its redox property is discussed from a viewpoint of steric influences of gold(I)-phosphine backbone on the coordination ability of SAA coordination donors on the basis of the crystal structures and the spectral and electrochemical data.

References.

[1] (a) L. H. Gade, *Angew. Chem. Int. Ed.* **2000**, *39*, 2658. (b) E. J. L. McInnes, S. Piligkos, G. A. Timco, R. E. P. Winpenny, *Coord. Chem. Rev.* **2005**, *249*, 2577. (c) H. Li, T. J. Marks, *Proc. Natl. Acad. Sci. U. S. A.* **2006**, *103*, 15295. (d) M. D. Ward, *Coord. Chem. Rev*. **2007**, *251*, 1663. (e) H. Hofneier, U. S. Schubert, *Chem. Soc. Rev.* **2004**, *33*, 373.

(f) C. F. Yocum, *Coord. Chem. Rev.* **2008**, *252*, 296. (g) Y.-G. Huang, F.-L. Jiang, M.-C. Hong, *Coord. Chem. Rev.* **2009**, *253*, 2814. (h) T. Nabeshima, *Bull. Chem. Soc. Jpn.* **2010**, *83*, 969. (i) S. K. Mandal, H. W. Roesky, *Designing Molecular Catalysts with Enhanced Lewis Acidity*, in *Advances in Catalysis*, vol. 54, B. C. Gates, H. Knözinger, Eds.; Elsevier Inc., pp. 1–61 (2011).

[2] (a) M. Hidai, S. Kuwata, Y. Mizobe, *Acc. Chem. Res.* **2000**, *33*, 46. (b) M. Ruben, J. Rojo, F. J. Romero-Salguero, L. H. Uppadine, J.-M. Lehn. *Angew. Chem. Int. Ed.* **2004**, *43*, 3644. (c) S. Kitagawa, R. Kitaura, S. Noro, *Angew. Chem. Int. Ed.* **2004**, *43*, 2334. (d) M. Andruh, J.-P. Costes, C. Dlaz, S. Gao, *Inorg. Chem*. **2009**, *48*, 3342. (e) I. Garcia-Bosch, X. Ribas, M. Costas, *Eur. J. Inorg. Chem.* **2012**, 179.

[3] (a) A. D. Garnovskii, B. I. Kharisov, L. M. Blanco, A. P. Sadimenko, A. I. Uraev, I. S. Vasilchenko, D. A. Garnovskii, *J. Coord. Chem.* **2002**, *55*, 1119. (b) E. Pardo, R. Ruiz-García, J. Cano, X. Ottenwaelder, R. Lescouëzec, Y. Journaux, F. Lloret, M. Julve, *Dalton Trans.* **2008**, 2780. (c) S. J. Garibay, J. R. Stork, S. M. Cohen, *The Use of Metalloligands in Metal-Organic Frameworks*, in *Progress in Inorganic Chemistry*, K. D. Karlin, Wiley, Chichester, vol. 56, pp. 335–378 (2009). (d) Y.-G. Huang, F.-L. Jiang, M.-C. Hong, *Coord. Chem. Rev.* **2009**, *253*, 2814. (e) M. C. Das, S. Xiang, Z. Zhang, B. Chen, *Angew. Chem. Int. Ed.* **2011**, *50*, 10510. (f) S. Wang, X.-H. Ding, J.-L. Zuo, X.-Z. You, W. Huang, *Coord. Chem. Rev.* **2011**, *255*, 1713. (g) G. Kumar, R. Gupta, *Chem. Soc. Rev.* **2013**, *42*, 9403.

[4] (a) L. G. Dance, *Polyhedron* **1986**, *5*, 1037. (b) P. J. Blower, J. R. Dilworth, *Coord. Chem. Rev.* **1987**, *76*, 121. (c) D. W. Stephan, T. T. Nadasdi, *Coord. Chem. Rev.* **1996**, *147*, 147.

[5] (a) D. W. Stephan, *Coord. Chem. Rev.* **1989**, *95*, 41. (b) T. Konno, *Bull. Chem. Soc. Jpn.* **2004**, *77*, 627. (c) H. Fleischer, *Coord. Chem. Rev.* **2005**, *249*, 799. (d) X.-Y. Tang, H.-Xi Li, J.-X. Chen, Z.-G. Ren, J.-P. Lang, *Coord. Chem. Rev.* **2008**, *252*, 2026.

[6] (a) *Supramolecular Assembly via Hydrogen Bonds I*, D. M. P. Mingos, Eds; Springer, Berlin Heidelberg (2004). (b) *Supramolecular Assembly via Hydrogen Bonds II*, D. M. P. Mingos, Eds; Springer, Berlin Heidelberg (2004). (c) *Proteins*, R. A. Meyers, Eds.; Wiley, Chichester (2006). (d) *Self-Organization of Molecular Systems: From Molecules and Clusters to Nanotubes and Proteins*, N. Russo, V. Ya Antonchenko, E. Kryachko, Eds.; Springer, Berlin Heidelberg (2009).

[7] part of recent examples: (a) H. Q. Yuan, A. Igashira-Kamiyama, T. Konno, *Chem. Lett.* **2010**, *39*, 1212. (b) N. Yoshinari, A. Igashira-Kamiyama, T. Konno, *Chem. -Eur. J.* **2010**, *16*, 14247. (c) Y. Yamada, M. Kono, Y. Miyoshi, T. Nagasaki, M. Koikawa, T. Tokii, *J. Coord. Chem.* **2010**, *63*, 742. (d) P. Thuery, *Inorg. Chem.* **2011**, *50*, 10558. (e) R. Lin, H. Zhang, S. Li, L. Chen, W. Zhang, T. B. Wen, H. Zhang, H. Xia, *Chem. -Eur. J.* **2011**, *17*, 2420. (f) R. Yoshida, S. Ogasahara, H. Akashi, T. Shibahara, *Inorg. Chim. Acta* **2012**,

383, 157. (g) N. Yoshinari, Y. Nagao, A. Yokoi, A. Igashira-Kamiyama, T. Konno, *Dalton Trans.* **2012**, *41*, 11259.

[8] (a) A. Toyota, T. Yamaguchi, A. Igashira- Kamiyama, T. Kawamoto, T. Konno, *Angew. Chem. Int. Ed.* **2005**, *44*, 1088. (b) M. Taguchi, A. Igashira-Kamiyama, T. Kajiwara, T. Konno, *Angew. Chem. Int. Ed.* **2007**, *46*, 2422. (c) M. Taguchi, Y. Sameshima, A. Igashira-Kamiyama, S. Akine, T. Nabeshima, T. Konno, *Chem. Lett.* **2008**, *37*, 244. (d) Y. Sameshima, N. Yoshinari, K. Tsuge, A. Igashira-Kamiyama, T. Konno, *Angew. Chem. Int. Ed.* **2009**, *48*, 8469. (e) T. Konno, N. Yoshinari, M. Taguchi, A. Igashira-Kamiyama, *Chem Lett.* **2009**, *38*, 526. (f) T. Konno, A. Toyota, A. Igashira-Kamiyama, *J. Chin. Chem. Soc.* **2009**, *56*, 26.

[9] A. Igashira-Kamiyama, T. Konno, *Dalton Trans.* **2011**, *40*, 7249.

[10] (a) P. Pyykkö, *Angew. Chem. Int. Ed.* **2004**, *43*, 4412. (b) P. Pyykkö, *Chem. Soc. Rev.* **2008**, *37*, 1967. (c) M. J. Katz, K. Sakai, D. B. Leznoff, *Chem. Soc. Rev.* **2008**, *37*, 1884. (d) H. Schmidbaur, A. Schier, *Chem. Soc. Rev.* **2012**, *41*, 370.

[11] (a) R. Lee, A. Igashira-Kamiyama, H. Motoyoshi, T. Konno, *CrystEngComm* **2012**, *14*, 1936. (b) A. Igashira-Kamiyama, N. Matsushita, R. Lee, K. Tsuge, T. Konno, *Bull. Chem. Soc. Jpn.* **2012**, *85*, 706. (c) R. Lee, A. Igashira-Kamiyama, M. Okumura, T. Konno, *Bull. Chem. Soc. Jpn.* **2013**, *86*, 908. (d) R. Lee, PhD thesis, Osaka University, Toyonaka, Japan, **2012**.

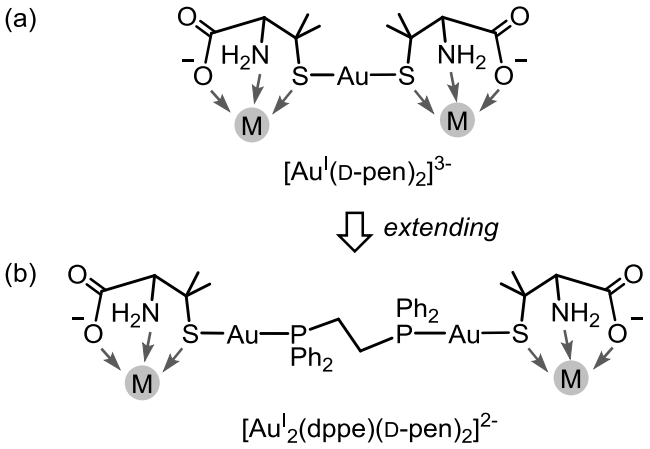

Chart 1. Previous coordination systems based on D-penicillaminato gold(I) metalloligands (a) without phosphines and (b) with dppe.

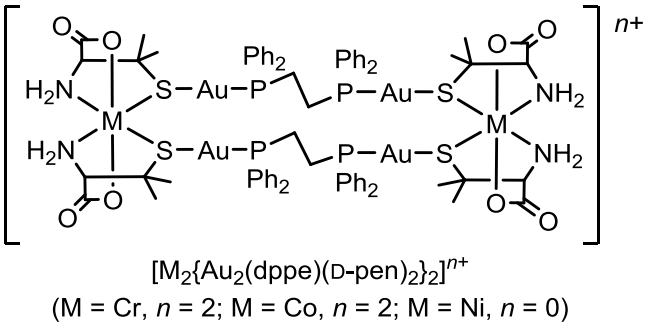

Chart 2. Hexanuclear complexes derived from $[Au^{I}_2(dppe)(D\text{-pen})_2]^{2-}$: $[M_2\{Au^{I}_2(dppe)(D\text{-pen})_2\}_2]^{n+}$ (M = Cr^{III}, n = 2; Co^{III}, n = 2; M = Ni^{II}; n = 0).

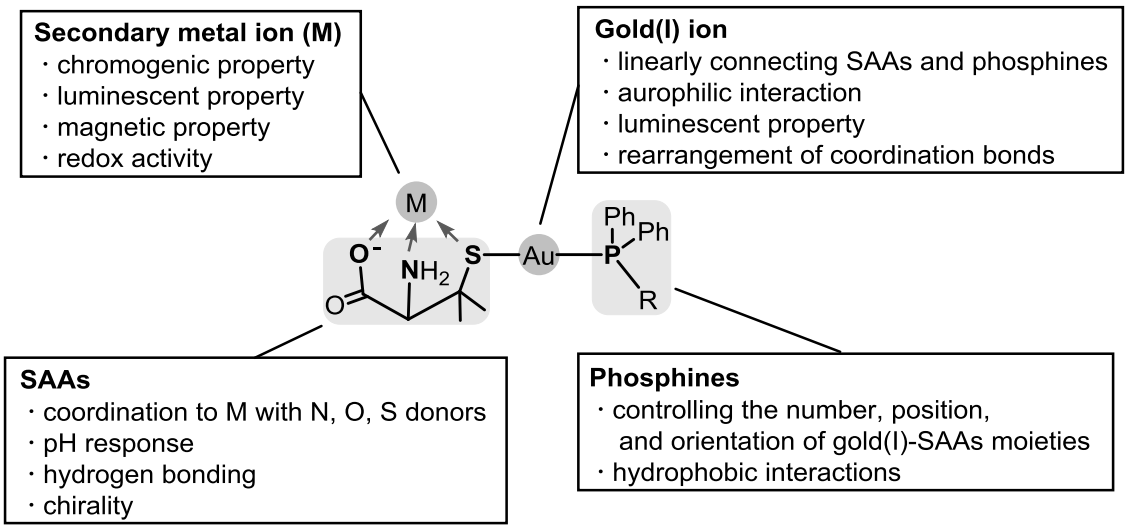

Chart 3. Concept of Au^{I}-M-SAAs-phosphines coordination systems.

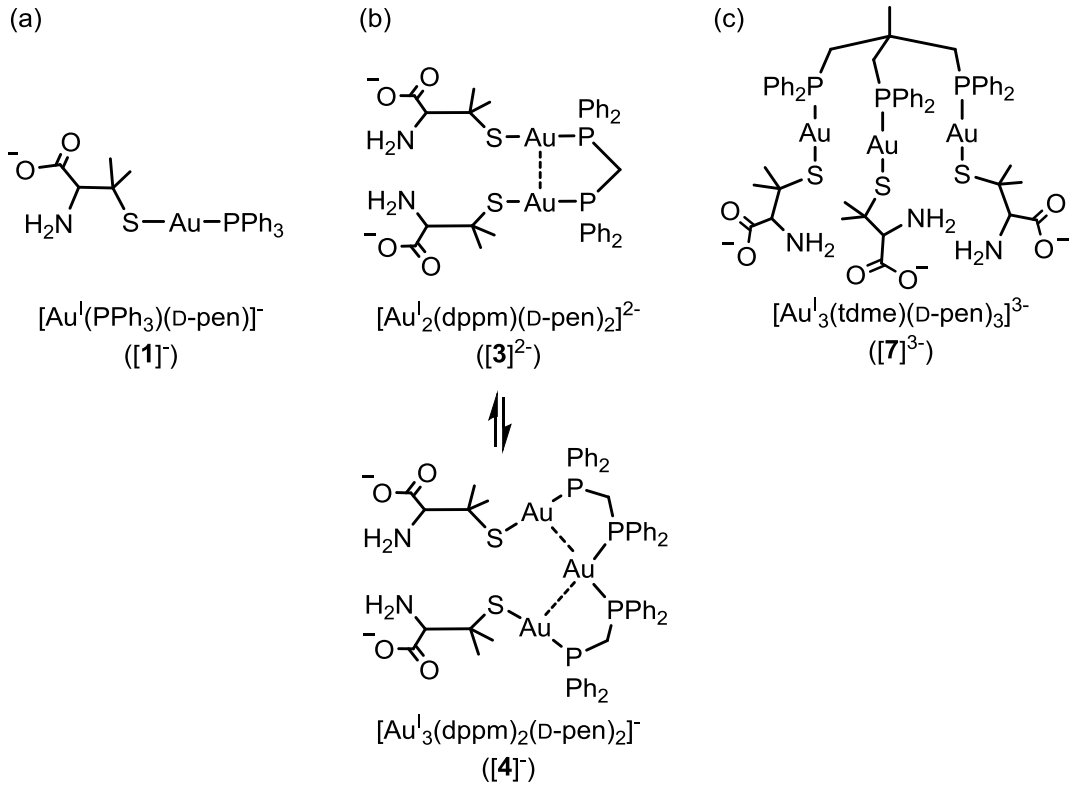

Chart 4. Gold(I) metalloligands with mixed D-pen and (a) monophosphine (PPh_3) presented in Chapter I, (b) diphosphine (dppm) in Chapter II, and (c) triphosphine (tdme) in Chapter III.

Chapter I. Monophosphine System.

I-1. Introduction.

Although there is a large number of reported gold(I) complexes coordinated by both thiolates and phosphines because of the excellent affinities of the soft Lewis pairs, Au–S and Au–P,[1] their coordination behavior as thiolato metalloligands has scarcely been investigated in the past. In particular, there are a few examples investigating the coordination behavior of this class of gold(I) complexes toward 3d transition metal ions,[2] while several reactions with thiophilic noble metals have been reported.[3] In coordination chemistry, however, 3d metal complexes are fundamental but very important even today due to their magnetic property, redox activity, rich spectroscopic information about ligand field, and so on.

In this chapter, the first systematic study for the coordination behavior of a thiolato gold(I) metalloligand with phosphine to three 3d group metal ions, cobalt(II), nickel(II), and zinc(II), is presented by using a monogold(I) complex with D-penicillaminate and triphenylphosphine, $[Au^{I}(PPh_3)(D\text{-pen})]^{-}$ ($[\mathbf{1}]^{-}$), as one of the simplest gold(I) metalloligands with mixed SAAs and phosphines. Cobalt ion is one of the most favorable metal ions to investigate ligand properties because cobalt exhibits different oxidation and spin state strongly depending on the coordination environment and, in particular, the d-d transition band of cobalt(III) complexes provides rich information about the ligand field thanks to an enormous libraries accumulated in the past.[4,5] Nickel(II) ion with $3d^8$ electron configuration is also intriguing because it can adopt octahedral and square-planar coordination geometry depending on the ligand character.[4,6] While zinc(II) ion give no information about the d electron structure, the $3d^{10}$ closed-shell metal ion allows the resulting heterometallic complex to show luminescence, which are often observed for the gold(I) complexes.[7]

The heterometallic multinuclear complexes obtained from the coordination of the monogold(I) metalloligand to the metal ions were characterized on the basis of electronic absorption, CD, and NMR spectra together with elemental analytical data. For the Au^{I}-Co^{III} complex, single-crystal X-ray analysis revealed the thiolato-bridged trinuclear structure, and the stable low-spin $3d^6$ state of the cobalt center was characterized by the spectroscopic data. For the Au^{I}-Ni^{II} complex, different coordination mode of the metalloligand depending on the solution pH to give drastic changes in the structure and property of nickel(II) center was shown by electronic absorption and CD spectra. For the Au^{I}-Zn^{II} complex, influences of metal chelation on photophysical property are discussed on the basis of luminescence spectra.

Moreover, by comparing with thiolato-bridged heterometallic complexes constructed from $[Au^{I}(D\text{-pen})_2]^{3-}$ [8] or $[Au^{I}_2(dppe)(D\text{-pen})_2]^{2-}$,[9] essential differences from the non-phosphine system and common features for the phosphine-containing system were brought out. The latter also rationalizes the formation of hexanuclear complexes reported in

the dppe system.

I-2. Experimental section.

I-2-1. Materials. A gold(I) complex, [Au(PPh_3)Cl], was prepared according to literature method.[10] All other chemicals were commercially available and used without further purification.

I-2-2. Synthesis of Au^I metalloligand with PPh_3: [Au^I(PPh_3)(D-Hpen)] ([H1]).

To a white suspension containing 1.00 g (2.02 mmol) of [Au(PPh_3)Cl] in 30 mL of ethanol was added 0.30 g (2.0 mmol) of D-H_2pen. The mixture was stirred at room temperature for 1.5 h, which gave a colorless solution. After addition of 20 mL (2.0 mmol) of an aqueous NaOH solution (0.10 M), the colorless solution was evaporated to give a white residue. The residue was washed by water to give a white powder, which was collected by filtration. Yield: 1.14 g (89%). Anal. Found: C, 43.75; H, 4.29; N, 2.22%. Calcd for [Au(PPh_3)(D-Hpen)]·1.5H_2O = $C_{23}H_{28}NO_{3.5}PSAu$: C, 43.54; H, 4.45; N, 2.21%. IR spectrum (cm^{-1}, KBr disk): 1626 (ν_{COO}). ^{1}H NMR spectrum (ppm from TMS, methanol-d_4): δ 1.38 (s, 3H), 1.84 (s, 3H), 3.56 (s, 1H), 7.52 - 7.60 (m, 15H). ^{31}P NMR spectrum (ppm from H_3PO_4, methanol-d_4): δ 38.5 (s).

I-2-3. Reactions of [H1] with metal ions.

(a) Synthesis of [Co^{III}{Au^I(PPh_3)(D-pen)}$_2$]ClO_4 ([2a]ClO_4). To a colorless solution containing 0.200 g (0.316 mmol) of [H**1**]·1.5H_2O in 10 mL of ethanol was added 1.60 mL (0.160 mmol) of aqueous $Co(CH_3COO)_2$ solution (0.1 M), which gave a pale orange solution. The mixture was stirred at room temperature for 2 h to turn a dark brown color, and then naturally concentrated after addition of 6.4 mL (0.64 mmol) of an aqueous $NaClO_4$ solution (0.1 M). After 7 days, purple-brown crystals were obtained together with a small amount of white powder. The white powder was removed from the mixture by washing with acetone to leave only purple-brown crystals. Yield: 0.11 g (48%). Anal. Found: C, 39.63; H, 3.61; N, 2.01%. Calcd for [Co{Au(PPh_3)(D-pen)}$_2$]ClO_4·H_2O = $C_{46}H_{50}N_2O_9P_2S_2ClCoAu_2$: C, 39.77; H, 3.63; N, 2.02%. IR spectrum (cm^{-1}, KBr disk): 1653 (ν_{COO}), 1097 (ν_{ClO4}). ^{1}H NMR spectrum (ppm from TMS, methanol-d_4): δ 1.49 (s, 3H), 1.79 (s, 3H), 3.81 (s, 1H), 7.42 - 7.47 (m, 12H), 7.55-7.58 (m, 3H). ^{31}P NMR spectrum (ppm from H_3PO_4, methanol-d_4): δ 37.0 (s).

(b) Synthesis of [Ni^{II}{Au^I(PPh_3)(D-pen)}$_2$] ([2b]). To a colorless solution containing 0.200 g (0.316 mmol) of [H**1**]·1.5H_2O in 20 mL of ethanol was added 43 mg (0.17 mmol) of $Ni(CH_3COO)_2$·4H_2O, which gave a pale green-blue solution. After the addition of 3.2 mL (0.32 mmol) of an aqueous NaOH solution (0.1 M) and 17 mL of water, the reaction mixture was concentrated to a volume of *ca.* 10 mL to give a pale green suspension. The resulting pale

green precipitate of [**2b**] was collected by filtration and washed with H_2O (4 mL × 2). Yield: 0.17 g (81%). Anal. Found: C, 41.15; H, 4.08; N, 2.16%. Calcd for $[Ni\{Au(PPh_3)(D\text{-pen})\}_2]\cdot 4H_2O$ = $C_{46}H_{56}N_2O_8P_2S_2NiAu_2$: C, 41.12; H, 4.20; N, 2.08%. IR spectrum (cm^{-1}, KBr disk): 1597 (ν_{COO}).

(c) Synthesis of $[Zn^{II}\{Au^{I}(PPh_3)(D\text{-pen})\}_2]$ ([2c]). To a colorless solution containing 0.200 g (0.315 mmol) of [H**1**]·1.5H_2O in 20 mL of ethanol was added 39 mg (0.18 mmol) of $Zn(CH_3COO)_2\cdot 2H_2O$, which gave a colorless solution. After the addition of 3.2 mL (0.32 mmol) of an aqueous NaOH solution (0.1 M) and 17 mL of water, the reaction mixture was concentrated to a volume of *ca.* 10 mL to give a white suspension. The resulting white precipitate of [**2c**] was collected by filtration and washed with H_2O (4 mL × 2). Yield: 0.19 g (90%). Anal. Found: C, 41.38; H, 4.13; N, 2.07%. Calcd for $[Zn\{Au(PPh_3)(D\text{-pen})\}_2]\cdot 3H_2O$ = $C_{46}H_{54}N_2O_7P_2S_2ZnAu_2$: C, 41.47; H, 4.09; N, 2.10%. IR spectrum (cm^{-1}, KBr disk): 1600 (ν_{COO}). ^{1}H NMR spectrum (ppm from TMS, methanol-d_4): δ 1.42 (s, 3H), 1.51 (s, 3H), 3.41 (s, 1H), 7.38 - 7.42 (m, 6H), 7.46 - 7.51 (m, 9H). ^{31}P NMR spectrum (ppm from H_3PO_4, methanol-d_4): δ 36.4 (s).

I-2-4. Reaction of [2b] with acid.

To a pale green-blue solution containing 0.030 g (0.022 mmol) of [**2b**]·4H_2O in 3 mL of ethanol was added 450 μL (0.045 mmol) of a 1.0 M ethanolic CF_3SO_3H solution, which gave a red solution immediately. The slow evaporation of the red solution gave a red crystalline solid which mainly contains $[Ni^{II}\{Au^{I}(PPh_3)(D\text{-Hpen})_2\}_2](CF_3SO_3)_2$ ($[H_2$**2b'**$](CF_3SO_3)_2$). Yield: 0.024 g. IR spectrum (cm^{-1}, KBr disk): 1723 ($\nu_{C=O}$).

I-2-5. Physical measurements. The electronic absorption spectra were recorded on a JASCO V570 or V-660 spectrophotometer at room temperature. The CD spectra were recorded on a JASCO J-600 or J-820 spectropolarimeter at room temperature. The IR spectra were recorded on a JASCO FT/IR-4100 spectrometer using KBr disks at room temperature. The solid-state luminescence spectra were recorded on a JASCO FP-6600 spectrometer at room temperature. The ^{1}H and ^{31}P NMR spectra were measured on a JEOL ECA-500 NMR spectrometer at room temperature using tetramethylsilane (TMS, δ 0.0 ppm) as the internal standard for ^{1}H NMR and triphenyl phosphate (δ –17.6 ppm) as the external standard for ^{31}P NMR. The X-ray fluorescence spectrometries were performed on a HORIBA MESA-500 or SHIMADZU EDX-720 spectrometer. The elemental analyses (C, H, N) were performed using a YANACO CHN coder MT-5 or MT-6.

I-2-6. X-ray structural determinations. Single-crystal X-ray diffraction measurement for [**2a**]$ClO_4\cdot 2H_2O$ was made on a Rigaku R-AXIS VII imaging plate diffractometer with graphite-monochromated Mo-Kα radiation at –73°C. The intensity data were collected by the

ω scan mode, and were corrected for Lorentz and polarization. Empirical absorption corrections were also applied.

The structure was solved by the direct method with SHELXS-97.[11] All calculations were performed using the Yadokari-XG software package [12] except for refinement, which was performed using SHELXL-97.[11] Hydrogen atoms except those of water molecules were placed at calculated positions but were not refined. All non-hydrogen atoms were refined anisotropically. Crystal data and selected bond distances and angles are summarized in Tables I-1 and I-2.

I-3. Results and discussion.

I-3-1. Synthesis and characterization of complexes.

(a) Au^{I} complex ([H1]). The reaction of $[Au^{I}(PPh_3)Cl]$ [10] with 1 molar equiv of D-H_2pen in ethanol, followed by the addition of NaOH, gave a colorless solution, from which [H**1**] was isolated as a white powder. The elemental analytical data of [H**1**] were in agreement with the formula of $[Au(PPh_3)(D\text{-Hpen})]\cdot 1.5H_2O$ (Scheme I-1). The ^{1}H and ^{31}P NMR spectra of [H**1**] in methanol-d_4 gave a single set of signals corresponding to [H**1**]. As shown in Figure I-1, the ^{1}H NMR spectrum shows three singlet signals at δ 1.38, 1.84, and 3.56 ppm attributed to two diastereotopic methyl groups and a methine group in D-pen, respectively, and some multiplet signals in the region of δ 7.52-7.60 derived from phenyl group in PPh_3. The ^{31}P NMR spectrum shows a singlet signal at δ 38.5 ppm (Figure I-2). The IR spectrum gave a strong absorption band assignable to asymmetric COO^{-} stretching at 1626 cm^{-1}, indicative of the presence of deprotonated carboxyl groups (Figure I-3).[13] Thus, D-$Hpen^{-}$ is assumed to exist in a zwitter ionic form with COO^{-} and NH_3^{+} groups, like D-$Hpen^{-}$ in the crystal of $NH_4[Au^{I}(D\text{-Hpen})_2]\cdot 3.667H_2O$ [14] and free DL-H_2pen.[15] Compound [H**1**] was very soluble in polar organic solvents such as methanol, ethanol and dichloromethane, but almost insoluble in water probably due to the introduction of the hydrophobic arylphosphine group, in contrast to the high water-solubility of $NH_4[Au^{I}(D\text{-Hpen})_2]$. Under UV irradiation, the white solid of [H**1**] emitted weak green light with an emission band peaked at 485 nm in the solid-state luminescence spectrum (Figure I-4).

(b) Au^{I}-Co^{III} complex ([2a]ClO_4). The reaction of [H**1**] with 0.5 molar equiv of $Co^{II}(CH_3COO)_2$ under an aerobic condition gave a dark colored solution indicating the formation of a cobalt(III) complex, and purple-brown crystals ([**2a**]ClO_4) were obtained from the solution by adding $NaClO_4$ to it. X-ray fluorescence spectrometry implied that [**2a**]ClO_4 contains Au and Ni atoms, and the elemental analytical data of [**2a**]ClO_4 are in agreement with the formula of $[Co\{Au(PPh_3)(D\text{-pen})\}_2]ClO_4\cdot H_2O$ (Scheme I-1). As shown in Figure I-3, a strong IR band at 1097 cm^{-1} showed the inclusion of ClO_4^{-} as a counter anion, which supports the cationic character of the obtained compound. The ^{1}H and ^{31}P NMR spectra of

[**2**]ClO_4 in methanol-d_4 also exhibited a single set of sharp signals corresponding to one PPh_3 and one D-pen moieties with some shifts from those of [H**1**] (^{1}H signals derived from CH_3 at δ 1.49 and 1.79 ppm, CH at δ 3.81 ppm, Ph in the range of δ 7.42 - 7.58 ppm, and a ^{31}P signal at δ 37.0 ppm), indicative of C_2-symmetrical molecular structure of [**2a**]$^+$ consisting of two [**1**]$^-$ metalloligands and a diamagnetic low-spin cobalt(III) ion, together with the analytical data described above (Figures I-1 and I-2).

The crystal structure of [**2a**]ClO_4 was determined by single-crystal X-ray crystallography, which revealed the presence of one and a half independent, yet nearly the same complex cations, which are at a general position and on a 2-fold axis, respectively, in the asymmetric unit, besides a corresponding number of perchlorate anions and some hydration water molecules. As shown in Figure I-5, [**2a**]$^+$ is a Au_2Co trinuclear complex in which two [**1**]$^-$ coordinate to a cobalt ion with a tridentate-N,O,S mode with retaining the original metalloligand structure (av. Au–P = 2.258(2) Å, Au–S = 2.323(2) Å, P–Au–S = 174.9(7)°). The coordination environment of the cobalt center is octahedral *trans*(*O*)-{Co(D-pen-*N*,*O*,*S*)$_2$} mode, which is basically the same as those observed in the previous system involving thiolato-bridged Au^I-Co^{III} complexes with D-pen.[8f,9a,9c] Among the three possibilities (trans(N), trans(O), and trans(S)) for the octahedral {M(D-pen-*N*,*O*,*S*)$_2$} unit,[8g] both [**2a**]$^+$ and [Co^{III}_3{Au^I(dppe)(D-pen)$_2$}$_2$]$^{2+}$ adopt the same trans(O) configuration (Chart 2 in General Introduction). Considering no restriction for relative position between the D-pen moieties in the monophosphine system, this specificity seems to be the intrinsic nature of the (D-pen-*S*)Au(PR_3)-type metalloligands on coordination to octahedral ions, while the other configurations have been found in some cases without gold(I)-phosphine moiety.[8] The bond lengths of [**2a**]$^+$ are in the region of typical low-spin cobalt(III) ion (av. Co–N = 1.95(1) Å, Co–O = 1.90(1) Å, Co–S = 2.259(2) Å, N–Co–S = 173.8(2)°, O–Co–O = 176.0(2)°), which is indicative of low-spin cobalt(III) state in [**2a**]$^+$, in accord with the NMR observation giving sharp signals with normal chemical shifts.

As shown in Figure I-6, the crystal of [**2a**]ClO_4 is mostly filled with the hydrophobic part consisting of PPh_3 groups connected to each other by many hydrophobic interactions such as CH$\cdots\pi$ contacts, and hydrophilic columns consisting of {Co(D-pen)$_2$}$^-$ moieties and water molecules penetrate the hydrophobic matrix along *c* axis. The complex cations form a trimer by ten NH$\cdots$OOC hydrogen bonds (NH$\cdots$O = 2.112(5) – 2.555(5) Å), which is further connected to two neighboring trimers via hydrogen bonds with water molecules in a column (Figure I-7). All ClO_4^- anions exist in hydrophobic space with many CH$\cdots$O contacts in the crystal (CH$\cdots$O = 2.590(8) – 2.661(9) Å).

The molecular structure of [**2a**]$^+$ can be regarded as the substructure of [Co^{III}_2{Au^I_2(dppe)(D-pen)$_2$}$_2$]$^{2+}$ in disregard of substitution groups on P atoms. This is consistent with the fact that electronic absorption and CD spectra of [**2a**]ClO_4 in ethanol, which have bands around 580 nm with a weakly positive cotton effect and 520 nm with a

negative cotton effect assignable to $^1T_{1g} \leftarrow {}^1A_{1g}$ and $^1T_{2g} \leftarrow {}^1A_{1g}$ d-d transitions derived from a low-spin octahedral cobalt(III) center, are similar to those of $[Co^{III}_2\{Au^I_2(dppe)(D\text{-pen})_2\}_2]^{2+}$ in visible region (Figure I-8).

(c) Au^I-Ni^{II} complex ([2b]). The reaction of [H**1**] with 0.5 molar equiv of $Ni^{II}(CH_3COO)_2$ gave a pale green-blue solution, from which a pale green powder of [**2b**] was obtained. X-ray fluorescence spectrometry implied that [**2b**] contains Au and Ni atoms, and the elemental analytical data of [**2b**] were in agreement with the formula of $[Ni\{Au(PPh_3)(D\text{-pen})\}_2]\cdot 4H_2O$. Unfortunately, attempt to obtain a single crystal of [**2b**] was unsuccessful, and the molecular structure of [**2b**] could not be determined by the crystallography. However, electronic absorption spectrum of [**2b**] in ethanol, that exhibited absorption bands at 976 and 591 nm assignable to $^3T_{2g} \leftarrow {}^3A_{2g}$ and $^3T_{1g} \leftarrow {}^3A_{2g}$ d-d transitions derived from an octahedral nickel(II) center, and the CD spectrum, that exhibited a positive band at 384 nm, and negative bands at 902, 847, and 563 nm, are very similar to those of known $[Ni^{II}_2\{Au^I_2(dppe)(D\text{-pen})_2\}_2]$ [9b] in visible and near IR region, strongly indicative of the coordination structure around nickel(II) center of *trans*(*O*)-$\{Ni^{II}(D\text{-pen-}N,O,S)_2\}^{2-}$ (Figure I-9). Therefore, [**2b**] can be assigned to a trinuclear $Au^I_2Ni^{II}$ complex that is essentially the same as $[\mathbf{2a}]^+$ despite the different charges and ionic radii between nickel(II) and cobalt(III) ions (Scheme I-1).

When 2 molar equiv of triflic acid (CF_3SO_3H) was added to the ethanolic solution of [**2b**], the absorption and CD spectra immediately changed to show an absorption band at 484 nm and positive cotton effects at 543 and 446 nm and negative one at 496 nm, together with drastic color change from green-blue to red (Figure I-10). The spectral patterns of the red solution are similar to those of $[Au^I_2\{Ni^{II}(D\text{-pen-}N,S)_2\}_2]^{2-}$ synthesized from $[Au(D\text{-pen})_2]^{3-}$ (Chart I-1).[8b] Therefore, it is indicated that geometrical conversion from [**2b**] with an octahedral $\{Ni(D\text{-pen-}N,O,S)_2\}^{2-}$ unit to $[Ni^{II}\{Au^I(PPh_3)(D\text{-Hpen})\}_2]^{2+}$ ($[H_2\mathbf{2b'}]^{2+}$) with a square-planar $\{Ni(D\text{-Hpen-}N,S)_2\}$ unit was caused by protonation of carboxylate groups. Although isolation of pure solid of $[H_2\mathbf{2b'}]X_2$ (X is counter anion) was unsuccessful, the hypothesis illustrated in Scheme I-2 is supported by an absorption band at 1723 cm^{-1} implying the existence of COOH in the IR spectrum of red dried residue obtained from the reaction solution, which should mainly consist of $[H_2\mathbf{2b'}](CF_3SO_3)_2$ (Figure I-3). The conversion between [**2b**] and $[H_2\mathbf{2b'}]^{2+}$ is reversible since the red solution of $[H_2\mathbf{2b'}]^{2+}$ reverted back to the green-blue solution showing the same spectral features as that of [**2b**] by the treatment with base (K_2CO_3). Note that the square-planar nickel(II) center generally shows a diamagnetic character ($S = 0$) due to a large energy gap between the unoccupied $3d_{x^2-y^2}$ and the other four occupied 3d orbitals, while the magnetically isolated octahedral nickel(II) center shows a paramagnetic character ($S = 1$). Therefore, the pair of two Au^I-Ni^{II} complexes [**2b**] and $[H_2\mathbf{2b'}]^{2+}$ builds an interconvertible system in which changes in the chromogenic and magnetic properties are caused by pH control.

(d) Au^{I}-Zn^{II} complex ([2c]). The reaction of [H**1**] with 0.5 molar equiv of $Zn^{II}(CH_3COO)_2$ gave a colorless solution, from which white powder of [**2c**] was obtained. X-ray fluorescence spectrometry implied that [**2c**] contains Au and Zn atoms, and the elemental analytical data of [**2c**] were in agreement with the formula of $[Zn\{Au(PPh_3)(D\text{-pen})\}_2]\cdot 3H_2O$. While the filled 3d orbitals of Zn^{II} ion forbid structural determination by UV-vis spectrum, the IR spectrum of [**2c**] is very similar to that of [**2b**] (Figure I-3). In addition, as in the case of [**2a**]ClO_4, ^1H and ^{31}P NMR spectra of [**2c**] in methanol-d_4 also showed signals derived from one metalloligand $[\mathbf{1}]^-$, which includes ^1H nuclei in two diastereomeric methyl (δ 1.42 and 1.51 ppm) and methine groups (δ 3.41 ppm) of D-pen, phenyl groups of PPh_3 (δ 7.38 - 7.51 ppm), and a ^{31}P nucleus of PPh_3 (δ 36.4 ppm). Therefore, it is indicated that [**2c**] is also the isostructural trinuclear $Au^{I}_2Zn^{II}$ complex like to $[\mathbf{2a}]^+$ and [**2b**] (Scheme I-1). The white solid of [**2c**] exhibited green luminescence under UV irradiation, which is similar to that of [H**1**] in color but much brighter than [H**1**]. In the solid-state emission spectrum, [**2c**] gave an emission band at 488 nm with about twice as intense as [H**1**] under the same conditions (Figure I-4). The origin of the emission for both [H**1**] and [**2c**] is assigned to phosphorescence arising primarily from a ^{3}LMCT (S $\rightarrow$ Au) transition, similar to the assignment for related luminescent gold(I) species having both phosphine and thiolate ligands.[7c,16] Despite the existence of two P–Au–S luminophores in a molecule of [**2c**], there is no significant shift in the emission and excitation energy from those of [H**1**], probably because of relatively distant Au^I centers as found in the crystal structure of [**2a**]ClO_4. On the other hand, the intensity of the emission significantly increased for [**2c**] as compared to that for [H**1**]. Coordination of $[\mathbf{1}]^-$ to zinc(II) ion can contribute to the increase of emission intensity by suppressing following two possible quenching mechanisms of [H**1**]: the vibrational energy loss by the flexible D-pen moiety, and the reductive quenching by electron transfer from free lone pairs in D-pen.

I-3-2. Comparison with coordination system without phosphines.

Since the metalloligand $[\mathbf{1}]^-$ is regarded as a derivative of $[Au^{I}(D\text{-pen})_2]^{3-}$ by replacement of one $D\text{-pen}^{2-}$ by PPh_3, the reactivity of $[\mathbf{1}]^-$ with metal ions was compared with that of $[Au^{I}(D\text{-pen})_2]^{3-}$. The reaction of $[\mathbf{1}]^-$ with metal ions gave the heterometallic Au^{I}_2M trinuclear complexes through coordination of amine, carboxylate, and thiolato donor groups to the metal ions, therefore, the fact shows that the coordination ability of $\{Au^{I}(D\text{-pen})\}^-$ moiety is still preserved on introduction of the phosphine group. In the structure of $[\mathbf{2a}]^+$, the two $[\mathbf{1}]^-$ metalloligands coordinate to the octahedral cobalt(III) center in a tridentate-N,O,S fashion to form a *trans*(*O*)-$N_2O_2S_2$ octahedron, which is similar to the case of $[Au^{I}_3\{Co^{III}(D\text{-pen-}N,O,S)_2\}_3]$ consisting of three $[Au^{I}(D\text{-pen})_2]^{3-}$ metalloligands and three Co^{III} ions, including their Au^{I}-Co^{III} oxidation states and *R* absolute configurations of μ_2-bridging sulfur atoms (Chart I-1).[8f] While $[Au^{I}_3\{Co^{III}(D\text{-pen-}N,S)\}_2]^{3-}$, where only N and

S atoms are used for coordination, was also formed in the reaction of $[Au^{I}(D\text{-pen})_2]^{3-}$ with cobalt(II) ion involving air-oxidation, no evidence for such coordination mode was obtained in the present system probably due to large steric repulsions between neighboring PPh_3 groups in the expected structure of the N,S-coordinate product, $[\{Au^{I}(PPh_3)\}_3\{Co^{III}(D\text{-pen-}N,S)\}]$ (Chart I-1).

In spite of the topological difference between the trinuclear structure of $[\mathbf{2a}]^{+}$ with terminal $\{Au(PPh_3)\}^{+}$ groups and the more restricted cyclic hexanuclear structure of $[Au^{I}_3\{Co^{III}(D\text{-pen})_2\}_3]$, their $[Au^{I}_2\{Co^{III}(D\text{-pen-}N,O,S)_2\}]^{+}$ substructures are almost superimposed except slight elongation of Au–S bonds in $[\mathbf{2a}]^{+}$ (av. Au–S = 2.323(2) Å for $[\mathbf{2a}]^{+}$, 2.306(3) Å for $[Au^{I}_3\{Co^{III}(D\text{-pen})_2\}_3]$). In addition, the very similar electronic absorption and CD spectra of those complexes indicate the similarity in the electronic state around the cobalt(III) center. From these results, monophosphine ligands may be widely used as terminal ligands to modify the structures containing S–Au–S linkage without critical changes in the property of thiolato-bridged metal centers by blocking one of two coordination sites on each linear gold(I) ion.

On the other hand, the largest difference between the systems with phosphines and without phosphines is the existence or absence of the hydrophobic groups. The presence of the hydrophobic parts affected the crystal packing through CH···π and π···π interactions, which played important role in the dppe system, as well as solubility in solvents. All the complexes of [H**1**], [**2a**]ClO_4, [**2b**], and [**2c**] are insoluble in pure water but very soluble in polar organic solvents such as alcohols and haloalkanes, in contrast to the non-phosphine system where water is commonly the best solvent.

Interestingly, it was revealed that the change of the solubility by introduction of the lipophilic arylphosphine affected the coordination behavior of the metalloligand in the case of Ni^{II}. Under almost neutral pH condition, $[\mathbf{1}]^{-}$ coordinated to nickel(II) ion with a tridentate-N,O,S mode to form [**2b**] with an octahedral nickel(II) center, although the reaction of $[Au(D\text{-pen})_2]^{3-}$ with nickel(II) ion mainly produced $[Au^{I}_2\{Ni^{II}(D\text{-pen-}N,S)_2\}_2]^{2-}$ with a square-planar nickel(II) center in neutral aqueous solution and the *trans*(*O*)-$N_2O_2S_2$ geometry has not been found in the combination of $[Au^{I}(D\text{-pen})_2]^{3-}$ and Ni^{II} ion (Chart I-1).[8b] In addition, under acidic condition, [**2b**] was converted to [H_2**2b'**] with square-planar Ni^{II} accompanied with protonation on carboxylate groups, while $[Au^{I}_2\{Ni^{II}(D\text{-pen-}N,S)\}_2]^{2-}$ was converted to $[Au^{I}_3\{Ni^{II}(D\text{-Hpen-}O,S)_3\}_2]^{+}$ triggered by the protonation on amino groups (Chart I-1). The difference of coordination modes is explained by the difference of solvent polarity between water and ethanol. In ethanol with relatively lower polarity, negative-charged COO^{-} group is less stable because of weak stabilization by solvation. The less stability of free carboxylate groups promotes coordination of carboxylate to metal ion, leading to $N_2O_2S_2$ six-coordinate structure of nickel(II) under neutral condition, although the ligand field of N_2S_2 environment is strong enough to stabilize a square-planar geometry. Since

free amino acids prefer a combination of the zwitter ionic NH_3^+/COO^- form rather than the uncharged NH_2/COOH form particularly in polar media, preferential protonation on amino groups rather than carboxylate groups leads to O,S-coordination in $[Au^I_3\{Ni^{II}(D\text{-Hpen-}O,S)_3\}_2]^+$. On the other hand, the NH_2/COOH form may be more stabilized in ethanol, but this stabilization seems not to be large enough to invert the preference of protonation, considering the free metalloligand [H**1**]. Nevertheless, the N_2S_2 square-planar structure with protonated COOH groups should be the most possible one under acidic condition in the present system, because steric hinderance of PPh_3 groups prevents to form $[\{Au^I(PPh_3)\}_3\{Ni^{II}(D\text{-Hpen-}O,S)_3\}]^{2+}$ and the ligand-field of O_2S_2 environment is probably not strong enough to stabilize the square-planar geometry of nickel(II) center.[17]

Another important feature that [H**1**] has and $NH_4[Au(D\text{-Hpen})_2]$ does not have is luminescence, and it was enhanced by coordination to zinc(II) ion. Introduction of arylphosphines to gold(I)-thiolate systems produced luminescent P–Au–S structure, and the aryl groups on phosphorus atoms may act as a light-harvesting antenna as well as bulky groups to protect the luminophore from quenchers.[18]

I-4. Conclusion.

In order to reveal general structural features, chemical and physical properties, and reactivity of the thiolato-bridged heterometallic Au^I-M multinuclear complexes with mixed D-penicillaminate and phosphines, the coordination behavior of [**1**]$^-$ as one of the simplest D-penicillaminato gold(I) metalloligand with phosphines toward three 3d metal ions (Co^{II}, Ni^{II}, and Zn^{II}) was investigated and compared to the traditional non-phosphine systems as well as the previously reported dppe system in this chapter.

All the reaction of [H**1**] with Co^{II}, Ni^{II}, and Zn^{II} ions gave the Au^I_2M trinuclear complexes ([**2a**]$^+$, [**2b**], and [**2c**], respectively), in which two [**1**]$^-$ coordinate to an octahedral metal ion with a tridentate-N,O,S mode through D-pen moiety, in spite of the difference in the number of valence electrons (3d) and the charges of the secondary metal ions. The detailed molecular structure of the trinuclear complex was revealed by the single-crystal X-ray structural analysis for [**2a**]ClO_4, which also indicated that the substructure of [**2a**]$^+$, $[Au^I_2\{Co^{III}(D\text{-pen-}N,O,S)_2\}]^+$, is quite similar to that in the previous phosphine-containing system as well as the non-phosphine system including its electronic state, together with the spectroscopic data. Therefore, the monophosphine system shown in this chapter will be significantly helpful as a basic model to explain properties of analogous systems with more complicated structures. Actually [**2a**]$^+$ will be referred in order to explain anomalous behavior of a cobalt complex in Chapter III. It is hoped that the methodology to terminate one of two coordination sites on a linear Au^I ion by monophosphine can be commonly applied to analyzing the structures and properties of complexes with RS–Au–SR moiety other than D-pen. [19]

On the other hand, it was also shown that the introduction of the arylphosphine group provides the hydrophobic interactions in the crystal phase, good solubility in organic solvents, and luminescent property. The previous study of the dppe system has already indicated that CH$\cdots\pi$ interaction has a quite important influence on the crystal packing structure when they function cooperatively and effectively, in spite of their relatively small stabilization energy compared with general hydrogen bonding interactions.[9] Moreover, the Au^{I}-Ni^{II} complexes in this system revealed that the change in the solubility affects the coordination behavior and its dependence on acid/base, and the behavior rationally explains the formation of the $[Ni^{II}_2\{Au_2(dppe)(D\text{-}pen)_2\}_2]$ as well as Au^{I}-Ni^{II} complexes described in Chapter II. The luminescent property given by the introduction of the arylphosphine group was additionally enhanced by coordination to a zinc(II) ion. Moreover, the luminescence arising from the LMCT excitation state from S to Au atoms can be modified also by aurophilic interaction as reported for other luminescent gold(I) complexes,[7] which is demonstrated in Chapter II.

I-5. References.

[1] (a) C. E. Housecroft, *Coord. Chem. Rev.* **1997**, *164*, 667. (b) P. Schwerdtfeger, H. L. Hermann, H. Schmidbaur, *Inorg. Chem.* **2003**, *42*, 1334. (c) M. C. Gimeno, A. Laguna, in *Comprehensive Coordination Chemistry II*, J. A. McCleverty, T. J. Meyer, Eds.; Elsevier Inc., vol. 6, pp. 911–1145 (2003). (d) J. J. Vittal, R. J. Puddephatt, *Gold: Inorganic & Coordination Chemistry*, Wiley, Chichester (2006).

[2] (a) L. Hao, M. A. Mansour, R. J. Lachicotte, H. J. Gysling, R. Eisenberg, *Inorg. Chem.* **2000**, *39*, 5520. (b) H. G. Raubenheimer, M. W. Esterhuysen, G. Frenking, A. Y. Timoshkin, C. Esterhuysen, U. E. I. Horvath, *Dalton Trans.* **2006**, 4580.

[3] (a) F. Canales, O. Crespo, M. C. Gimeno, A. Laguna, P. G. Jones, *Organometallics* **1999**, *18*, 3142. (b) I. d. Rio, R. Terroba, E. Cerrada, M. B. Hursthouse, M. Laguna, *Eur. J. Inorg. Chem.* **2001**, 2013. (c) S. Nogai, A. Schier, H. Schmidbaur, D. Schneider, *Inorg. Chim. Acta*, **2003**, *352*, 179. (d) M. Bardaji, M. J. Calhorda, P. J. Costa, P. G. Jones, A. Laguna, *Inorg. Chem.* **2006**, *45*, 1059. (e) E. Barreiro, J. S. Casas, M. D. Couce, A. Laguna, J. M. Lopez-de-Luzuriaga, *Eur. J. Inorg. Chem.* **2011**, 1322. (f) O. Crespo, M. C. Gimeno, A. Laguna, F. J. Lahoz, C. Larraz, *Inorg. Chem.* **2011**, *50*, 9533.

[4] F. Basolo, R. C. Johnson, *Coordination Chemisry; the Chemistry of Metal Complexes*, Benjamin, NY (1964).

[5] T. Ishii, S. Tsuboi, G. Sakane, M. Yamashita, B. K. Breedlove, *Dalton Trans.* **2009**, 680.

[6] R. J. Deeth, *Coord. Chem. Rev.* **2001**, *212*, 11.

[7] (a) A. Vogler, H. Kunkely, *Coord. Chem. Rev.* **2001**, *219-221*, 489. (b) V. W.-W. Yam, E. C.-C. Cheng, *Chem. Soc. Rev.* **2008**, *37*, 1806. (c) E. R. T. Tiekink, J.-G. Kang, *Coord. Chem. Rev.* **2009**, *253*, 1627. (d) X. He, V. W.-W. Yam, *Coord. Chem. Rev.* **2011**, *255*,

2111.

[8] (a) A. Toyota, T. Yamaguchi, A. Igashira- Kamiyama, T. Kawamoto, T. Konno, *Angew. Chem. Int. Ed.* **2005**, *44*, 1088. (b) M. Taguchi, A. Igashira-Kamiyama, T. Kajiwara, T. Konno, *Angew. Chem. Int. Ed.* **2007**, *46*, 2422. (c) M. Taguchi, Y. Sameshima, A. Igashira-Kamiyama, S. Akine, T. Nabeshima, T. Konno, *Chem. Lett.* **2008**, *37*, 244. (d) Y. Sameshima, N. Yoshinari, K. Tsuge, A. Igashira-Kamiyama, T. Konno, *Angew. Chem. Int. Ed.* **2009**, *48*, 8469. (e) T. Konno, N. Yoshinari, M. Taguchi, A. Igashira-Kamiyama, *Chem Lett.* **2009**, *38*, 526. (f) T. Konno, A. Toyota, A. Igashira-Kamiyama, *J. Chin. Chem. Soc.* **2009**, *56*, 26. (g) A. Igashira-Kamiyama, T. Konno, *Dalton Trans.* **2011**, *40*, 7249.

[9] (a) R. Lee, A. Igashira-Kamiyama, H. Motoyoshi, T. Konno, *CrystEngComm* **2012**, *14*, 1936. (b) A. Igashira-Kamiyama, N. Matsushita, R. Lee, K. Tsuge, T. Konno, *Bull. Chem. Soc. Jpn.* **2012**, *85*, 706. (c) R. Lee, A. Igashira-Kamiyama, M. Okumura, T. Konno, *Bull. Chem. Soc. Jpn.* **2013**, *86*, 908.

[10] McAuliffe, R. V. Parish, P. D. Randall, *J. Chem. Soc., Dalton Trans.* **1979**, 1730.

[11] G. M. Sheldrick, *Acta Crystallogr., Sect. A* **2008**, *64*, 112.

[12] C. Kabuto, S. Akine, E. Kwon, *J. Cryst. Soc. Jpn.* **2009**, *51*, 218.

[13] K. Nakamoto, *Infrared and Raman Spectra of Inorganic and Coordination Compounds*, 5th ed., Wiley, Chichester (1997).

[14] D. J. LeBlanc, J. F. Britten, Z. Wang, H. E. Howard-Lock, C. J. L. Lock, *Acta Crystallogr. Sect. C* **1997**, *53*, 1763.

[15] H. E. Howard-Lock, C. J. L. Lock, P. S. Smalley, *J. Chem. Crystallogr.* **1983**, *13*, 333.

[16] (a) B.-C. Tzeng, J.-H. Liao, G.-H. Lee, S.-M. Peng, *Inorg. Chim. Acta* **2004**, *357*, 1405. (b) C.-K. Li, X.-X. Lu, K. M.-C. Wong, C.-L. Chan, N. Zhu, V. W.-W. Yam, *Inorg. Chem.* **2004**, *43*, 7421. (c) M. Bardají, M. J. Calhorda, P. J. Costa, P. G. Jones, A. Laguna, M. R. Pérez, M. D. Villacampa, *Inorg. Chem.* **2006**, *45*, 1059. (d) P. J. Costa, M. J. Calhorda, *Inorg. Chim. Acta* **2006**, *359*, 3617. (e) J. Schneider, Y.-A. Lee, J. Pérez, W. W. Brennessel, C. Flaschenriem, R. Eisenberg, *Inorg. Chem.* **2008**, *47*, 957. (f) E. R. T. Tiekink, J.-G. Kang, *Coord. Chem. Rev.* **2009**, *253*, 1627. (g) I. O. Koshevoy, E. S. Smirnova, M. Haukka, A. Laguna, J. C. Chueca, T. A. Pakkanen, S. P. Tunik, I. Ospino, O. Crespo, *Dalton Trans.* **2011**, *40*, 7412. (h) O. Crespo, M. C. Gimeno, A. Laguna, F. J. Lahoz, C. Larraz, *Inorg. Chem.* **2011**, *50*, 9533.

[17] Only three examples of isolated square-planer [Ni^{II}(carboxylate-*O*)$_2$(thiolate-*S*)$_2$] complexes can be found in "Reaxys" database (https://www.reaxys.com/) and "Cambridge Structural Database (CSD)" (http://www.ccdc.cam.ac.uk/Solutions/CSDSystem/Pages/CSD.aspx): (a) K. A. Jensen, *Z. Anorg. Allg. Chem.* **1936**, 265. (b) A. A. Medzhidov, V. M. Farzaliev, V. T. Kasumov, M. A. Allakhverdiev, C. I. Mamedov, *J. Gen. Chem. USSR (English Translation)* **1982**,

93. (c) S. G. Rosenfield, M. L. Y. Wong, D. W. Stephen, P. K. Mascharak, *Inorg. Chem.* **1987**, *26*, 4119.

[18] (a) W. M. Campbell, A. K. Burrell, D. L. Officer, K. W. Jolley, *Coord. Chem. Rev.* **2004**, 1363. (b) L. Armelao, S. Quici, F. Barigelletti, G. Accorsi, G. Bottaro, M. Cavazzini, E. Tondello, *Coord. Chem. Rev.* **2010**, *254*, 487.

[19] (a) T. Konno, K. Tokuda, T. Abe, M. Hirotsu, *Mol. Cryst. Liq. Cryst. Sci. Technol., Sect.A* **2000**, *342*, 45. (b) T. Konno, Y. Chikamoto, K. Okamoto, T. Yamaguchi, T. Ito, M. Hirotsu, *Angew. Chem. Int. Ed.* **2000**, *39*, 4098. (c) T. Konno, M. Hattori, T. Yoshimura, M. Hirotsu, *Chem. Lett.* **2002**, 230. (d) Y. Yamada, Y. Miyashita, K. Fujisawa, K. Okamoto, *Bull. Chem. Soc. Jpn.* **2002**, *75*, 1151. (e) Y. Chikamoto, M. Hirotsu, T. Yamaguchi, T. Yoshimura, T. Konno, *Dalton Trans.* **2004**, 3654. (f) R. Y. C. Shin, G. K. Tan, L. L. Koh, J. J. Vittal, L. Y. Goh, R. D. Webster, *Organometallics* **2005**, *24*, 539. (g) T. Konno, M. Usami, A. Toyota, M. Hirotsu, T. Kawamoto, *Chem. Lett.* **2005**, *34*, 1146. (h) S. D. Robertson, A. M. Z. Slawin, J. D. Woollins, *Eur. J. Inorg. Chem.* **2007**, 247. (i) T. Aridomi, K. Takamura, A. Igashira-Kamiyama, T. Konno, *Chem. Lett.* **2008**, *37*, 170. (j) P. Chen, Y. Peng, C. Jia, J. Qu, *Eur. J. Inorg. Chem.* **2010**, 5239. (k) Y. Takino, N. Yoshinari, T. Kawamoto, T. Konno, *Chem. Lett.* **2012**, *41*, 834.

[20] (a) P. Pyykkö, *Chem. Rev.* **1997**, *97*, 597. (b) H. Schmidbaur, A. Schier, *Chem. Soc. Rev.* **2008**, *37*, 1931.

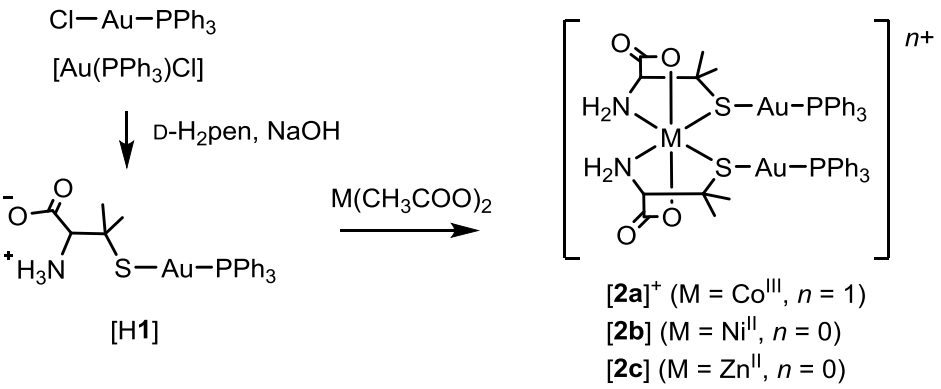

Scheme I-1. Syntheses of complexes, [H**1**], [**2a**]$^{+}$, [**2b**], and [**2c**].

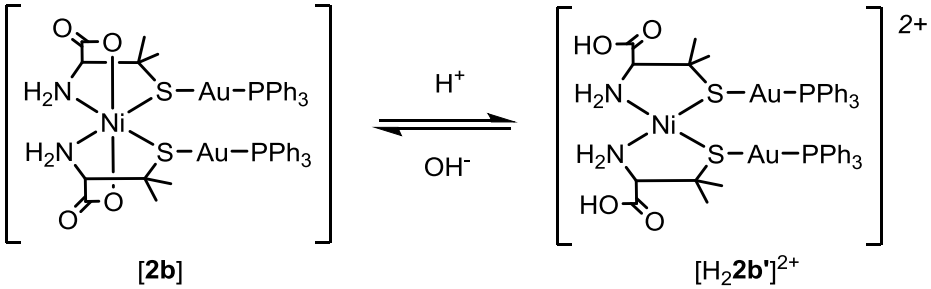

Scheme I-2. The acid/base-induced conversion between [**2b**] and [H_2**2b'**]$^{2+}$.

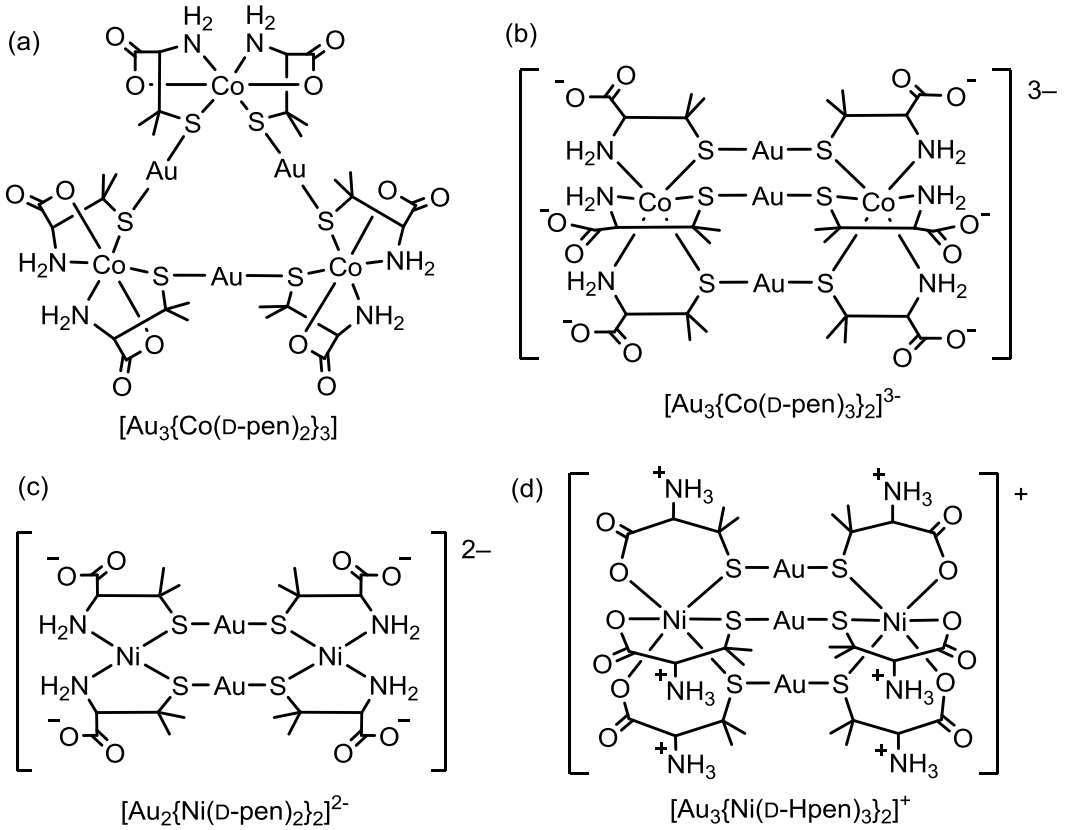

Chart I-1. Heterometallic complexes derived from $[Au^{I}(D\text{-pen})_2]^{3-}$: (a) $[Au^{I}_3(Co^{III}(D\text{-pen})_2)_3]$, (b) $[Au^{I}_3\{Co^{III}(D\text{-pen})_3\}_2]^{3-}$, (c) $[Au^{I}_2\{Ni^{II}(D\text{-pen})_2\}_2]^{2-}$, and (d) $[Au^{I}_3\{Ni(D\text{-Hpen})_3\}_2]^{+}$.

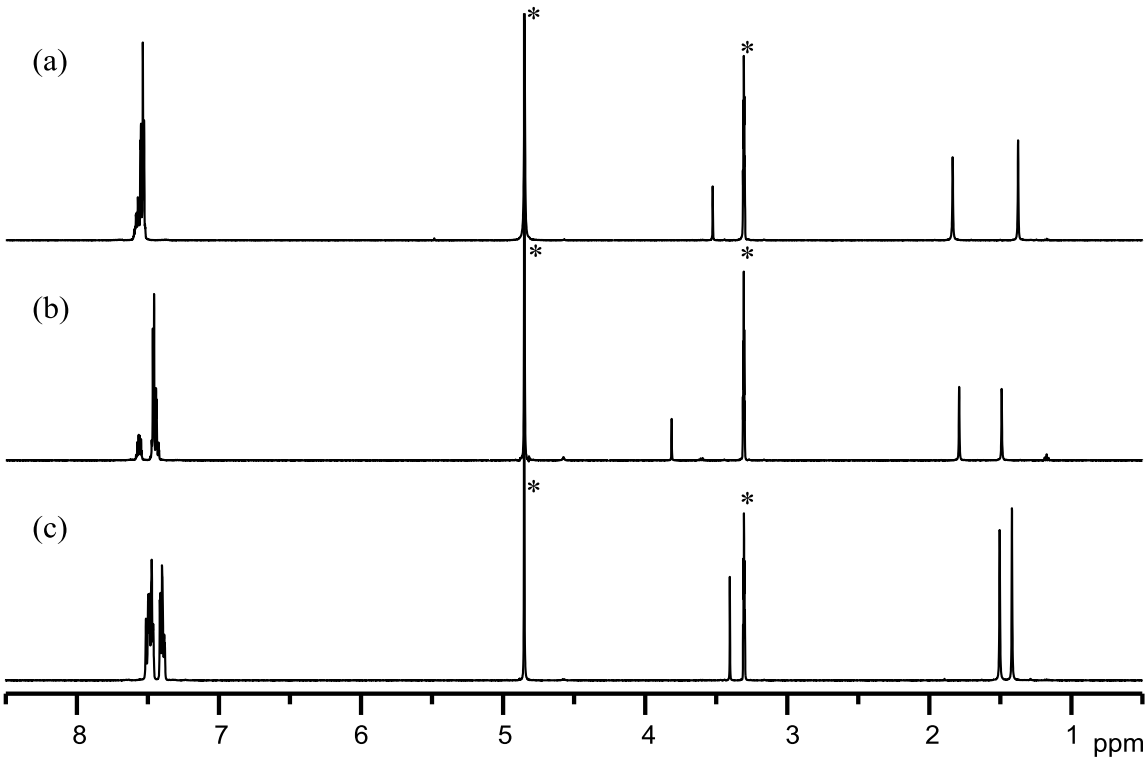

Figure I-1. ^{1}H NMR spectra of (a) [H**1**], (b) [**2a**]ClO_4, and (c) [**2c**] in methanol-d_4. (*) denotes the signals from solvents.

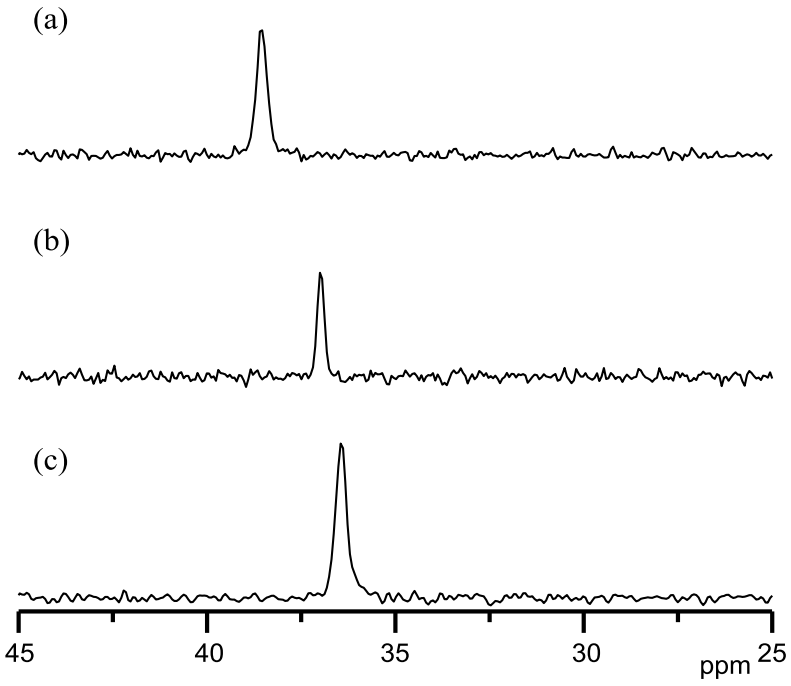

Figure I-2. ^{31}P NMR spectra of (a) [H**1**], (b) [**2a**]ClO_4, and (c) [**2c**] in methanol-d_4.

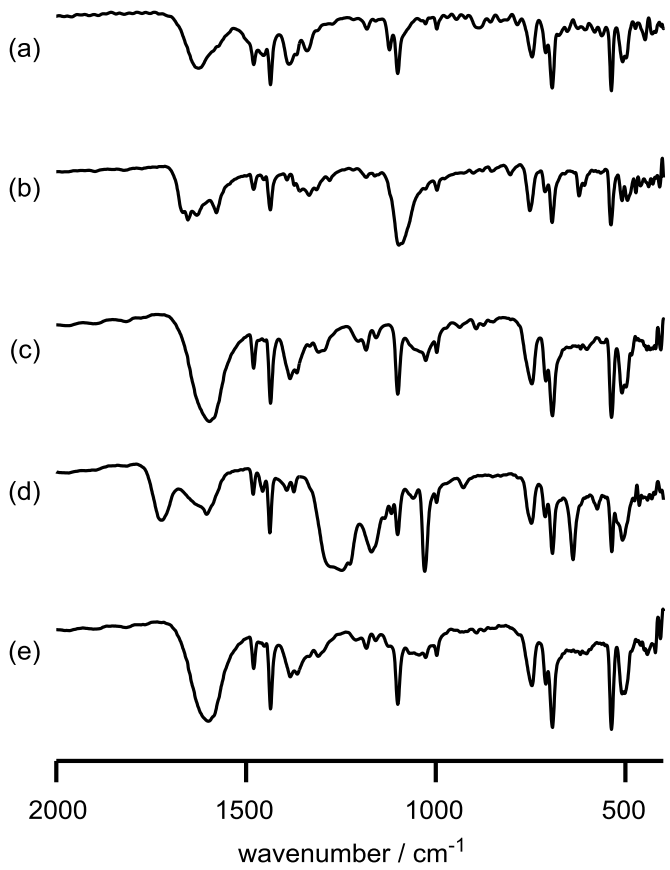

Figure I-3. IR spectra of (a) [H**1**], (b) [**2a**]ClO_4, (c) [**2b**], (d) [H_2**2b'**], and (e) [**2c**] (KBr disk).

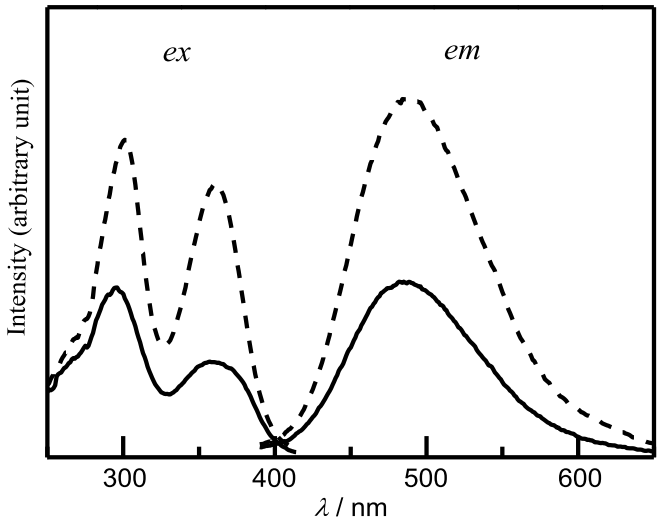

Figure I-4. Solid-state emission (*em*) and excitation (*ex*) spectra of [H**1**] (solid line) and [**2c**] (dashed line).

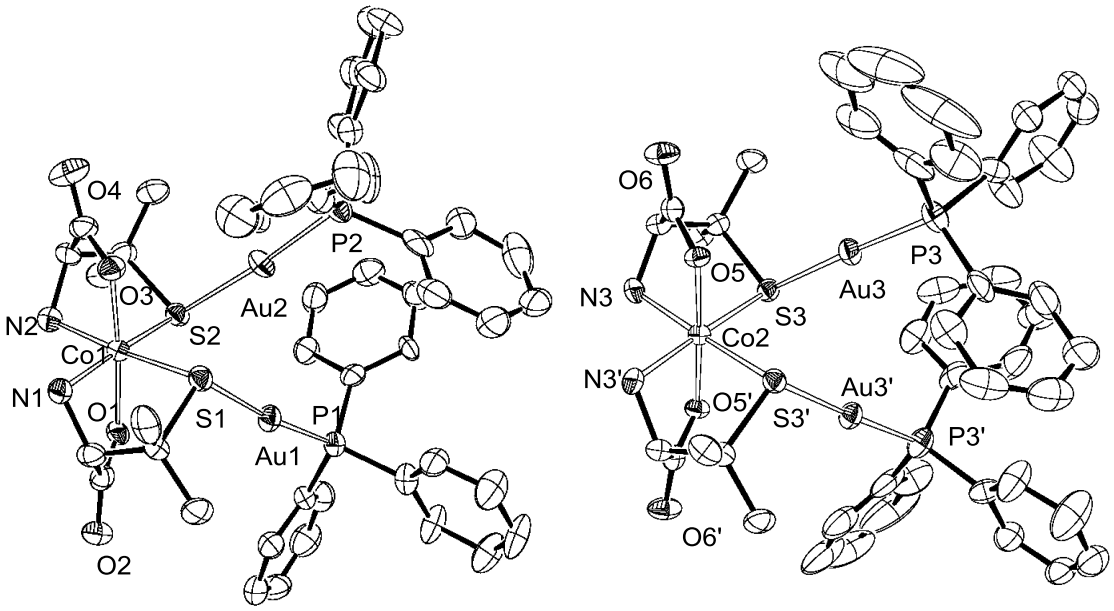

Figure I-5. ORTEP drawings of the complex cations in [**2a**]ClO_4 with 50% probability level of thermal ellipsoids. H atoms are omitted for clarity. Symmetry code ('): 1–x, y, –z.

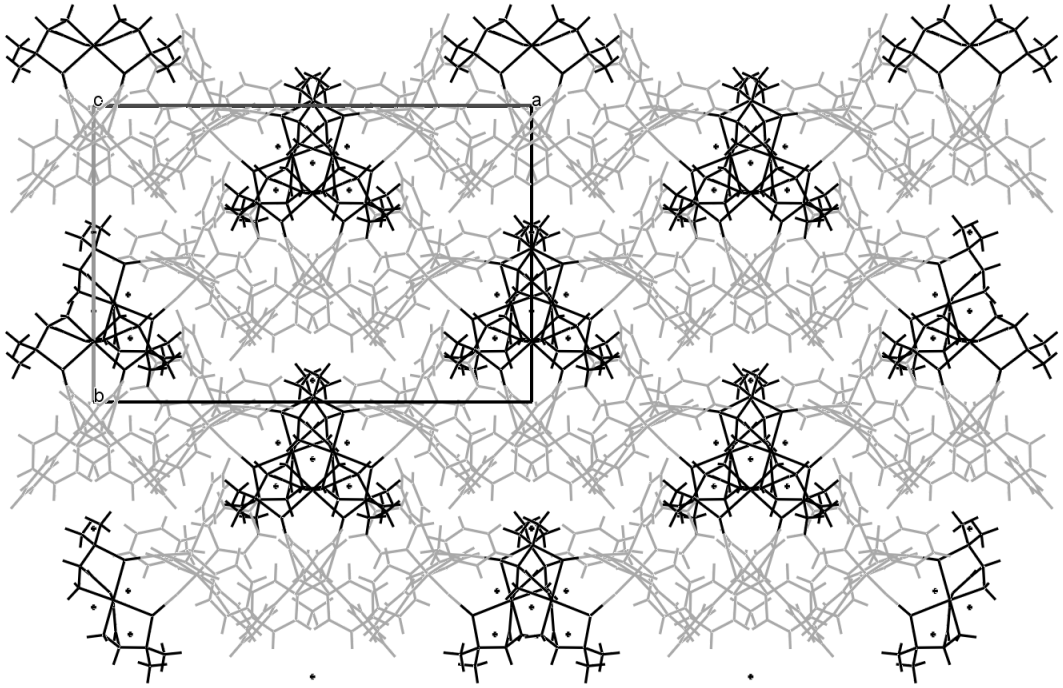

Figure I-6. Packing diagram of [**2a**]ClO_4 viewed along *c* axis. $\{Co^{III}(D\text{-pen})_2\}^-$ moieties and O atoms of water molecules are shown with black sticks and the other parts ($\{Au^{I}(PPh_3)\}^+$ and ClO_4^-) are shown with gray sticks.

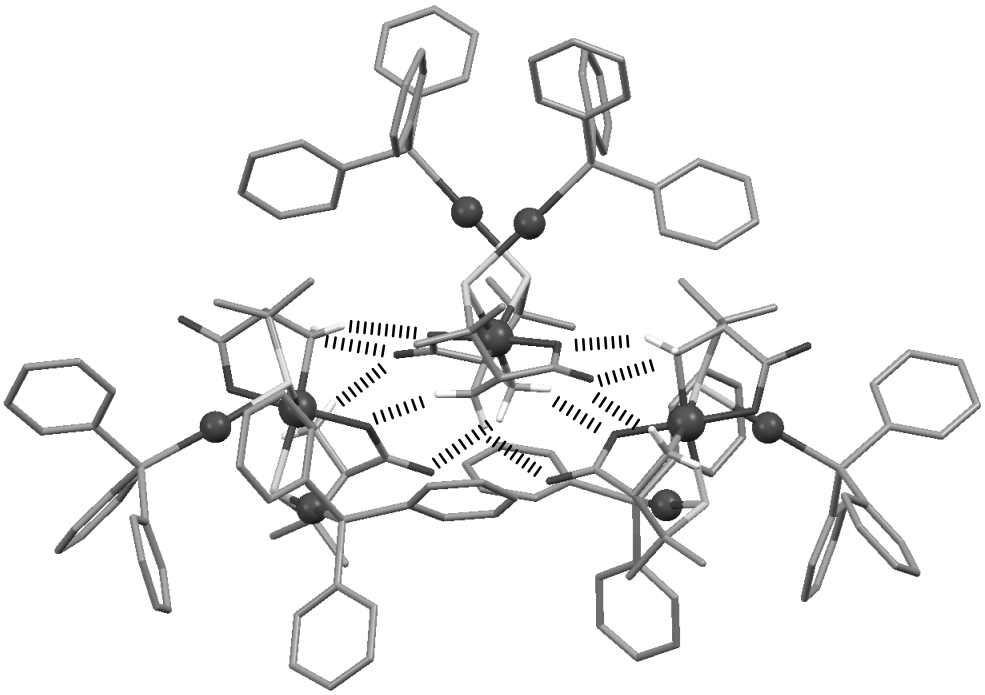

Figure I-7. Hydrogen-bonded trimer of [**2a**]ClO_4. H atoms except those on N are omitted for clarity. Hydrogen bonds are depicted with dashed lines.

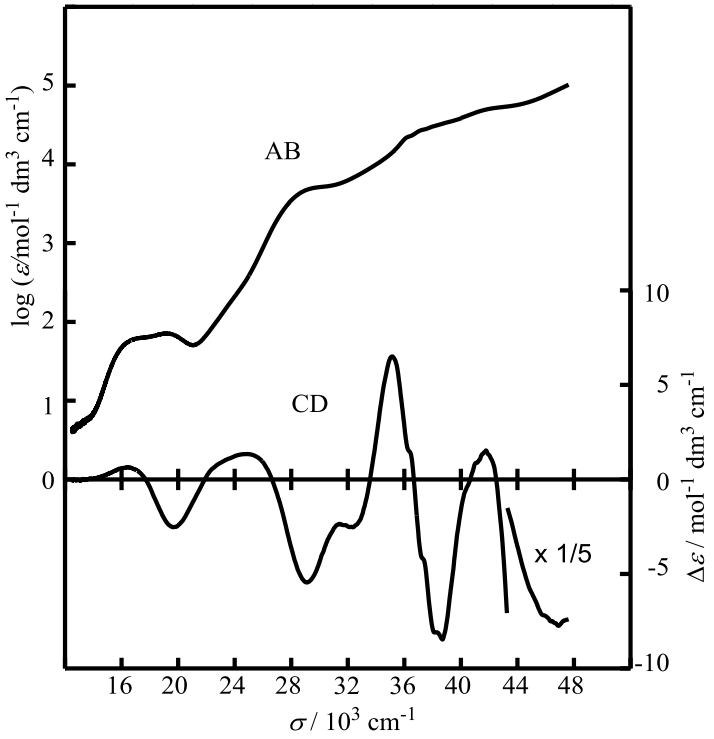

Figure I-8. Electronic absorption and CD spectra of [**2a**]ClO_4 in ethanol.

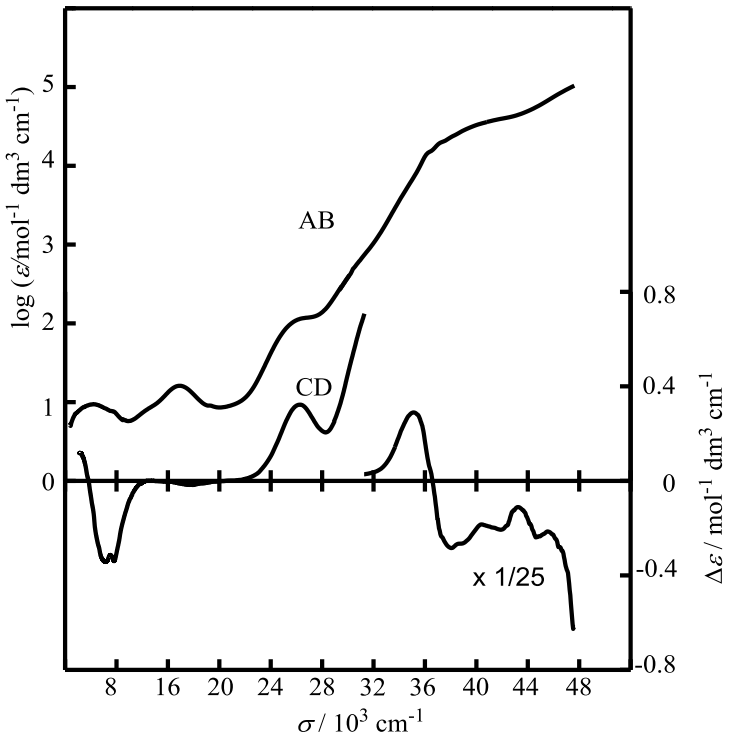

Figure I-9. Electronic absorption and CD spectra of [**2b**] in ethanol.

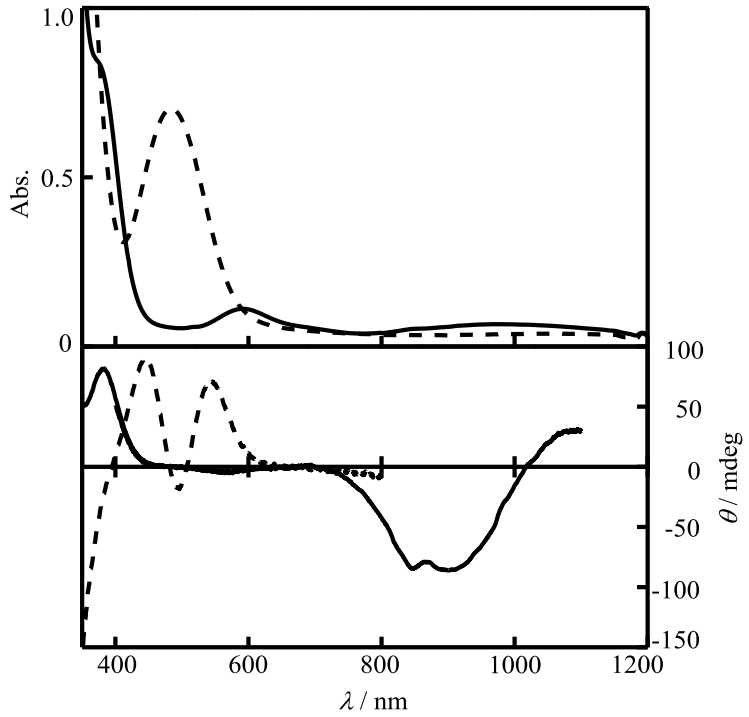

Figure I-10. Electronic absorption and CD spectra of ethanolic solution containing [**2b**] (solid line) and $[H_2\mathbf{2b'}]^{2+}$ generated from the reaction of [**2b**] with 2 molar equiv of triflic acid (dashed line).

Table I-1. Crystallographic data for [**2a**]ClO_4.

	[**2a**]$ClO_4 \cdot 2H_2O$
empirical formula	$C_{46}H_{52}Au_2ClCoN_2O_{10}P_2S_2$
formula weight	1407.27
color, form	purple, plate
crystal size /mm^3	$0.20 \times 0.20 \times 0.10$
crystal system	monoclinic
space group	*C*2
a/ Å	24.3383(18)
b/ Å	15.7892(12)
c/ Å	20.1003(16)
α (°)	90
β (°)	106.491(7)
γ (°)	90
V/ $Å^3$	7406.4(10)
Z	6
T/ K	200(2)
ρ_{calcd}/ g cm^{-3}	1.893
μ(Mo Kα)/ mm^{-1}	6.521
R_1[a] ($I>2\sigma(I)$)	0.0394
wR_2[b] (all data)	0.0628
flack parameter	0.004(3)

[a] $R_1 = (\Sigma|(|F_o| - c|F_c|)|)/(\Sigma|F_o|)$

[b] $wR_2 = [\{\Sigma w(F_o^2 - cF_c^2)^2\}/(\Sigma w|F_o^2|^2)]^{1/2}$

Table I-2. Selected bond distances (Å) and angles (°) for [**2a**]ClO_4.

		distances (Å)	
Au1–P1	2.2588(15)	Co2–N3	1.958(5)
Au2–P2	2.257(2)	Co1–O1	1.916(5)
Au3–P3	2.259(2)	Co1–O3	1.880(5)
Au1–S1	2.3163(16)	Co2–O5	1.890(4)
Au2–S2	2.3275(18)	Co1–S1	2.2559(18)
Au3–S3	2.3246(17)	Co1–S2	2.2624(17)
Co1–N1	1.958(4)	Co2–S3	2.2569(16)
Co1–N2	1.943(5)		
		angles (°)	
P1–Au1–S1	173.64(7)	N2–Co1–S1	174.1(2)
P2–Au2–S2	173.33(7)	N3–Co2–S3'	173.92(19)
P3–Au3–S3	177.64(6)	O1–Co1–O3	175.20(17)
N1–Co1–S2	173.47(19)	O5–Co2–O5'	177.5(2)

Symmetry code('): –x+1, y, –z

Table I-3. Electronic absorption and CD spectral data of [**2a**]ClO_4. (sh = shoulder)

absorption maxima: σ / 10^3 cm^{-1} (log (ε / mol^{-1} dm^3 cm^{-1}))		CD extrema: σ / 10^3 cm^{-1} ($\Delta\varepsilon$ / mol^{-1} dm^3 cm^{-1})	
[**2a**]ClO_4 in ethanol			
17.0	(1.79)sh	16.56	(+0.63)
19.10	(1.854)	19.58	(–2.51)
29.8	(3.72)sh	24.84	(+1.38)
36.4	(4.37)sh	29.05	(–5.44)
37.4	(4.45)sh	32.47	(–2.48)
43.0	(4.73)sh	35.19	(+6.49)
		38.76	(–8.38)
		41.84	(+1.47)
[**2b**] in ethanol			
10.25	(0.972)	11.11	(–0.34)
16.92	(1.208)	11.80	(–0.34)
27.1	(2.06)sh	17.76	(–0.02)
36.4	(4.17)sh	26.28	(+0.33)
37.5	(4.30)sh	35.19	(+7.35)
42.9	(4.63)sh	38.05	(–7.10)
		41.88	(–5.16)
		44.64	(–5.96)

Chapter II. Diphosphine System.

II-1. Introduction.

Advancing one more step from the simplest monophosphine system presented in the previous chapter, the research for another system with dppm (bis(diphenlyphosphino)methane), which is a very simple diphosphine ligand with two diphenylphosphino groups (PPh_2) bridged by only one methylene group (CH_2), is presented in this chapter. This diphosphine ligand was employed here in order to achieve structural control of thiolato-bridged complexes by gold(I)-phosphine backbone through aurophilic interactions.[1] Aurophilic interaction is an attractive interaction between gold atoms, and its moderate strength (typically 20 - 50 kJ/mol) is suitable to control some structural factors such as molecular conformations and supramolecular arrangements under ambient conditions.[1a,b]

In the previous study on a digold(I) metalloligand with D-pen and dppe (1,2-bis(diphenylphosphino)ethane), which is also a diphosphine but with an ethylene group (CH_2CH_2) separating two PPh_2 groups, it was shown that $[Au^I_2(dppe)(D\text{-pen})_2]^{2-}$ exclusively acts as a bis(tridentate-N,O,S) bridging metalloligand coordinating to two octahedral metal ions (Cr^{III}, Co^{III}, Ni^{II}).[2] This coordination behavior is very similar to that of $[Au^I(D\text{-pen})_2]^{3-}$, which also acts as a bridging ligand to the secondary metal ions.[3].

On the other hand, a digold(I) complex with dppm newly designed here, $[Au^I_2(dppm)(D\text{-pen})_2]^{2-}$ ($[\mathbf{3}]^{2-}$), is expected to prefer a bent conformation with two D-pen moieties in a parallel manner because of an effective intramolecular aurophilic interaction between two gold(I) ions bridged by dppm, which has been reported for a large number of gold(I)-dppm complexes in the past.[4] Indeed, it is shown in this chapter that the coordination behavior of $[\mathbf{3}]^-$ was controlled by gold(I)-dppm backbone through intramolecular aurophilic interaction to act as a hexadentate-N_2,O_2,S_2 chelating metalloligand toward the secondary metal ions, leading to a heterometallic Au^I_2M trinuclear ring structure including a metallo-chelate ring of $\{Au^I_2(dppm)\}^{2+}$, $[M\{Au^I_2(dppm)(D\text{-pen})_2\}]$ ([**5a**] or [**5b**]; M = Ni^{II} or Zn^{II}, respectively).

Moreover, it was also revealed that the Au^I_2M metalloring can be reversibly expanded to a larger Au^I_3M metalloring with a longer backbone consisting of $\{Au^I_3(dppm)_2\}^{3+}$ by incorporating $\{Au^I(dppm)\}^+$ extension agent, $[M\{Au^I_3(dppm)_2(D\text{-pen})_2\}]^+$ ($[\mathbf{6a}]^+$ or $[\mathbf{6b}]^+$; M = Ni^{II} or Zn^{II}, respectively). Although interconvertible metalloring structures have received attention not only as candidates of host molecules for molecular recognition but also because of their potential applicability in molecular devices and nanomachines,[5] this class of coordination systems is still challenging, probably because the structural expansion/contraction events require reversible reorganization of chemical bonds.[6] Herein rare examples of heterometallic and heteroleptic size-interconvertible ring system constructed

from the gold(I) metalloligands with mixed D-pen and dppm are demonstrated. Interestingly, the expansion/contraction reactions of the metallorings were caused by external stimuli, leading to physical property changes depending on the incorporated secondary metal ions.

The coordination behavior of $[\mathbf{3}]^{2-}$ as well as a trigold(I) metalloligand, $[Au^{I}_{3}(dppm)_2(D\text{-pen})_2]^{-}$ ($[\mathbf{4}]^{-}$), was investigated for two 3d transition metal ions, nickel(II) and zinc(II), leading to heterometallic $Au^{I}_{2}Ni^{II}$, $Au^{I}_{2}Zn^{II}$, $Au^{I}_{3}Ni^{II}$, and $Au^{I}_{3}Zn^{II}$ complexes. In addition, all the digold-/trigold-structural pairs including the free metalloligands exhibited structural expansion/contraction reactions by insertion/removal of $\{Au^{I}(dppm)\}^{+}$ extension agent. For the Au^{I}-Ni^{II} complexes, the structural conversion reaction was monitored by the electronic absorption and circular dichroism (CD) spectroscopy. In addition, structural conversions triggered by acid/base as well as oxidation/reduction are also explained on the basis of ligand field affected by the difference of the gold(I)-phosphine backbone. For the Au^{I}-Zn^{II} complexes, the structural conversion reaction was monitored in detail by NMR spectroscopy, which revealed its solvent-dependence. In addition, difference in the photophysical property depending on the difference of gold(I)-phosphine backbone between luminescent Au^{I}-Zn^{II} complexes is discussed together with the parental Au^{I} complexes.

II-2. Experimental section.

II-2-1. Materials. Gold(I) complexes, $NH_4[Au(D\text{-Hpen})_2]$,[3a] $[Au_2(dppm)Cl_2]$,[7] $[Au_2(dppm)_2]Cl_2$,[8] and [Au(tht)Cl] (tht = tetrahydrothiophene),[9] were prepared according to literature methods. All other chemicals were commercially available and used without further purification.

II-2-2. Synthesis of Au^{I} metalloligands with dppm.

(a) $[Au^{I}_{2}(dppm)(D\text{-Hpen})_2]$ ($[H_23]$). To a white suspension containing 1.02 g (1.20 mmol) of $[Au_2(dppm)Cl_2]$ in 40 mL of ethanol was added 0.39 g (2.63 mmol) of D-H_2pen. The mixture was stirred at room temperature for 2 h, which gave a colorless solution. After addition of 26.3 mL (2.63 mmol) of a 0.1 M NaOH ethanolic solution, the colorless solution was evaporated to dryness. The resulting pale yellow residue was suspended in 20 mL of water to remove NaCl. Then, the remaining pale yellow powder was collected by filtration and washed with 10 mL of water three times. Yield: 1.20 g (85%). Anal. Found: C, 36.06; H, 4.37; N, 2.57%. Calcd for $[\{Au_2(dppm)\}(D\text{-Hpen})_2]\cdot 5H_2O = C_{35}H_{52}N_2O_9P_2S_2Au_2$: C, 36.09; H, 4.50; N, 2.40%. IR spectrum (cm^{-1}, KBr disk): 1627 (ν_{COO}), 1437 (ν_{Ph}), 1101 and 781-691 (ν_{P-Ph}). ^{1}H NMR spectrum (ppm from TMS, methanol-d_4): δ 1.43 (s, 6H), 1.76 (s, 6H), 3.57 (s, 2H), 4.21 (t, J = 12.0 Hz, 2H), 7.35 - 7.45 (m, 12H), 7.68 - 7.74 (m, 8H). ^{31}P NMR spectrum (ppm from 85 % H_3PO_4, methanol-d_4): δ 32.0 (s).

(b) $[Au^{I}_{3}(dppm)_2(D\text{-}H_{0.5}pen)_2]$ ([H4]). To a colorless solution containing 1.00 g (1.30

mmol) of dppm in 25 mL of dichloromethane was added 0.63 g (1.95 mmol) of [Au(tht)Cl]. The mixture was stirred at room temperature in the dark, and 0.20 g (1.31 mmol) of D-H_2pen suspended in 8 mL of ethanol was added to the mixture. After additional 1 hour of stirring, 20 mL (2.0 mmol) of a 0.1 M NaOH ethanolic solution was added to the resulting pale yellow solution to give a yellow suspension. The yellow suspension was evaporated to dryness, and the resulting yellow residue was dissolved in 16 mL of methanol. After addition of 26 mL of water, the yellow solution was stood at room temperature for 5 weeks, which gave pale yellow crystals. Yield: 1.14 g (95%). Anal. Found: C, 39.05; H, 4.45; N, 1.56%. Calcd for $[Au_3(dppm)_2(D\text{-}H_{0.5}pen)]\cdot 10H_2O$ = $C_{60}H_{83}N_2O_{14}P_4S_2Au_3$: C, 39.27; H, 4.56; N, 1.53%. IR spectrum (cm^{-1}, KBr disk): 1619 (ν_{COO}), 1436 (ν_{Ph}), 1101 and 782-690 (ν_{P-Ph}). ^{1}H NMR spectrum (ppm from TMS, methanol-d_4): δ 1.17 (s, 6H), 1.32 (s, 6H), 3.28 (s, 2H), 7.1-7.9 (broad, 40H). ^{31}P NMR spectrum (ppm from H_3PO_4, methanol-d_4): δ 34.5 (s).

II-2-3. Reactions of [$H_2$3] with metal ions.

(a) Synthesis of [$Ni^{II}\{Au^{I}_2$(dppm)(D-pen)$_2$}] ([5a]). To a colorless solution containing 0.27 g (0.23 mmol) of [H_2**3**]·5H_2O in 12 mL of ethanol were added 2.4 mL (0.24 mmol) of a 0.1 M $NiCl_2\cdot 6H_2O$ ethanolic solution and 4.8 mL (0.48 mmol) of a 0.1 M NaOH aqueous solution, which gave a green solution immediately. The mixture was evaporated to dryness, and then the green residue was dissolved in 30 mL of water/ethanol (1:1). The green solution was allowed to stand at room temperature for 4 weeks, which gave green block crystals. Yield: 0.25 g (81%). Anal. Found: C, 33.88; H, 4.43; N, 2.15%. Calcd for $[Ni\{Au_2(dppm)(D\text{-}pen)_2\}]\cdot 7H_2O\cdot 0.5EtOH$ = $C_{36}H_{57}N_2O_{11.5}P_2S_2NiAu_2$: C, 33.77; H, 4.49; N, 2.19%. IR spectrum (cm^{-1}, KBr disk): 1596 (ν_{COO}), 1436 (ν_{Ph}), 1102 and 781-690 (ν_{P-Ph}). ESI-MS (in ethanol) *m*/*z*: 1153.08 ({Na[**5a**]}$^+$, 100%), 588.03 ({Na_2[**5a**]}$^{2+}$, 5.8%).

(b) Synthesis of [$Zn^{II}\{Au^{I}_2$(dppm)(D-pen)$_2$}] ([5b]). To a colorless solution containing 0.30 g (0.24 mmol) of [H_2**3**]·5H_2O in 10 mL of ethanol was added 2.6 mL (0.26 mmol) of a 0.1 M $ZnCl_2$ ethanolic solution and 5.2 mL (0.52 mmol) of a 0.1 M NaOH aqueous solution, which gave a colorless solution. After addition of 10 mL of water, the resulting solution was stood at room temperature for 5 weeks, which gave colorless block crystals. Yield: 0.27 g (84%). Anal. Found: C, 33.35; H, 4.24; N, 2.28%. Calcd for $[Zn\{Au_2(dppm)(D\text{-}pen)_2\}]\cdot 7H_2O$ = $C_{35}H_{54}N_2O_{11}P_2S_2ZnAu_2$: C, 33.25; H, 4.31; N, 2.22%. IR spectrum (cm^{-1}, KBr disk): 1592 (ν_{COO}), 1436 (ν_{Ph}), 1101 and 776-691 (ν_{P-Ph}). ^{1}H NMR spectrum (ppm from TMS, methanol-d_4): δ 1.47 (s, 6H), 1.55 (s, 6H), 3.40 (s, 2H), 4.21 (t, 0.1H), 7.32 - 7.35 (m, 8H), 7.40 (t, 4H), 7.63 - 7.72 (m, 8H). ^{31}P NMR spectrum (ppm from H_3PO_4, methanol-d_4): δ 32.4 (s). ESI-MS (in ethanol) *m*/*z*: 1137.04 ({H[**5b**]}$^+$, 100%), 1159.02 ({Na[**5a**]}$^+$, 69.7%).

(c) Synthesis of [$Ni^{II}\{Au^{I}_2$(dppm)(D-$H_{0.75}$pen)$_2$}](Et$_4$N)$_{0.5}Cl_2$ ([$H_{1.5}$5a'](Et$_4$N)$_{0.5}Cl_2$). To a white suspension containing 0.50 g (0.43 mmol) of [H_2**3**]·5H_2O in 10 mL of ethanol was added 4.9 mL (0.49 mmol) of a 0.1 M $NiCl_2\cdot 6H_2O$ ethanolic solution, which gave a red

solution after sonication for a few minutes. To the resulting red solution was added 5.0 mL (5.0 mmol) of 1 M Et_4NCl ethanolic solution, and the mixture was stood at room temperature in the dark for 4 weeks, which gave red platelet crystals. Yield: 0.31 g (56%). Anal. Found: C, 35.47; H, 4.35; N, 2.86%. Calcd for $[Ni\{Au_2(dppm)(D\text{-}H_{0.75}pen)_2\}](Et_4N)_{0.5}Cl_2\cdot 2.5H_2O$ = $C_{39}H_{56.5}N_{2.5}O_{6.5}P_2S_2Cl_2NiAu_2$: C, 35.65; H, 4.33; N, 2.66%. IR spectrum (cm^{-1}, KBr disk): 1728 and 1716 (ν_{CO}), 1437 (ν_{Ph}), 1103 and 788-688 ($\nu_{P\text{-}Ph}$).

II-2-4. Reactions of [H4] with metal ions.

(a) Synthesis of [$Ni^{II}\{Au^{I}_3(dppm)_2(D\text{-}pen)_2\}$]Cl ([6a]Cl). To a yellow solution containing 0.50 g (0.27 mmol) of [H**4**]·$10H_2O$ in 5 mL of ethanol were added 2.8 mL (0.28 mmol) of a 0.1 M $NiCl_2$ ethanolic solution and 2.7 mL (0.27 mmol) of a 0.1 M NaOH aqueous solution, which gave a yellow-green solution. After the addition of 50 mL of water and 0.11 mL (0.55 mmol) of a 5 M NaCl aqueous solution, the reaction mixture was stood at room temperature in the dark. After 17 days, the resulting yellow-green needle-like crystals were collected by filtration. Yield: 0.52 g (93%). Anal. Found: C, 35.13; H, 4.58; N, 1.35%. Calcd for $[Ni\{Au_3(dppm)_2(D\text{-}pen)_2\}]Cl\cdot 17H_2O$ = $C_{60}H_{96}N_2O_{21}P_4S_2ClNiAu_3$: C, 35.08; H, 4.71; N, 1.36%. IR spectrum (cm^{-1}, KBr disk): 1599 (ν_{COO}), 1436 (ν_{Ph}), 1101 and 785-690 (ν_{P-Ph}). ESI-MS (in ethanol) *m*/*z*: 1711.20 ([**6a**]$^+$, 100%), 867.08 ({Na[**6a**]}$^{2+}$, 17.2%).

(b) Synthesis of [$Zn^{II}\{Au^{I}_3(dppm)_2(D\text{-}pen)_2\}$]Cl ([6b]Cl). To a yellow solution containing 0.30 g (0.16 mmol) of [H**4**]·$10H_2O$ in 3 mL of ethanol were added 4 mL of water, 1.7 mL (0.17 mmol) of a 0.1 M $ZnCl_2$ ethanolic solution, and 1.6 mL (0.16 mmol) of a 0.1 M NaOH aqueous solution, which gave a pale yellow solution. The addition of 25 mL of water and 1.6 mL (82 mmol) of a 5 M NaCl aqueous solution to this solution gave a white suspension, which turned to an almost clear solution by adding 3 mL of ethanol. After 4 days, a small amount of white powder was precipitated. The white powder was removed by filtration through Celite, and the filtrate was stood at room temperature in the dark. After 1 month, the resulting colorless needle-like crystals were collected by filtration. Yield: 0.28 g (85%). Anal. Found: C, 35.76; H, 4.66; N, 1.40%. Calcd for $[Zn\{Au_3(dppm)_2(D\text{-}pen)_2\}]Cl\cdot 14.5H_2O$ = $C_{60}H_{91}N_2O_{18.5}P_4S_2ClZnAu_3$: C, 35.74; H, 4.55; N, 1.39%. IR spectrum (cm^{-1}, KBr disk): 1612 (ν_{COO}), 1436 (ν_{Ph}), 1102 and 784-691 (ν_{P-Ph}). ^1H NMR spectrum (ppm from TMS, methanol-d_4): δ 1.27 (s, 6H), 1.37 (s, 6H), 1.47 (s, 2.5H), 1.55 (s, 2.5H), 3.37 (s, 2H), 3.40 (s, 0.8H), 7.06 (s, 4H), 7.21 (s, 4H), 7.31 - 7.83 (m, 42H), 7.99 (s, 4H), 8.09 (s, 4H). ^{31}P NMR spectrum (ppm from H_3PO_4, methanol-d_4): δ 32.4 (s, 0.4P), 33.1 (d, 1P), 33.7 (s, 0.4P), 34.8 (s, 1P). ESI-MS (in ethanol) *m*/*z*: 1717.12 ([**6b**]$^+$).

II-2-5. Structural conversion.

(a) Conversion from [$H_2$3] to [H4]. To a colorless solution containing 0.10 g (0.087 mmol) of [H_2**3**]·$5H_2O$ in 4 mL of methanol was added 0.06 g (0.05 mmol) of $[Au_2(dppm)_2]Cl_2$,

followed by the addition of 0.9 mL (0.09 mmol) of a 0.1 M NaOH aqueous solution, which gave a bright yellow solution, by way of a pale yellow solution. After the addition of 5 mL of water, the yellow solution was stood at room temperature for 3 days, which gave pale yellow crystals of [H**4**]·10H_2O. Yield: 0.10 g (63%). Reaction monitoring by NMR measurement was also carried out as follows. To a pale yellow solution containing 13 mg (11 μmol) of [H_2**3**]·5H_2O in 0.6 mL of methanol-d_4 was added 7 mg (5 μmol) of [Au^I_2(dppm)$_2$]Cl_2, which gave a bright yellow solution. The ^{1}H NMR spectrum of this solution was consistent with that of [H**4**] in methanol-d_4.

(b) Conversion from [H4] to [$H_2$3]. To a bright yellow solution containing 17 mg (9.0 μmol) of [H**4**]·10H_2O in 0.6 mL of methanol-*d*4 was added 5.5 mg (9.5 μmol) of NH_4[Au(D-Hpen)$_2$]·3.5H_2O, which gave a pale yellow solution. The ^{1}H NMR spectrum of this solution was consistent with that of [H_2**3**] in methanol-d_4.

(c) Conversion from [5a] to [6a]$^+$. To a green solution containing 0.11 g (0.089 mmol) of [**5a**]·7H_2O·0.5EtOH in 1 mL of ethanol was added 0.056 g (0.046 mmol) of [Au_2(dppm)$_2$]Cl_2, which gave a yellow-green solution immediately. To the resulting yellow-green solution was added 18 mL of water, followed by the addition of 0.071 mL (0.36 mmol) of a 5 M NaCl aqueous solution. The mixture was allowed to stand at room temperature for 1 week, and the resulting yellow-green needle-like crystals of [**6a**]Cl were collected by filtration. Yield: 0.15 g (81%).

(d) Conversion from [6a]$^+$ to [5a]. To a solution containing 0.030 g (0.015 mmol) of [**6a**]Cl·17H_2O in 3 mL of ethanol was added 0.0085 g (0.015 mmol) of NH_4[Au(D-Hpen)$_2$]·3.5H_2O and 0.6 mL (0.06 mmol) of a 0.1 M ethanolic NaOH solution. After the mixture was stirred at room temperature for a few minutes, 0.15 mL (0.015 mmol) of a 0.1 M ethanolic $NiCl_2$ solution was added to it, which quickly gave a green solution. The absorption and CD spectra of this solution were identical with those of [**5a**]. To the solution was added 2 mL of water, and the mixture was allowed to stand at room temperature for 18 days. The resulting green crystals of [**5a**] were collected by filtration. Yield: 0.031 g (83%).

(e) Conversion from [5b] to [6b]. To a colorless solution containing 0.10 g (0.08 mmol) of [**5b**]·7H_2O in 3 mL of ethanol was added 0.05 g (0.04 mmol) of [Au_2(dppm)$_2$]Cl_2, which gave a pale yellow solution. The addition of 15 mL of water and 0.80 mL (4.0 mmol) of a 5 M NaCl aqueous solution gave a white suspension, which turned to an almost clear solution by adding 1 mL of ethanol. After filtration, the resulting solution was stood at room temperature in the dark. After 6 weeks, the resulting colorless needle-like crystals of [**6b**]Cl were collected by filtration. Yield: 0.13 g (79%).

(f) Conversion from [6b]$^+$ to [5b]. To a solution containing 0.050 g (0.025 mmol) of [**6b**]Cl·14.5H_2O in 3 mL of ethanol were added 0.015 g (0.025 mmol) of NH_4[Au(D-Hpen)$_2$]·3.5H_2O and 1 mL (0.1 mmol) of a 0.1 M ethanolic NaOH solution. After the mixture was stirred at room temperature for a few minutes, 0.25 mL (0.025 mmol) of a 0.1

M ethanolic $ZnCl_2$ solution was added to it. The colorless reaction solution was evaporated to dryness, and the white residue, which showed a ^{1}H NMR spectrum (methanol-d_4) essentially the same as that of [**5b**], were recrystallized from 3 mL of ethanol/water (1:1) to give colorless crystals of [**5b**]. Yield: 0.034 mg (54%).

(g) Interconversion between [5a] and [H$_n$5a']$^{n+}$. To a green solution containing 0.050 g (0.039 mmol) of [**5a**]·7H_2O·0.5EtOH in 3 mL of ethanol was added 80 μL (0.080 mmol) of a 1.0 M ethanolic CF_3SO_3H solution, which gave a red solution immediately. Its absorption and CD spectral features were quite similar to the reflection and CD spectra of [$H_{1.5}$**5a'**]$(Et_4N)_{0.5}Cl_2$ in the solid state, respectively. Treatment of the resulting red solution with excess K_2CO_3 gave an initial green solution, whose absorption and CD spectra are essentially the same as those of [**5a**].

When HCl was used instead of CF_3SO_3H, the red crystals of [$H_{1.5}$**5a'**]$(Et_4N)_{0.5}Cl_2$ was isolated as a following procedure. To a green solution containing 0.100 g (0.078 mmol) of [**5a**]·7H_2O·0.5EtOH in 3 mL of ethanol was added 160 μL (0.080 mmol) of a 1.0 M HCl solution prepared by mixing 12 M HCl aqueous solution and ethanol in 1:11 volume ratio, which gave a red solution immediately. To the resulting red solution was added 0.130 g (0.782 mmol) of Et_4NCl, and the mixture was stood at room temperature in the dark for 3 weeks, which gave red platelet crystals of [$H_{1.5}$**5a'**]$(Et_4N)_{0.5}Cl_2$. Yield: 0.066 g (64%).

(h) Interconversion between [6a]$^+$ and [H$_n$5a']$^{n+}$. To a yellow-green solution containing 0.080 g (0.039 mmol) of [**6a**]Cl·17H_2O in 3 mL of ethanol was added 80 μL (0.080 mmol) of a 1.0 M ethanolic CF_3SO_3H solution, which gave a red solution immediately. The absorption and CD spectra of this solution were very similar to those of the reaction solution of [**5a**] treated with CF_3SO_3H. Treatment of the resulting red solution with excess K_2CO_3 gave an initial yellow-green solution, whose absorption and CD spectra are essentially the same as those of [**6a**]Cl.

II-2-6. Physical measurements. The electronic absorption spectra were recorded on a JASCO V570 or V-660 spectrophotometer at room temperature. The CD spectra were recorded on JASCO J-600 or J-820 spectropolarimeter at room temperature. The IR spectra were recorded on a JASCO FT/IR-4100 spectrometer using KBr disks at room temperature. The ^{1}H and ^{31}P NMR spectra were measured on a JEOL ECA-500 NMR spectrometer using tetramethylsilane (TMS, δ 0.0 ppm) as the internal standard for ^{1}H NMR and triphenyl phosphate (δ –17.6 ppm) as the external standard for ^{31}P NMR. The X-ray fluorescence spectrometries were performed on a HORIBA MESA-500 or SHIMADZU EDX-720 spectrometer. The elemental analyses (C, H, N) were performed using YANACO CHN coder MT-5 or MT-6. The electrospray ionization mass spectra (ESI-MS) were measured on a QSTAR Elite LC/MS/MS system in ethanol. Cyclic voltammetric studies were performed with a BAS CV-600A apparatus by using glassy-carbon working electrode (3 mmϕ), an

Ag/AgCl (3 M NaCl aq.) reference electrode with a salt bridge (0.1 M Bu_4NPF_6 in methanol), and a Pt wire auxiliary electrode. Electrochemical experiments were conducted at room temperature in a methanolic solution of 0.1 M Bu_4NPF_6. The potential of ferrocenium/ferrocene (Fc^+/Fc) couple was + 0.40 V (*v.s.* Ag/AgCl) under this condition. The solid-state luminescence spectra were recorded on a JASCO FP-6600 spectrometer at room temperature and at 77 K with liquid nitrogen. The emission quantum yields (Φ) were measured with a lab-made absolute emission quantum yield measuring system using an integrating sphere (6 inch, Labsphere Inc.) of which the internal surface was coated with highly reflective Spectralon. A sample powder in a flat quartz cell (10 mm diameter, 1 mm height) placed at the bottom of the integrating sphere was excited with a monochromated light (355 – 365 nm) introduced from the top of the integrating sphere through a liquid light guide (deep UV model, Newport Co.). The emission from a detection exit of the integrating sphere was focused into a grating spectromator (Triax 1900, Jobin Yvon) equipped with a CCD image sensor (S7031, Hamamatsu). The absolute quantum yield of emission was calculated according to the method described in the literature.[10] The emission lifetimes were determined using the measuring system previously reported.[11] The sample was photo-excited using the third harmonic of a Q-switched Nd^{3+}:YAG laser (Continuum Surelite I-10, λ = 355 nm). The observed decay profile of the emission intensity was fit to two or three exponential functions with convolution of the instrumental response function of the measuring system.

II-2-7. X-ray structural determinations. Single-crystal X-ray diffraction measurements for [H**4**]·10H_2O, [**5a**]·7H_2O·0.5EtOH, [**5b**]·7H_2O·0.5EtOH, [$H_{1.5}$**5a'**]($Et_4N)_{0.5}Cl_2$·1.5H_2O·EtOH, [**6a**]Cl·17H_2O, and [**6b**]Cl·17H_2O were made on a Rigaku RAXIS-RAPID imaging plate diffractometer with graphite-monochromated Mo-Kα radiation at –73°C. The intensity data were collected by the ω scan mode, and were corrected for Lorentz and polarization. Empirical absorption corrections were also applied.

The structure was solved by the direct method with SIR97 [12] or SHELXS-97 [13] All calculations were performed using the Yadokari-XG software package [14] except for refinement, which was performed using SHELXL-97.[13] Hydrogen atoms except those of a part of solvation molecules and on N atoms in [H**4**]·10H_2O were placed at calculated positions but were not refined. All non-hydrogen atoms except those in a part of solvation molecules and disordered chloride anions were refined anisotropically. Crystal data and selected bond distances and angles are summarized in Tables II-1 – II-8.

II-3. Results and discussion.

II-3-1. Synthesis, characterization, and structural conversion reaction of complexes.

(a) Au^I complexes ([H_2**3**], [H**4**]).

Synthesis and characterization of [$H_2$3]. The digold(I) metalloligand with dppm, [Au^I_2(dppm)(D-Hpen)$_2$] ([H_2**3**]), was also prepared from its corresponding chlorido precursor [Au^I_2(dppm)Cl_2],[7] in analogy to [H**1**] in Chapter I. The reaction of [Au^I_2(dppm)Cl_2] with 2 molar equiv of D-H_2pen in ethanol, followed by the addition of NaOH, gave a colorless solution, from which [H_2**3**] was isolated as a white powder (Scheme II-1). The elemental analytical data of [H_2**3**] were in agreement with the formula of [Au_2(dppm)(D-Hpen)$_2$]·5H_2O, and the presence of Au atom was confirmed by X-ray fluorescence spectrometry. The ^{1}H and ^{31}P NMR spectra of [H_2**3**] in methanol-d_4 gave signals corresponding to a half of [H_2**3**], thus the C_2-symmetrical structure expected for [H_2**3**] was confirmed. As shown in Figure II-1, the ^{1}H NMR spectrum exhibits three singlet signals at δ 1.43, 1.76 and 3.57 ppm attributed to two diastereotopic methyl groups and a methine group in D-pen, respectively, and a signal at δ 4.21 from a methylene group of dppm, which is split to triplet due to the spin coupling with two ^{31}P nuclei ($^2J_{H–P}$ = 12 Hz), and some multiplet signals in the region of δ 7.68 - 7.74 and 7.35 - 7.45 derived from phenyl groups of dppm. The ^{31}P NMR spectrum shows a singlet signal at δ 32.0 (Figure II-2). In the IR spectrum, [H_2**3**] gave a strong ν_{COO} band at 1627 cm^{-1}, indicative of the presence of deprotonated carboxyl groups (Figure II-3).[15] Thus, D-$Hpen^-$ is also assumed to exist in a zwitter ionic form like the other D-penicillaminato gold(I) metalloligands [2a,d,3a] and free D-H_2pen.[16]

Synthesis and characterization of [H4]. Despite the analytically enough purity of isolated [H_2**3**], a single set of minor signals was observed with a very small intensity (< 3% as compared to [H_2**3**] on the basis of integral intensities of signals derived from methyl group) in the ^{1}H NMR spectrum of [H_2**3**], which implied the possibility that [H_2**3**] is partially converted to another species. The minor species was initially discovered as a metalloligand in a $Au^I_3Ni^{II}$ complex described below and surely assigned to a trigold(I) complex with {Au^I_3(dppm)$_2$}$^{2+}$ backbone by isolation of the second metal-free metalloligand, [Au^I_3(dppm)$_2$(D-$H_{0.5}$pen)$_2$] ([H**4**]). It has been known that the combination of Au^I, dppm, and chloride also produces a trigold(I) complex, [Au^I_3(dppm)$_2Cl_2$]$^+$, other than [Au^I_2(dppm)Cl_2] employed as the precursor of [H**3**], and interconversion between them has been reported.[17] The trigold(I) metalloligand [H**4**] was synthesized from the reaction of [$Au^I_3Cl_2$(dppm)$_2$]$^+$, prepared *in situ* from [Au^I(tht)Cl] (tht = tetrahydrothiophene) and dppm,[9,17a] with D-H_2pen in a 1:2 ratio, and isolated as pale yellow crystals (Scheme II-1). The elemental analytical data of [H**4**] were in agreement with the formula of [Au_3(dppm)$_2$(D-$H_{0.5}$pen)$_2$]·10H_2O, and the presence of Au atom was confirmed by X-ray fluorescence spectrometry. The ^{1}H NMR spectrum of [H**4**] in

methanol-d_4 gave two methyl and a methine singlet signals due to D-pen (δ 1.17, 1.32, and 3.28 ppm) and strongly broadened signals due to dppm in aromatic region (δ 7.1 - 7.9 ppm) in an integral intensity ratio of 3:3:1:20, consistent with the presence of D-pen and dppm in a 1:1 ratio in the complex (Figure II-1). As shown in Figure II-3, the IR spectrum of [H**4**] also exhibited a strong band assignable to an asymmetric COO stretching mode at 1619 cm^{-1}.

The crystal structure of [H**4**] was determined by single-crystal X-ray crystallography, which revealed the presence of two trigold complex molecules and some hydration water molecules in the unit cell (Figure II-4). The two complex molecules have similar structures. Each trigold complex has two terminal Au^I ions coordinated to P and S atoms in a linear geometry (av. Au–P = 2.273(12) Å, Au–S = 2.288(7) Å, P–Au–S = 176.8(7)°) and a central Au^I ion coordinated to two P atoms in a distorted linear geometry (av. Au–P = 2.318(7) Å, P–Au–P = 155.3(8)°). Furthermore, each complex exhibits Au···Au contacts indicating aurophilic interaction between the terminal and the central Au^I ions (av. $Au_{terminal}\cdots Au_{central}$ = 3.03(2) Å). Those two complex molecules both adopt a quite similar conformation with a bent Au_3 arrangement (av. $Au_{terminal}\cdots Au_{central}\cdots Au_{terminal}$ = 75.51(5)°), but their bending directions are opposite. Regarding the central Au^I ion as a distorted tetrahedral geometry linked to two P atoms and two terminal Au^I ions, one of the complex molecules has an *R*-configured Au^I ion (Au2) and the other has an *S*-configured one (Au5) based on the Cahn–Ingold–Prelog priority rules.[18] The diastereomeric conformers based on two chiral centers of the central Au^I ion and D-pen with *S*-configured α-carbon hold each other's "hands" via $NH_3^+\cdots NH_2$ hydrogen bonds to form a dimer in the crystal as shown in Figure II-5 (av. N···N = 2.81(9) Å). While the X-ray crystallography could not confirm which amino group has an additional H^+ involved in the hydrogen bonding, the hydrogen-bonding mode suggests the electrically neutral form of each trigold complex, in agreement with the formula of [H**4**] from the analytical data.

The strongly broadened ^{1}H NMR signals from phenyl groups, together with ^{31}P NMR spectrum showing only a broad signal at δ 34.5 ppm in spite of two different ^{31}P nuclei in one complex molecule [H**4**] (Figure II-2), can be attributed to the inversion of the bending conformation of the $\{Au^I_3(dppm)_2\}^{3+}$ backbone. The inversion of the conformation may occur quickly in solution at room temperature through an intermediate state with a perfectly linear central Au^I ion, which would cause strong broadening of the ^{1}H NMR signals from the phenyl groups. The ^{1}H resonance of phenyl groups split into several sharp signals when the solution was cooled, and the ^{1}H NMR spectrum measured at –40°C, which shows seven sharp aromatic signals from the phenyl groups and three aliphatic signals from D-pen, indicates that only one conformer among those found in the crystal structure exists at low temperature (Figure II-6).

Other properties and structural conversion. Solubility of [H_2**3**] and [H**4**] are also almost the same as that of [H**1**], which was very soluble in alcohols but almost insoluble in water. The digold(I) metalloligand [H_2**3**] is also luminescent but its brightness is somehow

weaker than that of [H**1**], and the trigold(I) metalloligand [H**4**] is almost non-emissive in the solid state at ambient temperature, while both are highly emissive at 77 K. The luminescent properties are discussed in detail below together with those of Au^{I}-Zn^{II} complexes derived from these metalloligands.

The interconversion of gold(I)-dppm backbone between D-penicillaminato derivatives [H_2**3**] and [H**4**] was examined in the wake of the method reported for their chlorido precursors. The reaction of [H_2**3**] with 0.5 molar equiv of $[Au^{I}_2(dppm)_2]Cl_2$ [8] in methanol-d_4 followed by the addition of NaOH caused a change in the solution color from pale yellow to bright yellow, and the ^{1}H NMR spectral features of the bright yellow reaction solution were essentially the same as those of [**4**]$^-$ (Figure II-1). On the other hand, the reaction of [H**4**] with 1 molar equiv of NH_4[Au(D-Hpen)$_2$] [3a] in methanol-d_4 gave a pale yellow solution, the ^{1}H NMR spectral features of which were the same as those of [**3**]$^{2-}$ (Figure II-1). Thus, it was confirmed that [**3**]$^{2-}$ and [**4**]$^-$ are interconvertible with each other, accompanied by the insertion/removal of a $\{Au^{I}(dppm)\}^+$ extension linker supplied from $[Au^{I}_2(dppm)_2]^{2+}$ (Scheme II-1).

(b) Au^{I}-Ni^{II} complexes ([5a], $[H_{1.5}5a'](Et_4N)_{0.5}Cl_2$, [6a]Cl).

Synthesis and characterization of [5a]. First, the reaction of [H_2**3**] with Ni^{II} ion was examined in order to elucidate the coordination ability of [**3**]$^{2-}$ designed as a hexadentate chelating metalloligand. Treatment of [H_2**3**] with 1 molar equiv of $Ni^{II}Cl_2\cdot 6H_2O$ in ethanol, followed by the addition of NaOH, gave a green solution, from which green crystals with a block-like shape ([**5a**]) were obtained. X-ray fluorescence spectrometry implied that [**5a**] contains Ni and Au atoms, and the elemental analytical data of [**5a**] were in agreement with the formula of $[Ni\{Au_2(dppm)(D\text{-}pen)_2\}]\cdot 7H_2O\cdot 0.5EtOH$ (Scheme II-1).

The crystal structure of [**5a**] was determined by single-crystal X-ray crystallography, which revealed the presence of two independent, yet nearly the same complex molecules in the asymmetric unit, besides solvation water and ethanol molecules. As shown in Figure II-7, [**5a**] is a $Au^{I}_2Ni^{II}$ trinuclear complex in which [**3**]$^{2-}$ coordinate to a Ni^{II} ion with a hexadentate-N_2,O_2,S_2 mode with retaining the original metalloligand structure (av. Au–P = 2.2681(8) Å, Au–S = 2.3172(8) Å, P–Au–S = 174.52(3)°). As expected, there is a Au···Au contact that is shorter than twice the van der Waals radius of Au atom (1.66 Å), indicative of an aurophilic interaction between two Au^{I} ions in a molecule (av. Au···Au = 3.1346(2) Å). This attractive force should direct two D-pen moieties in the metalloligand to appropriate orientation to chelate a metal ion, as a result, [**3**]$^{2-}$ vises a Ni^{II} ion as a hexadentate chelating metalloligand to form a 8-membered $CAu_2NiP_2S_2$ metalloring structure. The coordination environment of the Ni^{II} center, which adopts a distorted $N_2O_2S_2$ octahedral geometry with a trans(O) configuration (av. Ni–N = 2.076(3) Å, Ni–O = 2.093(2) Å, Ni–S = 2.4267(8) Å, N–Ni–S = 175.54(8)°, O–Ni–O = 167.52(13)°), is essentially the same as that of [**2b**] (Scheme I-1 in Chapter I). A notable difference from [**2b**] is found on the absolute configurations of

two μ_2-bridging S atoms, each of which adopts *R* and *S* configurations to retain the intramolecular aurophilic interaction, thus, [**5a**] adopts non-symmetric (C_1) molecular structure containing the 8-membered metalloring with a twist-boat conformation in contrast to the C_2-symmetrical structure of [**2b**] expected on the basis of the crystal structure of [**2a**]ClO_4.

As shown in Figure II-9, the electronic absorption spectrum of [**5a**] in ethanol shows a broad near IR band at 1020 nm and a visible band at 589 nm assignable to $^3T_{2g}\leftarrow{}^3A_{2g}$ and $^3T_{1g}\leftarrow{}^3A_{2g}$ transitions, respectively. This spectral feature is similar to that of [**2b**] containing a *trans*(*O*)-{Ni(D-pen-*N*,*O*,*S*)$_2$}$^{2-}$ unit. On the other hand, the CD spectra of them are somewhat different. The visible band of [**5a**] clearly shows positive cotton effect peaked at 576 nm whereas the corresponding CD signal of [**2b**] is weakly negative, probably as a result of the difference in chiral configuration on S atoms.

Synthesis and characterization of [6a]Cl, and structural conversion by insertion/removal of extending agent. Inspired by the reported conversion reaction between [Au^I_2(dppm)Cl_2] and [Au^I_3(dppm)$_2Cl_2$]$^+$ through [Au^I_2(dppm)$_2$]$^{2+}$,[17] conversion from [**5a**] with {Au^I_2(dppm)}$^{2+}$ backbone to another Au^I-Ni^{II} complex with {Au^I_3(dppm)$_2$}$^{3+}$ was examined. A green ethanolic solution containing [**5a**] turned to a yellow-green solution by adding 0.5 molar equiv of [Au^I_2(dppm)$_2$]Cl_2, and yellow-green needle-like crystals of [**6a**]Cl were obtained from the reaction solution (Scheme II-1). The elemental analytical data of [**6a**]Cl were in agreement with the formula of [Ni{Au_3(dppm)$_2$(D-pen)$_2$}]Cl·17H_2O, and X-ray fluorescence spectrometric data were also consistent with 3:1 ratio of Au and Ni. The IR spectrum of [**6a**]Cl, which shows a ν_{COO} band at 1599 cm^{-1} and ν_{Ph} band at 1436 cm^{-1}, is quite similar to that of [**5a**] except the intensity ratio of the signals derived from D-pen and dppm (Figure II-3).

Single-crystal X-ray structural analysis for the yellow green crystal of [**6a**]Cl clearly showed the presence of complex cation, [Ni^{II}{Au^I_3(dppm)$_2$(D-pen)$_2$}$_2$]$^+$, and a chloride anion in a 1:1 ratio, besides some hydration water molecules. As shown Figure II-10, complex cation [**6a**]$^+$ has a 12-membered $C_2Au_3NiS_2P_4$ metalloring including a {Au^I_3(dppm)$_2$}$^{3+}$ backbone instead of {Au^I_2(dppm)}$^{2+}$ observed in [**5a**], while the coordination structure around Ni^{II} center is essentially the same as that of [**5a**] (Ni–N = 2.061(4) Å, Ni–O = 2.076(3) Å, Ni–S = 2.4624(15) Å, N–Ni–S = 177.48(13)°, O–Ni–O = 167.7(2)°). The shorter distance between Au^I ions in [**6a**]$^+$ than that in [**5a**] indicates the presence of stronger aurophilic interactions, which seems to sustain the larger metalloring structure of [**6a**]$^+$ ($Au_{terminal}\cdots Au_{central}$ = 2.9774(3) Å). The overall arrangement of trigold(I) metalloligand part, {Au^I_3(dppm)$_2$(D-pen)$_2$}$^-$, in [**6a**]$^+$ is very similar to that of the *S*-configured diastereo-conformer found in the crystal structure of [H**4**] ($Au_{central}$–P = 2.3347(12) Å, $Au_{terminal}$–P = 2.2737(14) Å, Au–S = 2.3262(13) Å, P–Au–S = 174.30(5)°, $Au_{terminal}\cdots Au_{central}\cdots Au_{terminal}$ = 88.827(10)°). Indeed, the same yellow-green crystals of [**6a**]Cl

was also obtained from the reaction of [H**4**] with Ni^{II} ion, therefore it has been confirmed that [**4**]$^{-}$ also functions as a hexadentate-N_2,O_2,S_2 chelating metalloligand toward an octahedral metal ion as to [**3**]$^{2-}$.

It is noteworthy that only one conformer of [H**4**] coordinated to nickel(II) ion to form the heterometallic $Au^{I}_3Ni^{II}$ complex [**6a**]$^{+}$. When a D-pen binds to a metal ion in a tridentate-N,O,S mode, 5-membered N,S chelate ring adopts the λ conformation so as to the coordination of carboxylate group. Then Au^{I} ion on S atom seems to select an equatorial orientation to lead to the *R* configuration of the S atom because of lesser steric crowding of it compared with the axial orientation with the *S* configuration. Thus the chirality of D-pen led the chiral conformation of the metalloligand [**4**]$^{-}$ to only the *S* conformer on chelation to an octahedral metal ion, while it is not enough to fix the chiral conformation of [H**4**] in the crystal as well as in the solution at room temperature. While the electronic absorption spectrum of [**6a**]Cl in ethanol, showing a near IR band at 1020 nm and a visible band at 593 nm assignable to $^{3}T_{2g}\leftarrow{}^{3}A_{2g}$ and $^{3}T_{1g}\leftarrow{}^{3}A_{2g}$ transitions from an octahedral nickel(II) center, respectively, is very similar to that of [**5a**], the CD spectrum of [**6a**]Cl is similar to [**5a**] in visible region and to [**2b**] at the long-wavelength edge (Figure II-9). This observation is consistent with the equilibrium behavior of [**6a**]$^{+}$ with R_2 configuration of bridging S atoms between [**5a**] with *R,S* configuration in alcohols, which is explained below in detail for Au^{I}-Zn^{II} complexes by NMR monitoring (Scheme II-2).

As described above, the reaction of [**5a**] having an 8-membered metalloring with $[Au^{I}_2(dppm)_2]Cl_2$ in a 2:1 ratio gave [**6a**]$^{+}$ having a 12-membered metalloring, that is, the 8-membered metalloring in [**5a**] was expanded to the 12-membered metalloring in [**6a**]$^{+}$ by the insertion of a $\{Au^{I}(dppm)\}^{+}$ extension linker generated from $[Au^{I}_2(dppm)_2]^{2+}$, accompanied by the change in chirality, though the coordination environment of the nickel(II) center was retained during the metalloring expansion process. Moreover, the addition of 1 molar equiv each of $NH_4[Au^{I}$(D-Hpen)$_2]$ and $Ni^{II}Cl_2\cdot6H_2O$ to a yellow-green ethanolic solution containing [**6a**]Cl, together with NaOH, gave a green solution. This solution showed electronic absorption and CD spectra corresponding to those of [**5a**], from which green crystals of [**5a**] were obtained. Therefore, the reverse conversion, namely the contraction of the 12-membered metalloring was also confirmed (Scheme II-1).

Synthesis and characterization of $[H_{1.5}$5a'$](Et_4N)_{0.5}Cl_2$, and structural conversion by acid/base. According to the method used for the PPh_3 system in Chapter I, the responsiveness of the Au^{I}-Ni^{II} complexes with dppm to acid was also examined. When 2 molar equiv of triflic acid (CF_3SO_3H) was added to the ethanolic solution of [**5a**], very similar behavior to the case of [**2b**] was observed (Scheme I-2 in Chapter I). The solution color changed from green to red, and the absorption and CD spectra of the resulting red solution ($[H_2$**5a'**$]^{2+}$) exhibited a relatively strong absorption band at 494 nm and positive CD signals at 543 and 427 nm and negative one at 483 nm, respectively, which are largely assignable to $^{1}B_{1g}\leftarrow{}^{1}A_{1g}$ transitions

from square-planer d^8 nickel(II) center (Figure II-12). In addition, the reversibility of this reaction was confirmed by adding base (K_2CO_3) to the red solution to reproduce the green solution showing the same spectra as those of [**5a**]. Therefore, the same type of the structural conversion on nickel(II) center from an octahedral *trans*(*O*)-$N_2O_2S_2$ geometry to a square-planar *cis*-N_2S_2 geometry was also expected for [**5a**] (Scheme II-3).

The red compound was successfully isolated as red platelet crystals of [$H_{1.5}$**5a'**]$(Et_4N)_{0.5}Cl_2$ from the reaction of the metalloligand [H_2**3**] with $Ni^{II}Cl_2$ or the treatment of [**5a**] with HCl as acid instead of triflic acid in ethanol followed by adding an excess amount of tetraethylammonium chloride (Et_4NCl) as illustrated in Scheme II-1. The elemental analytical data of [$H_{1.5}$**5a'**]$(Et_4N)_{0.5}Cl_2$ were in agreement with the formula of [Ni{Au_2(dppm)(D-$H_{0.75}$pen)$_2$}]$(Et_4N)_{0.5}Cl_2\cdot 2.5H_2O$, and X-ray fluorescence spectrometry also supported this formula. These results, together with the presence of a ν_{CO} stretching band at 1720 cm^{-1} in the IR spectrum indicative of the presence of COOH group (Figure II-3), strongly suggested that the red compound [$H_{1.5}$**5a'**]$(Et_4N)_{0.5}Cl_2$ is the $Au^I_2Ni^{II}$ trinuclear complex with a square-planar $\{Ni^{II}$(D-pen-*N*,*S*)$_2\}^{2-}$ moiety formed through geometrical conversion from [**5a**] induced by protonation of carboxylate groups.

The crystal structure of [$H_{1.5}$**5a'**]$(Et_4N)_{0.5}Cl_2$ was determined by single-crystal X-ray crystallography, which shows the presence of two $Au^I_2Ni^{II}$ trinuclear complex cations, $[Ni^{II}\{Au^I_2$(dppm)(D-$H_{0.75}$pen)$_2\}]^{1.5+}$, having essentially the same structure with a square-planar Ni^{II} ion coordinated by two N and two S atoms in a cis geometrical fashion. As shown Figure II-13, $[H_{1.5}$**5a'**$]^{1.5+}$ is a $Au^I_2Ni^{II}$ trinuclear complex where $[H_{1.5}$**3**$]^{0.5-}$ with partially protonated carboxy groups coordinate to a Ni^{II} ion in a tetradentate-N_2,S_2 mode to form an 8-membered $CAu_2NiP_2S_2$ metalloring with a twist-boat conformation, which is similar to that of [**5a**]. While the coordination bonds of Au^I ions in $[H_{1.5}$**5a'**$]^{1.5+}$ are similar to those of [**5a**] (av. Au–P = 2.272(2) Å, Au–S = 2.329(2) Å, P–Au–S = 175.03(7)°), Au···Au distance of $[H_{1.5}$**5a'**$]^{1.5+}$ becomes obviously shorter than that of [**5a**] (av. Au···Au = 2.9620 Å), probably because of the shorter S···S separation associated with contractions of coordination bonds of the four-coordinate Ni^{II} ion in $[H_{1.5}$**5a'**$]^{1.5+}$ as compared with octahedral one (av. Ni–N = 1.935(6) Å, Ni–S = 2.182(2) Å, N–Ni–S = 177.1(2)°). The carboxyl groups did not participate in the coordination due to the protonation, which was evidenced by the different C–O bond distances with the averaged longer C–O distance of 1.304(10) Å and the averaged shorter C–O distance of 1.209(10) Å. One of the two D-pen ligands in the complex cation forms a λ-conformational 5-membered chelate ring, and thus, the carboxyl group retains the axial orientation like in [**5a**], but does not coordinate to the Ni^{II} ion with the long Ni···O separations (Ni1···O2 = 2.975(6), Ni2···O6 = 3.136(6) Å). The other D-pen forms a δ-conformational chelate ring, whose carboxyl group is directed to an equatorial position to form an intermolecular hydrogen bond (O3···O7 = 2.582(11) Å). As a result, a dimeric structure is formed by sharing one proton between two carboxylate groups each from two

complex-cations (Figure II-14). The pseudo-meso structure of $[H_{1.5}\mathbf{5a'}]^{1.5+}$ with both δ- and λ-conformational N,S-chelate ring, which has not been found for $[Au^{I}_{2}\{Ni^{II}(\text{D-pen-}N,S)_2\}_2]^{2-}$,[3c,19] may be associated to the chiralities of S atoms with both *R* and *S* configurations due to the intramolecular aurophilic interaction supported by dppm discussed above for the crystals structure of [**5a**], which seems to be more effective in $[H_{1.5}\mathbf{5a'}]^{1.5+}$.

The treatment of [**6a**]Cl with acid was also examined. As shown in Figure II-15, however, the CD spectral feature of the solution was almost the same as that of $[H_2\mathbf{5a'}]^{2+}$, indicating that the protonation of the carboxylate groups in the tetranuclear $Au^{I}_{3}Ni^{II}$ complex $[\mathbf{6a}]^{+}$ causes the elimination of a $\{Au^{I}(\text{dppm})\}^{+}$ part as $[Au^{I}_{2}(\text{dppm})_2]^{2+}$ to form the protonated trinuclear $Au^{I}_{2}Ni^{II}$ complex $[H_2\mathbf{5a'}]^{2+}$ (Scheme II-3). The formation of a protonated tetranuclear $Au^{I}_{3}Ni^{II}$ species with a square-planar nickel(II) center was not observed, probably because of its instability explained as follows. If the carboxylate groups of $[\mathbf{6a}]^{+}$ was protonated, the resulting tetranuclear complex cation should have positive charge (+2 or +3) higher than the trinuclear species (+1 or +2), and the higher charged structure is commonly unstable particularly in organic solvents. Influences of structural factors are also considerable. It is assumed that the formation of a square-planar nickel(II) center prevents the reservation of the tetranuclear structure, because the shorter intramolecular S···S distances due to the shorter Ni–S bonds observed in the crystal structure of $[H_{1.5}\mathbf{5a'}](Et_4N)_{0.5}Cl_2$ may be unfavorable for the larger metalloring of the tetranuclear structure. In addition, the pseudo-meso structure with the λ- and δ-conformational N,S-chelate rings and the *R*- and *S*-configurational S atoms observed in the crystal structure of $[H_{1.5}\mathbf{5a'}](Et_4N)_{0.5}Cl_2$ may be unconformable to the tetranuclear complex, because the bent $\{Au^{I}_{3}(\text{dppm})_2\}^{3+}$ backbone leads to the C_2-symmetrical structure with only the λ and *R* chiralities. The red solution derived from [**6a**]Cl also turned back to a yellow-green solution by adding base (K_2CO_3), showing the same absorption and CD spectra as those of [**6a**]Cl. Therefore, the interesting acid/base-induced reversible ring-contraction that shows the changes in coordination structure, color, and magnetism, was observed (Scheme II-3).

Structural conversion by electric potentials. It was revealed by the cyclic voltammetry that the interconversion between $Au^{I}_{2}Ni^{II}$ trinuclear and $Au^{I}_{3}Ni^{II}$ tetranuclear structures is also controlled by oxidation state in addition to protonation. The cyclic voltammogram recorded for [**5a**] in methanol with Bu_4NPF_6 as a supporting electrolyte showed an electrochemically reversible pair of waves at $E_{1/2}$ = +0.60 V (*v.s.* Ag/AgCl) assignable to a Ni^{III}/Ni^{II} redox couple in [**5a**] (Figure II-16). On the other hand, the cyclic voltammogram recorded for [**6a**]Cl under the same condition showed another electrochemically reversible pair of waves at $E_{1/2}$ = +0.77 V with a relatively weak pair of signals at almost the same potential as that for [**5a**] (Figure I-16). The current ratio of the reduction waves at higher and lower potential varied depending on scan rates, while the ratio of oxidation waves was independent of scan

rates. When the voltammogram was recorded at the faster rate of 1.0 V/s, the reduction current for the high-potential signal was more intense than the other. When the voltammogram was recorded at the slower rate of 0.03 V/s, conversely, the reduction current for the high-potential signal was weaker than the other. Considering these observation together with the equilibrium between [**5a**] and [**6a**]$^+$ in the solution, the high-potential signal at $E_{1/2}$ = +0.77 V is assignable to a Ni^{III}/Ni^{II} redox couple in [**6a**]$^+$ and the low-potential signal around $E_{1/2}$ = +0.60 V should be derived from [**5a**] generated from the elimination of a $\{Au^{I}(dppm)\}^+$ part from [**6a**]$^+$. Moreover, the rate dependence of the reduction waves in the replicated negative scan, together with the reproducibility in a multiple scan measurement, suggests a square EC-EC process in the redox cycle shown in Scheme II-4. According to this result, the +III oxidation state of nickel is preferred in the trinuclear Au_2Ni structure rather than the tetranuclear Au_3Ni one, and the equilibrium between these two structures is shifted to the trinuclear side by oxidation of the nickel center. This trend is consistent with the hypothesis that the digold(I) metalloligand can provide the shorter coordination bonds and the stronger ligand field than the trigold(I) one, because nickel(III) complexes show shorter bond lengths than nickel(II) complexes in general.[20]

(c) Au^{I}-Zn^{II} complexes ([5b], [6b]Cl).

Synthesis and characterization of [5b]. In order to reveal the reaction behavior of the interconvertible metalloring structures in solution in detail, their zinc(II) analogues were also prepared, and their structural interconversion was monitored by NMR spectroscopy. Treatment of [H_2**3**] with 1 molar equiv of $Zn^{II}Cl_2$ in ethanol, followed by the addition of NaOH, gave a colorless solution, from which colorless crystals with a block-like shape ([**5b**]) were obtained. X-ray fluorescence spectrometry implied that [**5b**] contains Zn and Au atoms, and the elemental analytical data of [**5b**] were in agreement with the formula of $[Zn\{Au_2(dppm)(D\text{-}pen)_2\}]\cdot 7H_2O$ (Scheme II-1). From these analytical data together with the IR spectrum of [**5b**], which is essentially the same as that of [**5a**], it was concluded that complex [**5b**] has also the trinuclear structure quite similar to that of [**5a**] in analogy with the PPh_3 system in Chapter I (Figure II-3).

The structural similarity between [**5a**] and [**5b**] was further demonstrated by the X-ray structural analysis for the single-crystal of [**5b**]. Complex [**5b**] crystallizes in a monoclinic system with space group $P2_1$, which is the same as that of [**5a**], meaning that their structures are isomorphs. There are two independent, yet nearly the same $Au^{I}_2Zn^{II}$ trinuclear complex molecules, where an 8-membered $CAu_2P_2S_2Zn$ metalloring is formed by chelation of the metalloligand [**3**]$^{2-}$ to a Zn^{II} ion (Figure II-17). The coordination bond lengths around the Zn^{II} center in [**5a**] (av. Zn–N = 2.13(2) Å, Zn–O = 2.14(2) Å, Zn–S = 2.514(13) Å) are somewhat longer, and its geometry is more distorted from an ideal octahedron (av. N–Zn–S = 172(3)°, O–Zn–O = 163.3(13)°) compared with those of the Ni^{II} center in [**5a**]. The differences can be

reasonably explained by the weaker coordination due to the lack of LFSE (ligand field stabilization energy) of the Zn^{II} ion with filled 3d orbitals. In [**5b**], two Au^{I} ions are each coordinated to P and S atoms with a slightly distorted linear geometry (av. Au–P = 2.269(5) Å, Au–S = 2.315(4) Å, P–Au–S = 174.5(15)°), and the intramolecular Au···Au separation of 3.14(2) Å suggests the presence of aurophilic interactions, as found in [**5a**]. The two S atoms bridging the Au^{I} and Zn^{II} ions have *R* and *S* absolute configurations, such that the 8-membered metalloring adopts a twist boat conformation, leading to the C_1-symmetrical crystal structure of [**5a**]. In the crystal packing, hydrophilic parts containing $\{Zn^{II}(\text{D-pen})_2\}^{2-}$ moieties of the complex molecules and solvation molecules are aggregated to form a hydrophilic layer in the *ac*-plane through the formation of hydrogen bonds. On the other hand, hydrophobic parts consisting of the phenyl groups of the dppm ligands are also aggregated to form a hydrophobic layer. As a result, these layers are alternately stacked along the *b*-axis (Figure II-18). It is noteworthy that no other crystallographically determined structures consisting of chalcogen-bridged Au and Zn centers (Au–E–Zn) have been reported in the past.

Synthesis and characterization of [6b]Cl, and structural conversion by insertion/removal of extending agent. By imitating the metalloring expansion reaction of the Au^{I}-Ni^{II} complex [**5a**], the structural conversion from the $Au^{I}_2Zn^{II}$ trinuclear structure [**5b**] to the $Au^{I}_3Zn^{II}$ tetranuclear structure was examined. The reaction of [**5b**] with 0.5 molar equiv of $[Au^{I}_2(dppm)_2]Cl_2$ in ethanol gave a pale-yellow solution, from which colorless needle-like crystals of [**6b**]Cl were isolated. The elemental analytical data for [**6b**]Cl were in agreement with the formula of $[Zn\{Au_3(dppm)_2(\text{D-pen})_2\}]Cl\cdot 14.5H_2O$, and the X-ray fluorescence spectrometric data were also consistent with a 3:1 ratio of Au and Zn. In addition, the IR spectrum of [**6b**]Cl is essentially the same as that of [**5a**]Cl in whole region (Figure II-3). Therefore, it is strongly suggested that the structural conversion shown in Scheme II-1 from the $Au^{I}_2Zn^{II}$ trinuclear complex to the $Au^{I}_3Zn^{II}$ tetranuclear complex occurred, as in the case of Au^{I}-Ni^{II} complexes. Note that the same colorless crystals of [**6b**]Cl was also obtained from the reaction of [H**4**] with $Zn^{II}Cl_2$ together with NaOH (Scheme II-1).

The successful ring expansion reaction was confirmed by the X-ray structural analysis for a single crystal of [**6b**]Cl. The single-crystal X-ray analysis showed that [**6b**]Cl also crystallized in the orthorhombic space group $P2_12_12$, in a structure isomorphic to the corresponding Au^{I}-Ni^{II} complex, [**5a**]Cl. The existence of the $Au^{I}_3Zn^{II}$ complex cation in the crystal provided evidence of the structural expansion due to the insertion of the $\{Au^{I}(dppm)\}^{+}$ extension linker into the $\{Au^{I}_2(dppm)\}^{2+}$ backbone of the trinuclear complex [**5b**] (Figure II-19). Moreover, the 8-membered metalloring in [**5b**] has changed to a C_2-symmetrically skewed 12-membered $C_2Au_3S_2P_4Zn$ metalloring in $[\mathbf{6b}]^{+}$, which is sustained by the stronger aurophilic interactions compared to those in the 8-membered ring ($Au_{terminal}\cdots Au_{central}$ = 2.9929(3) Å). The coordination sphere of the Zn^{II} center in $[\mathbf{6b}]^{+}$ is strongly distorted from an ideal octahedron (Zn–N = 2.127(5) Å, Zn–O = 2.112(4) Å, Zn–S = 2.5603(15) Å, N–Zn–S =

174.33(14)°, O–Zn–O = 165.8(2)°), as found in [**5b**]. The structure including the two symmetrically related Au^{I} ions ($Au_{terinal}$) coordinated to P and S atoms in a linear geometry also has little difference from that in [**5b**], except for the chirality of one S atom, while a newly formed Au^{I} ion ($Au_{central}$) coordinated to two P atoms is significantly distorted from a linear structure because of the aurophilic interactions with the other two Au ions ($Au_{terminal}$–P = 2.2713(15) Å, $Au_{terminal}$–S = 2.3183(14) Å, P–$Au_{terminal}$–S = 174.99(5)°, $Au_{central}$–P = 2.3357(13) Å, P–$Au_{central}$–P = 162.53(7)°). In the crystal structure, the $\{Zn^{II}(D\text{-pen})_2\}^{2-}$ moieties of the complex cations are separated from each other because of the steric effects of the bulky $\{Au^{I}_3(dppm)_2\}^{3+}$ moieties and the amino groups form hydrogen bonds with the chloride ions. As a result, the alternate stacking of waved hydrophilic and hydrophobic layers in the crystal of [**6b**]Cl is rather fuzzy (Figure II-20).

The reverse conversion from the tetranuclear $Au^{I}_3Zn^{II}$ structure of complex $[\mathbf{6b}]^{+}$ to the $Au^{I}_2Zn^{II}$ trinuclear structure of complex [**5b**] was also carried out using a method analogous to that for the Au^{I}-Ni^{II} complexes. The addition of 1 molar equiv each of $NH_4[Au^{I}(D\text{-Hpen})_2]$ and $Zn^{II}Cl_2$ to a pale yellow ethanolic solution containing [**6b**]Cl, together with NaOH, gave a colorless solution. The white residue obtained after the evaporation of the colorless solution was recrystallized to give the colorless crystals of [**5b**]. Therefore, the reversible metalloring expansion/contraction through insertion/removal of the $\{Au^{I}(dppm)\}^{+}$ linker was also confirmed for the Au^{I}-Zn^{II} complexes.

NMR studies revealing solvent dependence of structural conversion. The Au^{I}-Zn^{II} complexes [**5b**] and [**6b**]Cl, which consist only of closed-shell atoms, are doubtlessly diamagnetic species, so NMR study can provide a wealth of information on these compounds in solution state as well as on the structural conversion. As shown in Figure II-21, the ^{1}H NMR spectrum of [**5b**] in methanol-d_4 gave three singlet signals at δ 1.47, 1.55, and 3.40 ppm and multiplet signals in aromatic region (δ 7.32 - 7.72 ppm), which are attributed to two diastereotopic methyl groups and a methine group of D-pen and phenyl groups of the dppm, respectively. The single set of proton signals with an integral intensity ratio corresponding to the 1:2 molar ratio of dppm:D-pen in the ^{1}H NMR spectrum indicates the existence of pure complex [**5b**]. In addition, the ^{31}P NMR spectrum of [**5b**] gave only one singlet signal at δ 32.4 ppm (Figure II-22). However, the number of signals observed in the ^{1}H and ^{31}P NMR spectra corresponds to only half of the complex molecule, which is inconsistent with the C_1-symmetrical molecular structure observed in the crystal. This discrepancy is presumably due to the quick inversion of the absolute configuration around the S atoms in solution.

The ^{1}H and ^{31}P NMR spectra of [**6b**]Cl in methanol-d_4 showed not only a single set of signals assignable to $[\mathbf{6b}]^{+}$, but also signals of [**5b**] and $[Au^{I}_2(dppm)_2]^{2+}$ (Figures II-21 and II-22). As shown in Scheme II-2, complexes [**5b**] and $[Au^{I}_2(dppm)_2]^{2+}$ can be formed by disaggregation of $[\mathbf{6b}]^{+}$, and they must be in an equilibrium in solution, because the spectra showed no significant change over a few days. In the ^{1}H NMR spectrum of [**6b**]Cl in

methanol-d_4, signals due to phenyl groups were found in the region of δ 7.06 - 8.09 ppm, but it was hard to precisely analyze the signals from [**6b**]$^+$ because they overlap with many signals from [**5b**] and $[Au^I_2(dppm)_2]^{2+}$. However, the signals derived from D-pen at δ 1.27, 1.37, and 3.37 ppm attributed to two diastereotopic methyl groups and a methine group, respectively, were distinguishable from those of [**5b**]. From the relative intensities of these signals, it was estimated that about 1/3 of the [**6b**]$^+$ was disaggregated to [**5b**] and $[Au_2(dppm)_2]^{2+}$ in the solution ([**6b**]$^+$:[**5b**]:$[Au^I_2(dppm)_2]^{2+}$ ≈ 2:1:0.5). The ^{31}P NMR spectrum also contained two signals due to [**5b**] at δ 32.4 ppm and $[Au_2(dppm)_2]^{2+}$ at δ 33.7 ppm and two new signals due to [**6b**]$^+$ at δ 33.1 and 34.8 ppm with a reasonable intensity ratio.

Interestingly, the aggregation ratio in solution is strongly influenced by the solvent. The cationic tetranuclear complexes [**6a**]Cl and [**6b**]Cl are slightly soluble in water in addition to polar organic solvents probably due to their ionic character, while neutral trinuclear complexes [**5a**] and [**5b**] are practically insoluble in water. Therefore, the NMR spectra of [**6b**]Cl in several solvents were measured. The ^{1}H and ^{31}P NMR spectra of [**6b**]Cl in chloroform-*d* showed only two sets of signals, unlike those in methanol-d_4 (Figures II-21 and II-22). These signals were assigned to a 2:1 mixture of [**5b**] and $[Au^I_2(dppm)_2]Cl_2$ on the basis of the NMR spectra of pure [**5b**] and $[Au_2(dppm)_2]Cl_2$ in chloroform-*d*, and signals assignable to [**6b**]$^+$ were not found in the spectrum. On the other hand, the ^{1}H and ^{31}P NMR spectra of [**6b**]Cl in D_2O only showed a single set of signals assignable to [**6b**]$^+$ (Figures II-21 and II-22). The difference between the aggregation ratios in the different solutions can be explained by polarity of the solvents. In a less polar solvent such as chloroform, an ion pair of [**6b**]$^+$ and Cl^- is restructured into [**5b**] and $[Au_2(dppm)_2]Cl_2$, which has coordinated chlorido ligands in nonpolar solvents,[8,17a,21] because ionic species are not effectively stabilized by solvation, whereas electrically neutral ones are. Conversely, more polar solvents such as water should effectively stabilize ionic species and facilitate the aggregation into [**6b**]$^+$. In fact, these results demonstrate that the structural conversion between [**5b**] and [**6b**]$^+$ can be controlled by changing the polarity of the solvent. The much better isolated yield of [**6b**]Cl obtained from a mixed solvent of ethanol and water, as compared to that in methanol, also supports this result.

These observations also imply that the absorption and CD spectra of [**6a**]Cl in ethanol can be attributed to a mixture containing [**6a**]$^+$ as the major constituent and [**5a**] as the minor one, which is consistent with the CD spectrum of [**6a**]Cl in ethanol showing the spectral features similar to both [**5a**] and [**2b**] as discussed above. In addition, the CD spectra of [**6a**]Cl in chloroform and water exhibited the spectral features similar to those of [**5a**] and [**2b**], respectively, indicative of the same type of solvent dependence for Au^I-Ni^{II} complexes (Figure II-24).

Photophysical properties of Au^I and Au^I-Zn^{II} complexes. The Au^I and Au^I-Zn^{II} complexes [H_2**3**], [H**4**], [**5b**], and [**6b**]Cl exhibited luminescence under UV irradiation in the solid state with different colors and brightness levels. The luminescence spectra of solid

samples of those complexes were collected at ambient temperature as summarized in Table II-10. The solid samples of [H_2**3**] and [H**4**] were almost non-emissive at ambient temperature (Φ = 0.004 for [H_2**3**] and Φ < 0.001 for [H**4**]), whereas those of [**5b**] and [**6b**]Cl displayed yellow and green emission, respectively. The emission bands for [**5b**] and [**6b**]Cl were centered at 546 nm and 522 nm with corresponding quantum yields of Φ = 0.033 and Φ = 0.13, respectively (Figure II-25). The increasing of emission intensity on zinc(II)-binding is reminiscent of the PPh_3 system in Chapter I, where the reductive quenching of the excited state and the vibrational energy loss by D-pen moiety has been expected as major quenching process, which was supported by significant emission property at low temperature (77 K) of the zinc-free metalloligands [H_2**3**] and [H**4**] (Figure II-26). The larger quantum yield for [**6b**]Cl rather than that of [**5b**] can be attributed to the more significant aurophilic interactions, which is expected to contribute stabilization of the structure particularly in the excited state,[22] and the bulky $\{Au^I_3(dppm)_2\}^{3+}$ backbone, which keeps the complex cation isolated in the crystal structure and so can protect the luminophore. The origin of the emission for these complexes is assigned to phosphorescence arising primarily from a charge transfer transition from S to Au perturbed by aurophilic interaction (^{3}LMMCT), similar to the assignment for related luminescent gold(I) species having both phosphine and thiolate ligands.[23,24] Consistent with this assignment, the emission lifetimes of [**5b**] (τ = 4.3, 0.54, and 0.049 μs) and [**6b**]Cl (τ = 12, 2.9, and 0.61 μs) are on the order of microseconds.

II-3-2. Structural control by Au^I-phosphine backbone with aurophilic interaction.

The most critical difference between two diphosphine systems, the present dppm system and the previous dppe system, is presence or absence of the intramolecular aurophilic interaction. In all of the crystal structures shown in this chapter, the short $Au^I\cdots Au^I$ contacts indicating the presence of aurophilic interaction were observed. In addition, considering the spectral features in solution largely consistent with their crystal structures, it is expected that the $Au^I\cdots Au^I$ contacts in their structure, probably including complex [H_2**3**] whose crystal structure is unknown, are retained also in the solution. These results and a large number of previously reported complexes with the $\{Au^I_2(dppm)\}^{2+}$ substructure suggest that two P donors bridged by a methylene group in dppm quite efficiently promote the formation of the intramolecular $Au^I\cdots Au^I$ contact to be a significant determinant for the molecular structure and conformation.[4] Actually the use of the intramolecular aurophilic interaction led to not only the achievement of the objective D-penicillaminato digold(I) metalloligand coordinating with hexadentate-N_2,O_2,S_2 chelating mode toward a metal ion but also an accidental formation of additional trigold(I) structure, which is stabilized by the folding conformation of $\{Au^I_3(dppm)_2\}^{3+}$ moiety via aurophilic interaction, as well as interconversion between them.

In addition to the stabilization of their structures by aurophilic interactions, another key factor of the interesting structural interconversion system presented here is kinetically labile

character for ligand exchange reaction of gold(I) complexes.[25,26] Two-coordinate gold(I) center has an accessible coordination sphere to easily permit ligand exchange reaction through an associative mechanism,[27] which can be facilitated on coordination of phosphine ligands because they also stabilize three- or four-coordinate gold(I) centers and show strong trans effect.[28,29] On the other hand, the combinations of Au and P atoms, and Au and S atoms generally show quite good affinity to form thermally stable coordination bonds with a high covalent character.[25,30,31] Thus the coordination system constructed from gold(I) metalloligands with thiolates and phosphines can quickly and reversibly convert between plural stable structures without decomposition or irreversible reaction in the dynamic process, as demonstrated here for the dppm system.

II-4. Conclusion.

In this chapter, the coordination behavior of D-penicillaminato gold(I) metalloligands with the diphosphine, dppm, was investigated to achieve functionalization of thiolato-bridged heterometallic complexes through structural control by gold(I)-phosphine backbone with aurophilic interaction. The dppm system produced not only the expected digold(I) chelating metalloligand $[\mathbf{3}]^{2-}$ but also the unexpected trigold(I) metalloligand $[\mathbf{4}]^{-}$, both of which can coordinate to octahedral metal ions in a hexadentate-N_2,O_2,S_2 mode to give the thiolato-bridged heterometallic complexes.

According to the concept presented in General Introduction, a pair of D-pen arms acted as coordination donor groups that strongly bound to a metal ion with six donors to form a {M(D-pen)$_2$} functional part, which can response to external stimuli and express physical property change depending on the secondary metal ions (M), and the gold(I)-dppm backbones connected to the functional part through S atoms worked as a structural-controlling part to regulate the orientation of D-pen arms in the metalloligands as well as the functionality of {M(D-pen)$_2$} part in the heterometallic complexes. Particularly, the metalloring interconversion between the $Au^{I}_2Ni^{II}$ trinuclear and $Au^{I}_3Ni^{II}$ tetranuclear structures is a prime example. The $\{Ni^{II}(D\text{-pen})_2\}^{2-}$ moiety responded to the external stimuli (presence of extension agent, solvent polarity, solution pH, and electrical potentials) and exerted the various properties (chromogenic, chiroptical, and magnetic properties), and the gold(I)-dppm backbones produced the preference and the different properties of two states. As a result of cooperation of the functional part and the structural-controlling part, the interesting coordination system with a stimuli-responsive structural interconversion accompanied by changes in physical properties was achieved. The regulation of ligand field by gold(I)-phosphine backbone, which was indicated by the experiments of acid-induced conversion and cyclic voltammetry of Au^{I}-Ni^{II} complexes, is also discussed for Au^{I}-$Co^{II/III}$ complexes in Chapter III.

On the other hand, in the case of the closed shell Au^{I}-Zn^{II} system, the structural conversion reaction in solution was revealed in detail by NMR spectroscopy with different solvents. Moreover, the fascinating phenomenon was found in their photophysical properties where increasing of emission intensity was also observed on enhancement of aurophilic interactions from $\{Au^{I}_{2}(dppm)\}^{2+}$ to $\{Au^{I}_{3}(dppm)_{2}\}^{3+}$ in addition to the increasing by zinc(II)-binding, which was also observed in the PPh_3 system.

In contrast to the dppe system, which demonstrated the significant impact of hydrogen-bonding interactions, including CH···π interactions as a kind of weak hydrogen bond,[32] the present system emphasizes benefit of aurophilic interaction as another attractive force applicable for structural control. Although both aurophilic and hydrogen-bonding interactions are classified to non-bonded attractive forces with similar magnitude of energy, their characteristics and origins are quite different; aurophilic interaction is less-directional attractive force between gold atoms, which is thought today to arise from an electronic correlation effect considerably strengthened by the relativistic effect,[33] while hydrogen bonds generally possess higher-directionality and largely arise from an electrostatic potential energy because they are formed through sharing a hydrogen atom between the hydrogen-bonding donor with an acidic hydrogen and the acceptor with a lone pair.[34] While hydrogen bonds have been generally used to control structures and functionalities of compounds as well as crystal engineering since early times,[34,35] use of aurophilic interactions for structural control are still developing today. The usage of aurophilic interactions together with hydrogen bonds will facilitate more rational molecular designing, because they are strong enough to control the structures and uncompetitive attractions with quite different characteristics to each other. While the control of the molecular structure by the intramolecular interactions was demonstrated in this work, intermolecular interactions leading to supramolecular architectures will be available by selecting proper phosphine backbones.

Finally, it was also demonstrated that thermally stable but kinetically reactive character of Au^{I}–P and Au^{I}–S coordination bonds play important role for the interconvertible system, in which the structural conversion processes were quickly completed within several seconds without any decomposition or irreversible reactions.

II-5. References.

[1] (a) P. Pyykkö, *Chem. Rev.* **1997**, *97*, 597. (b) P. Pyykkö, *Chem. Soc. Rev.* **2008**, *37*, 1967. (c) M. J. Katz, K. Sakai, D. B. Leznoff, *Chem. Soc. Rev.* **2008**, *37*, 1884. (d) H. Schmidbaur, A. Schier, *Chem. Soc. Rev.* **2012**, *41*, 370.

[2] (a) R. Lee, A. Igashira-Kamiyama, H. Motoyoshi, T. Konno, *CrystEngComm* **2012**, *14*, 1936. (b) A. Igashira-Kamiyama, N. Matsushita, R. Lee, K. Tsuge, T. Konno, *Bull. Chem. Soc. Jpn.* **2012**, *85*, 706. (c) R. Lee, A. Igashira-Kamiyama, M. Okumura, T.

Konno, *Bull. Chem. Soc. Jpn.* **2013**, *86*, 908.C. A. (d) R. Lee, PhD thesis, Osaka University, Toyonaka, Japan, **2012**.

[3] (a) D. J. LeBlanc, J. F. Britten, Z. Wang, H. E. Howard-Lock, C. J. L. Lock, *Acta Crystallogr. Sect. C Cryst. Struct. Commun.* **1997**, *53*, 1763. (b) A. Toyota, T. Yamaguchi, A. Igashira-Kamiyama, T. Kawamoto, T. Konno, *Angew. Chem. Int. Ed.* **2005**, *44*, 1088. (c) M. Taguchi, A. Igashira-Kamiyama, T. Kajiwara, T. Konno, *Angew. Chem. Int. Ed.* **2007**, *46*, 2422. (d) M. Taguchi, Y. Sameshima, A. Igashira-Kamiyama, S. Akine, T. Nabeshima, T. Konno, *Chem. Lett.* **2008**, *37*, 244. (e) Y. Sameshima, N. Yoshinari, K. Tsuge, A. Igashira-Kamiyama, T. Konno, *Angew. Chem. Int. Ed.* **2009**, *48*, 8469. (f) T. Konno, N. Yoshinari, M. Taguchi, A. Igashira-Kamiyama, *Chem Lett.* **2009**, *38*, 526. (g) T. Konno, A. Toyota, A. Igashira-Kamiyama, *J. Chin. Chem. Soc.* **2009**, *56*, 26. (h) A. Igashira-Kamiyama, T. Konno, *Dalton Trans.* **2011**, *40*, 7249.

[4] Recent examples for structural determination containing a {Au_2(dppm)} substracture with an intramolecular Au···Au contact are follows: (a) J. Arias, M. Bardaji, P. Espinet, *Inorg. Chem.* **2008**, *47*, 1597. (b) J. Vicente, J. Gil-Rubio, N. Barquero, P. G. Jones, D. Bautista, *Organometallics* **2008**, *27*, 646. (c) J. Schneider, Y.-A Lee, J. Perez, W. W. Brennessel, C. Flaschenriem, R. Eisenberg, *Inorg. Chem.* **2008**, *47*, 957. (d) P. Teo, J. Wang, L. L. Koh, T. S. A. Hor, *Dalton Trans.* **2009**, 5009. (e) C. R. Wade, A. A. Yakovenko, F. P. Gabbai, *New J. Chem.* **2010**, *34*, 1646. (f) R. V. Bojan, J. M. Lopez-de-Luzuriaga, M. Monge, M. E. Olmos, *J. Organomet. Chem.* **2010**, *695*, 2385. (g) A. M. Kuchison, M. O. Wolf, B. O. Patrick, *Inorg. Chem.* **2010**, *49*, 8802. (h) M. Dennehy, O. V. Quinzani, R. M. Ferullo, A. Granados, R. A. Burrow, *Inorg. Chim. Acta,* **2011**, *377*, 77. (i) M. H. Mir, J. X. Ong, G. K. Kole, G. K. Tan, M. J. McGlinchey, Y. Wu, J. J. Vittal, *Chem. Commun.* **2011**, *47*, 11633. (j) A. Ilie, C. I. Rat, S. Scheutzow, C. Kiske, K. Lux, T. M. Klapotke, C. Silvestru, K. Karaghiosoff, *Inorg. Chem.* **2011**, *50*, 2675. (k) X.-L. Li, M. Tan, Ke-J. Zhang, Bo Yang, J. Chen, Yu-Bo Ai, *Inorg. Chem.* **2012**, *51*, 109.

[5] (a) *Molecular Machines*, T. L. Kelly, Eds.; Springer, Berlin Heidelberg (2005). (b) V. Balzani, A. Credi, M. Venturi, *Molecular Devices and Machines: Concepts and Perspectives for the Nanoworld*, 2nd Ed., Wiley, Chichester (2008). (c) *Molecular Switches*, B. L. Feringa, W. R. Browne, Eds.; Wiley, Chichester (2011).

[6] (a) J. R. Nitschke, *Acc. Chem. Res.* **2007**, *40*, 103. (b) V. E. Campbell, J. R. Nitschke, *Synlett* **2008**, 3077. (c) N. B. Debata, D. Tripathy, D. K. Chand, *Coord. Chem. Rev.* **2012**, *256*, 1831. (d) M. Tegoni, M. Remelli, *Coord. Chem. Rev.* **2012**, *256*, 289.

[7] C. K. Mirabelli, D. T. Hill, L. F. Faucette, F. L. McCabe, G. R. Girard, D. B. Bryan, B. M. Sutton, J. O'L. Bartus, S. T. Crooke, R. K. Johnson, *J. Med. Chem.* **1987**, *30*, 2181.

[8] H. Schmidbaur, A. Wohlleben, U. Schubert, A. Frank, G. Huttner, *Chem. Ber.* **1977**, *110*, 2751.

[9] R. Usón, A. Laguna, M. Laguna, *Inorg. Synth.* **1989**, *26*, 85.

[10] K. Suzuki, A. Kobayashi, S. Kaneko, K. Takehira, T. Yoshihara, H. Ishida, Y. Shiina, S. Oishi, S. Tobita, *Phys. Chem. Chem. Phys.* **2009**, *11*, 9850.

[11] T. Yutaka, S. Obara, S. Ogawa, K. Nozaki, N. Ikeda, T. Ohno, Y. Ishii, K. Sakai, M. Haga, *Inorg. Chem.* **2005**, *44*, 4737.

[12] A. Altomare, G. Cascarano, C. Giacovazzo, A. Guagliardi, A. G. G. Moliterni, M. C. Burla, G. Polidori, M. Camalli, R. Spagna, *J. Appl. Crystallogr.* **1999**, *32*, 115.

[13] G. M. Sheldrick, *Acta Crystallogr., Sect. A* **2008**, *64*, 112.

[14] C. Kabuto, S. Akine, E. Kwon, *J. Cryst. Soc. Jpn.* **2009**, *51*, 218.

[15] K. Nakamoto, *Infrared and Raman Spectra of Inorganic and Coordination Compounds*, 5th ed., Wiley, Chichester (1997).

[16] H. E. Howard-Lock, C. J. L. Lock, P. S. Smalley, *J. Chem. Crystallogr.* **1983**, *13*, 333.

[17] (a) I. J. B. Lin, J. M. Hwang, D.-F. Feng, M. C. Cheng, Y. Wang, *Inorg. Chem.* **1994**, *33*, 3467. (b) M. Bardaji, A. Laguna, M. Laguna, *J. Chem. Soc. Dalton Trans.* **1995**, 1255.

[18] *Nomenclature of Organic Chemistry: Iupac Recommendations 2012 and Preferred Iupac Names*, H. Favre, W. H. Powel, Eds; Royal Society of Chemistry (2012).

[19] P. J. M. W. L. Birker, G. C. Verschoor, *Inorg. Chem.* **1982**, *21*, 990.

[20] R. D. Shannon, *Acta Crystallogr. Sect. A* **1976**, *32*, 751.

[21] H. de la Riva, A. Pintado-Alba, M. Nieuwenhuyzen, C. Hardacre, M. C. Lagunas, *Chem. Commun.* **2005**, 4970.

[22] (a) M. A. Rawashdeh-omary, M. A. Omary, H. H. Patterson, J. P. Fackler, *J. Am. Chem. Soc.* **2001**, *123*, 11237. (b) Q.-J. Pan, H.-X. Zhang, *J. Mol. Struct. THEOCHEM* **2004**, *671*, 53.

[23] H. Schmidbaur, Schier, A.; *Chem. Soc. Rev.* **2008**, *37*, 1931.

[24] (a) B.-C. Tzeng, J.-H. Liao, G.-H. Lee, S.-M. Peng, *Inorg. Chim. Acta* **2004**, *357*, 1405. (b) C.-K. Li, X.-X. Lu, K. M.-C. Wong, C.-L. Chan, N. Zhu, V. W.-W. Yam, *Inorg. Chem.* **2004**, *43*, 7421. (c) M. Bardají, M. J. Calhorda, P. J. Costa, P. G. Jones, A. Laguna, M. R. Pérez, M. D. Villacampa, *Inorg. Chem.* **2006**, *45*, 1059. (d) P. J. Costa, M. J. Calhorda, *Inorg. Chim. Acta* **2006**, *359*, 3617. (e) J. Schneider, Y.-A Lee, J. Pérez, W. W. Brennessel, C. Flaschenriem, R. Eisenberg, *Inorg. Chem.* **2008**, *47*, 957. (f) E. R. T. Tiekink, J.-G. Kang, *Coord. Chem. Rev.* **2009**, *253*, 1627. (g) I. O. Koshevoy, E. S. Smirnova, M. Haukka, A. Laguna, J. C. Chueca, T. A. Pakkanen, S. P. Tunik, I. Ospino, O. Crespo, *Dalton Trans.* **2011**, *40*, 7412. (h) O. Crespo, M. C. Gimeno, A. Laguna, F. J. Lahoz, C. Larraz, *Inorg. Chem.* **2011**, *50*, 9533.

[25] M. C. Gimeno, A. Laguna, in *Comprehensive Coordination Chemistry II*, J. A. McCleverty, T. J. Meyer, Eds.; Elsevier Inc., vol. 6, pp. 911–1145 (2003).

[26] (a) M. J. Mays, P. A. Vergnano, *J. Chem. Soc. Dalt. Trans.* **1979**, 1112. (b) P. D. Akrivos, H. J. Katsikis, A. Koumoutsi, *Coord. Chem. Rev.* **1997**, *167*, 95. (c) P. Schwerdtfeger, H.

L. Hermann, H. Schmidbaur, *Inorg. Chem.* **2003**, *42*, 1334.

[27] D. F. Shriver, P. W. Atkins, *Inorganic Chemistry*, 3rd ed., Oxford University Press (1999).

[28] M. A. Carvajal, J. J. Novoa, S. Alvarez, *J. Am. Chem. Soc.* **2004**, *126*, 1465.

[29] (a) A. Y. Sokolov, O. V. Sizova, *Russ. J. Gen. Chem.* **2010**, *80*, 1057. (b) P. G. Jones, A. F. Williams, *J. Chem. Soc. Dalt. Trans.* **1977**, 1430.

[30] (a) C. E. Housecroft, *Coord. Chem. Rev.* **1997**, *164*, 667. (b) P. Schwerdtfeger, H. L. Hermann, H. Schmidbaur, *Inorg. Chem.* **2003**, *42*, 1334. (c) J. J. Vittal, R. J. Puddephatt, *Gold: Inorganic & Coordination Chemistry*, Wiley, Chichester (2006).

[31] L.-S. Wang, *Phys. Chem. Chem. Phys.* **2010**, *12*, 8694.

[32] (a) M. Nishio, M., Hirota, Y. Umezawa, *The CH/π Interaction: Evidence, Nature, and Consequences*, Wiley-VCH, New York (1998). (b) G. R. Desiraju, T. Steiner, The Weak Hydrogen Bond: In Structural Chemistry and Biology, Oxford University Press, USA (2001). (c) M. Nishio, *CrystEngComm* **2004**, *6*, 130.

[33] (a) M. Bardají, A. Laguna, *J. Chem. Educ.* **1999**, *76*, 201. (b) P. Pyykkö, *Angew. Chem. Int. Ed.* **2004**, *43*, 4412.

[34] (a) S. Scheiner, *Hydrogen Bonding: A Theoretical Perspective*, Oxford University Press, USA (1997). (b) G. A. Jeffrey, *An Introduction to Hydrogen Bonding*, Oxford University Press, USA (1997). (c) G. Gilli, P. Gilli, *The Nature of the Hydrogen Bond: Outline of a Comprehensive Hydrogen Bond Theory*, Oxford University Press, USA (1999). (d) *Hydrogen Bonding - New Insights*, S. Grabowski, Eds.; Springer, Berlin Heidelberg (2006).

[35] (a) T. Steiner, *Angew. Chem. Int. Ed.* **2002**, *41*, 48. (b) G. R. Desiraju, *Acc. Chem. Res.* **2002**, *35*, 565. (c) *Supramolecular Assembly via Hydrogen Bonds I*, D. M. P. Mingos, Eds; Springer, Berlin Heidelberg (2004). (d) *Supramolecular Assembly via Hydrogen Bonds II*, D. M. P. Mingos, Eds; Springer, Berlin Heidelberg (2004).

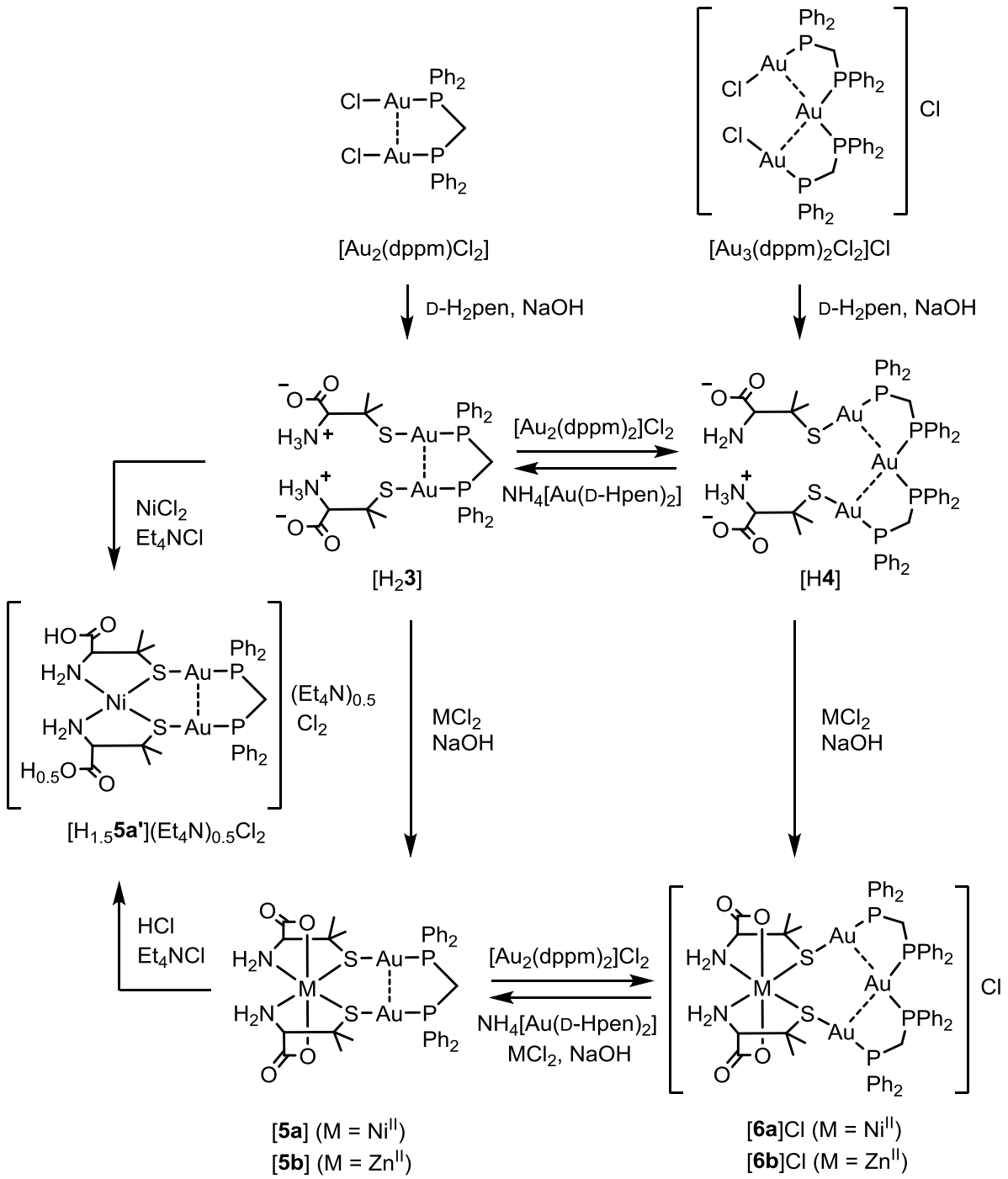

Scheme II-1. Syntheses and conversions of complexes [H_2**3**], [H**4**], [**5a**], [$H_{1.5}$**5a'**]$(Et_4N)_{0.5}Cl_2$, [**5b**], [**6a**]Cl, and [**6b**]Cl.

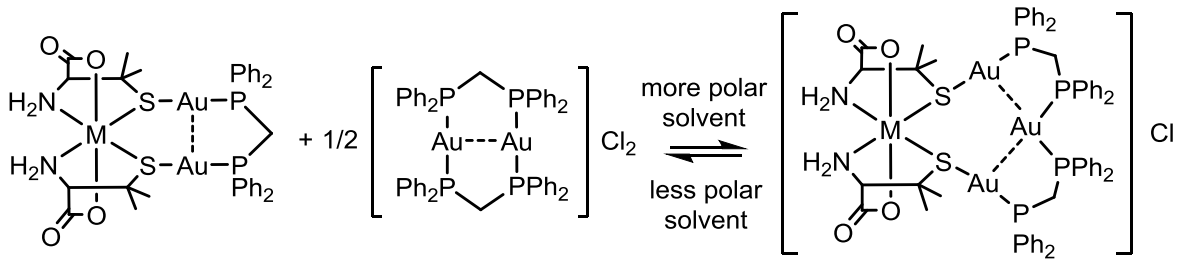

[**5a**] (M = Ni^{II})
[**5b**] (M = Zn^{II})

$[Au_2(dppm)_2]Cl_2$

[**6a**]Cl (M = Ni^{II})
[**6b**]Cl (M = Zn^{II})

Scheme II-2. Equilibrium among [**5**], $[Au^{I}_2(dppm)_2]Cl_2$, and [**6**]Cl depending on solvent.

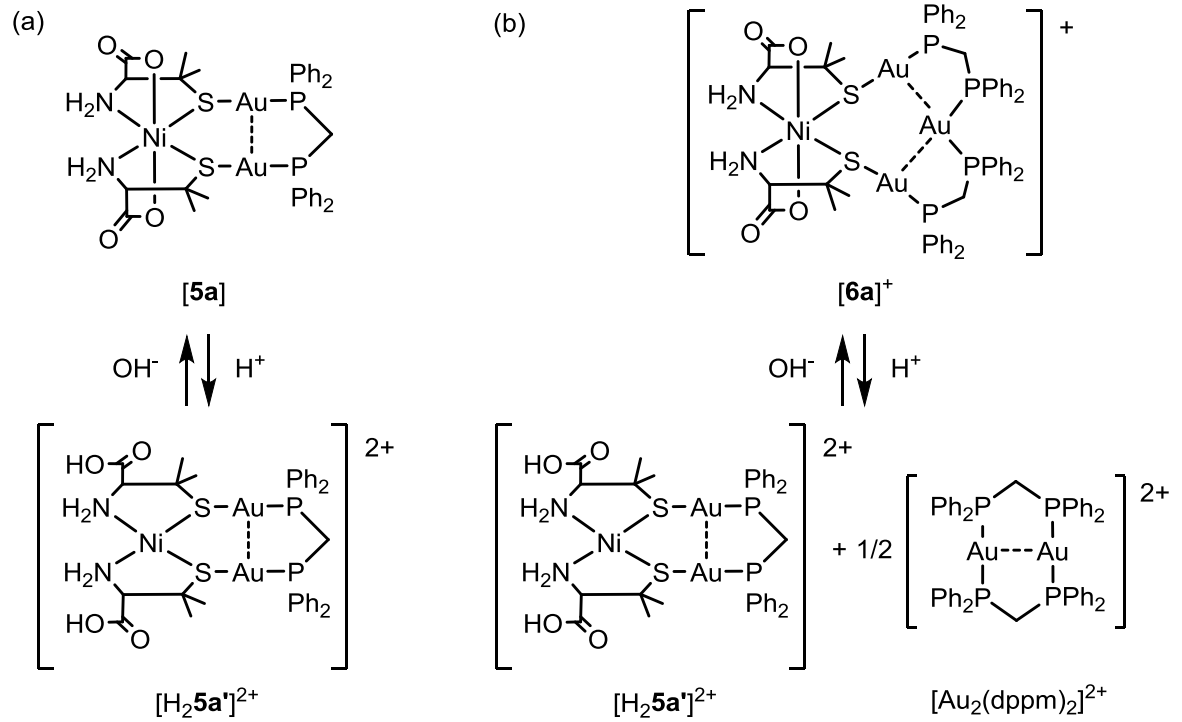

[**5a**] [**6a**]$^+$

$[H_2$**5a'**$]^{2+}$ $[H_2$**5a'**$]^{2+}$ $[Au_2(dppm)_2]^{2+}$

Scheme II-3. Acid/base-induced conversions between (a) [**5a**] and $[H_2$**5b'**$]^{2+}$, and [**6a**]$^+$ and $[H_2$**5b'**$]^{2+}$.

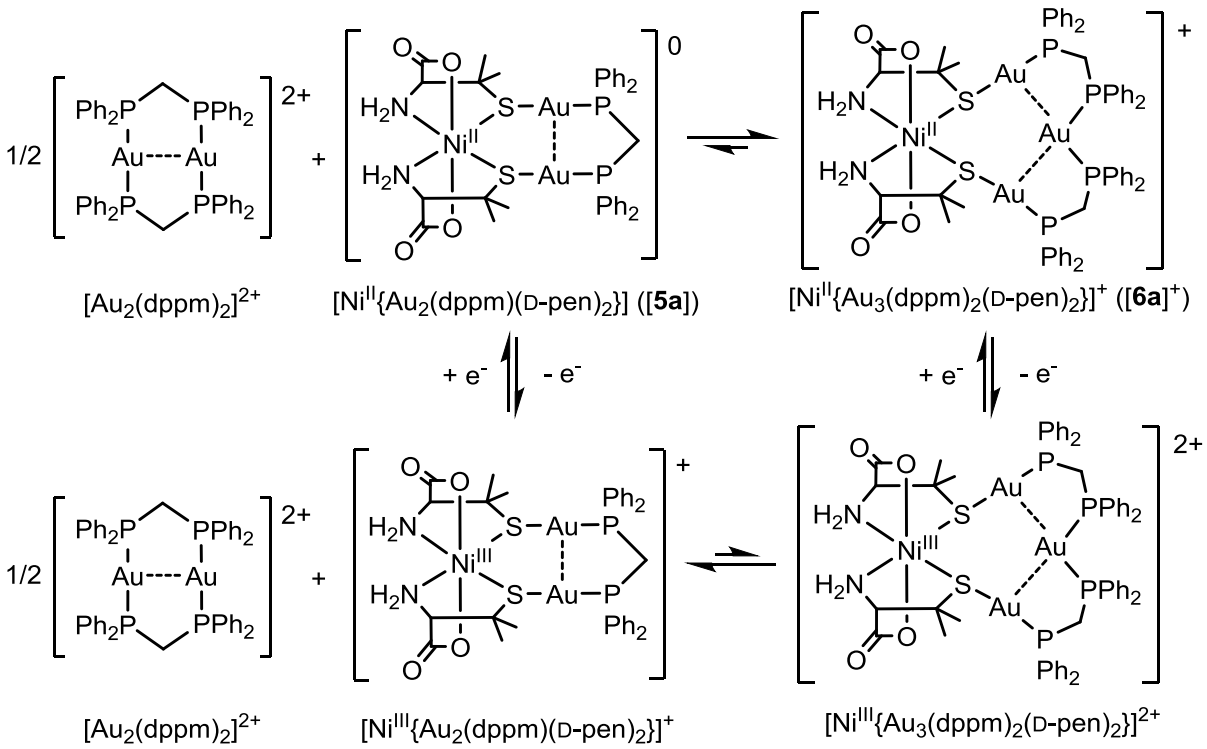

Scheme II-4. EC-EC process in cyclic voltammetry for [**6a**]Cl.

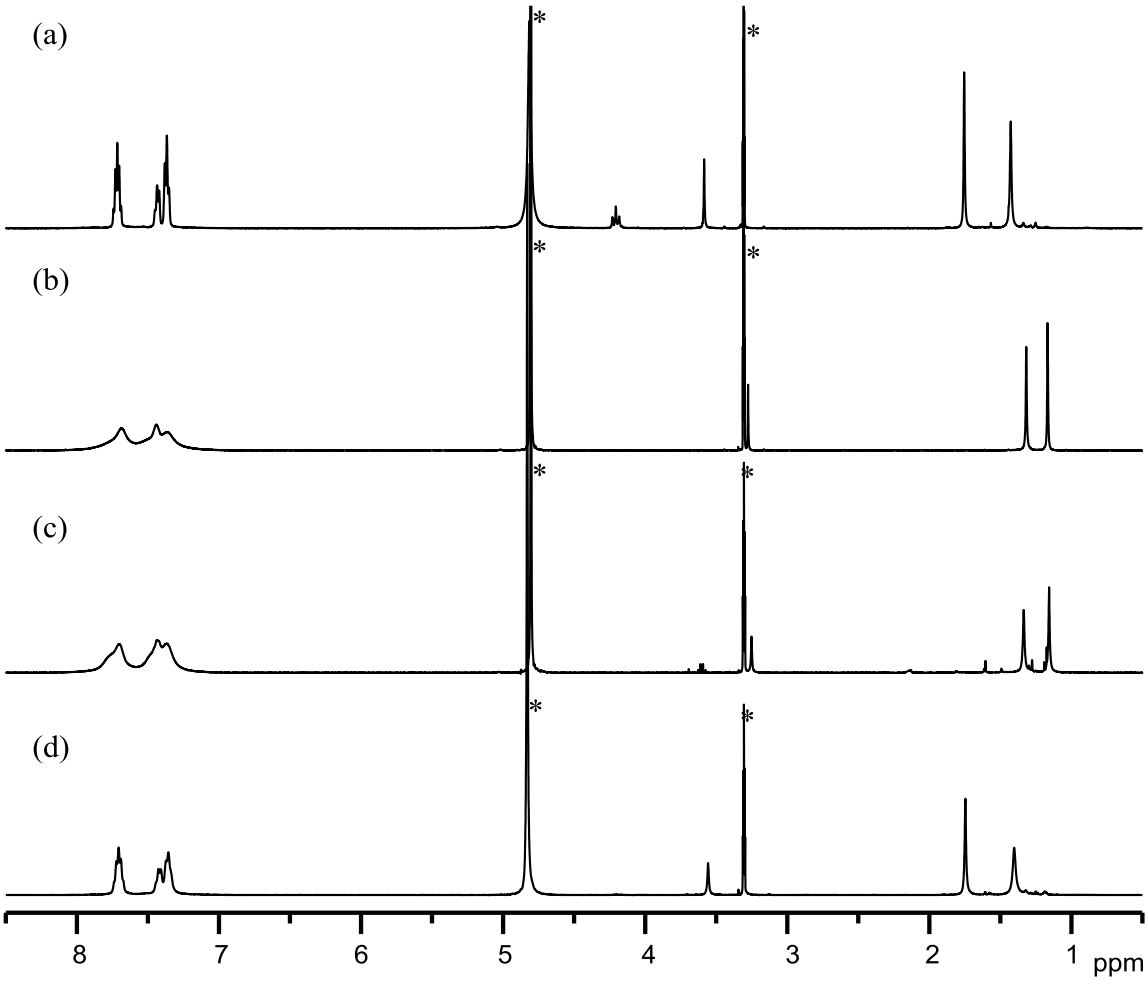

Figure II-1. ^{1}H NMR spectra of (a) [H_2**3**], (b) [H**4**], (c) reaction solution of [H_2**3**] with [Au^{I}_2(dppm)$_2$]Cl_2, and (d) reaction solution of [H**4**] with NH_4[Au^{I}(D-Hpen)$_2$] in methanol-d_4. (*) denotes the signals from solvents.

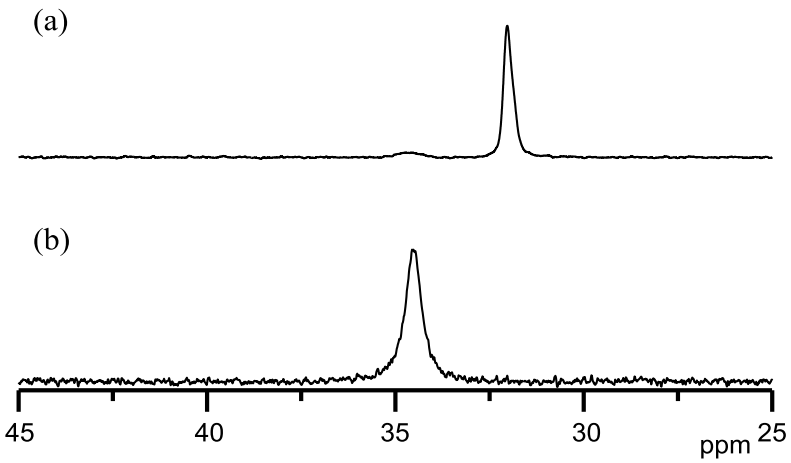

Figure II-2. ^{31}P NMR spectra of (a) [H_2**3**], (b) [H**4**] in methanol-d_4.

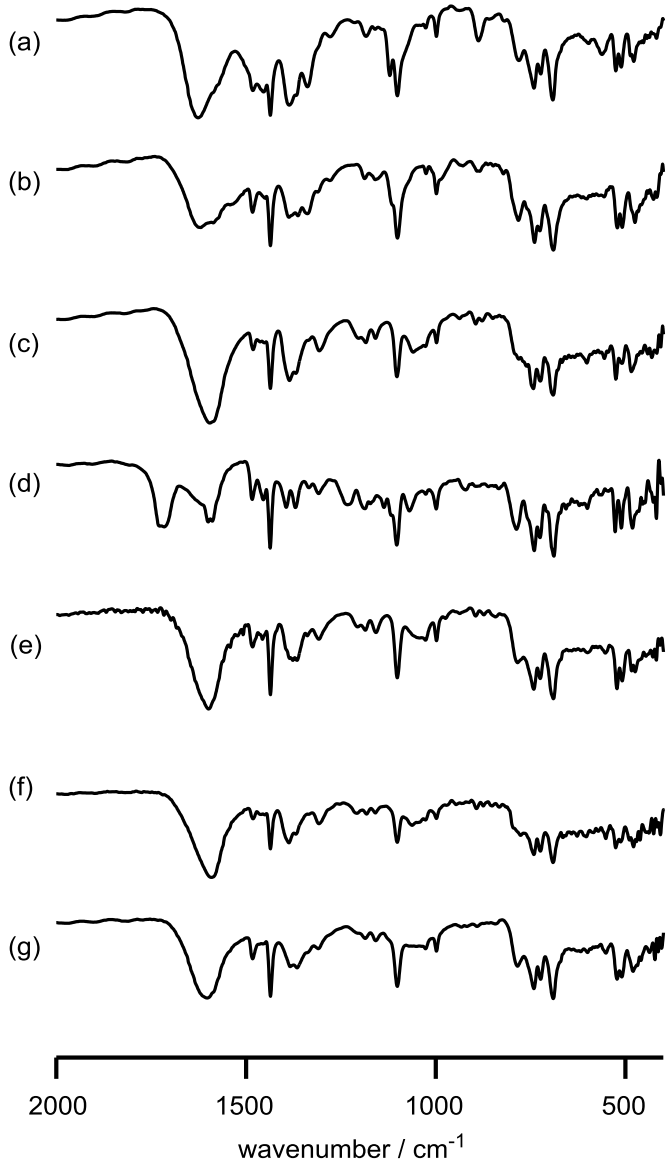

Figure II-3. IR spectra of (a) [H_2**3**], (b) [H**4**], (c) [**5a**], (d) [$H_{1.5}$**5a'**]$(Et_4N)_{0.5}Cl_2$, (e) [**6a**]Cl, (f) [**5b**], and (g) [**6b**]Cl (KBr disk).

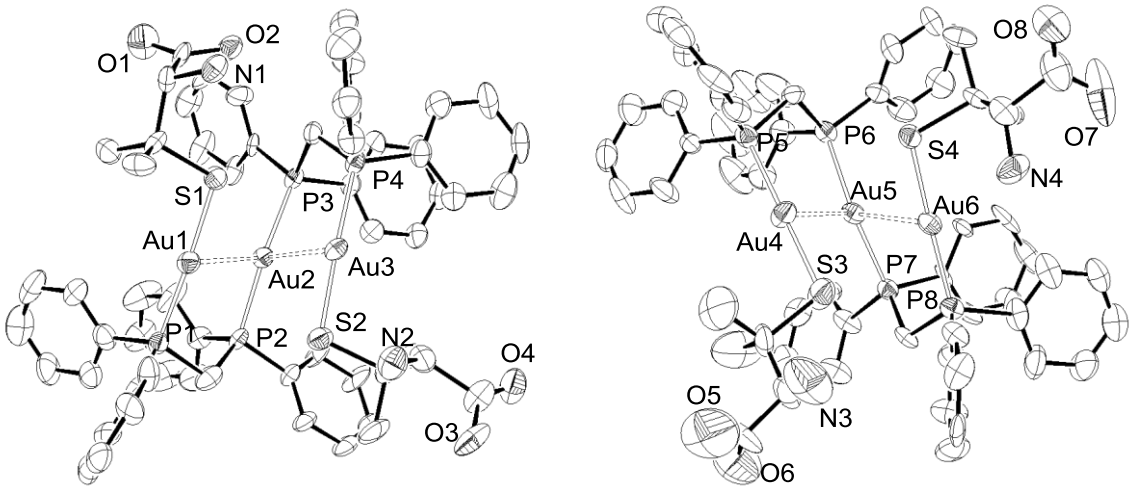

Figure II-4. ORTEP drawings of [H**4**] with 50% probability level of thermal ellipsoids. H atoms are omitted for clarity.

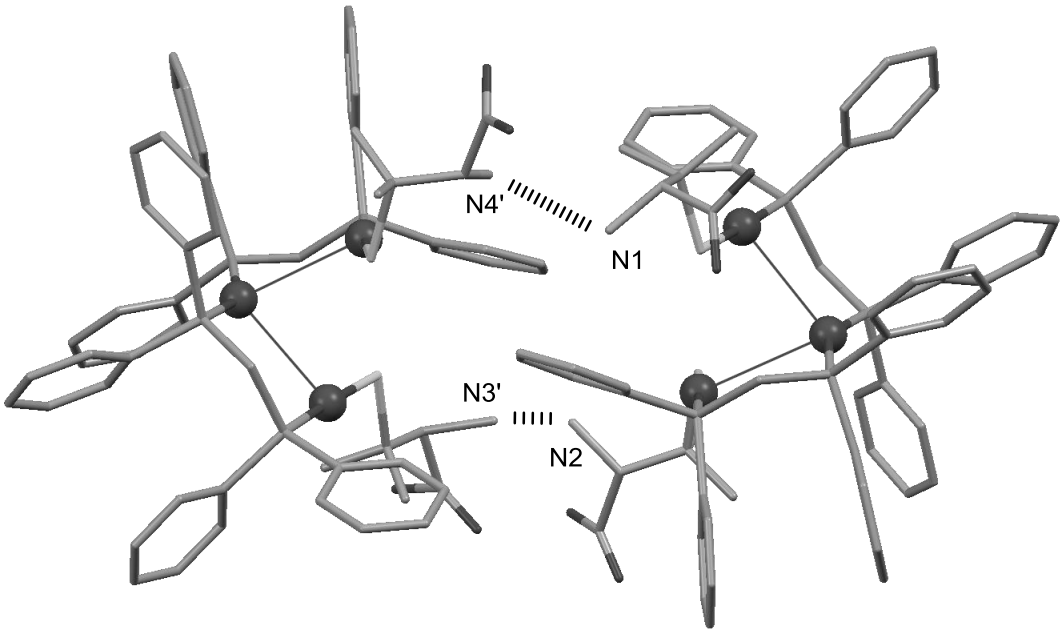

Figure II-5. Hydrogen-bonded dimer of [H**4**]. H atoms are omitted for clarity. Hydrogen bonds are depicted with dashed lines. Symmetry code ('): x, 1+y, –1+z.

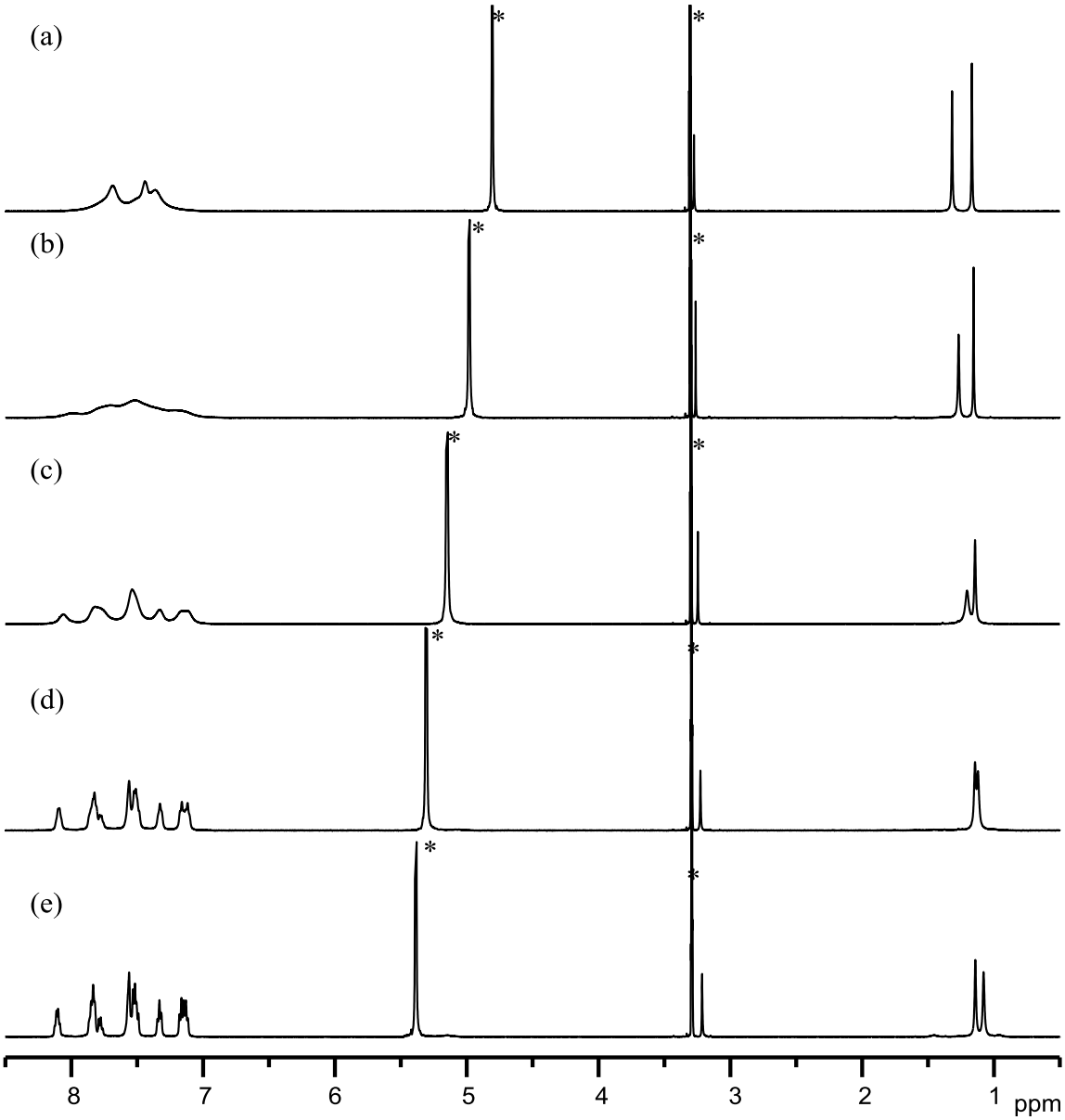

Figure II-6. ^{1}H NMR spectra of [H**4**] in methanol-d_4 measured at (a) 30°C, (b) 10°C, (a) –10°C, (a) –30°C, (a) –40°C. (*) denotes the signals from solvents.

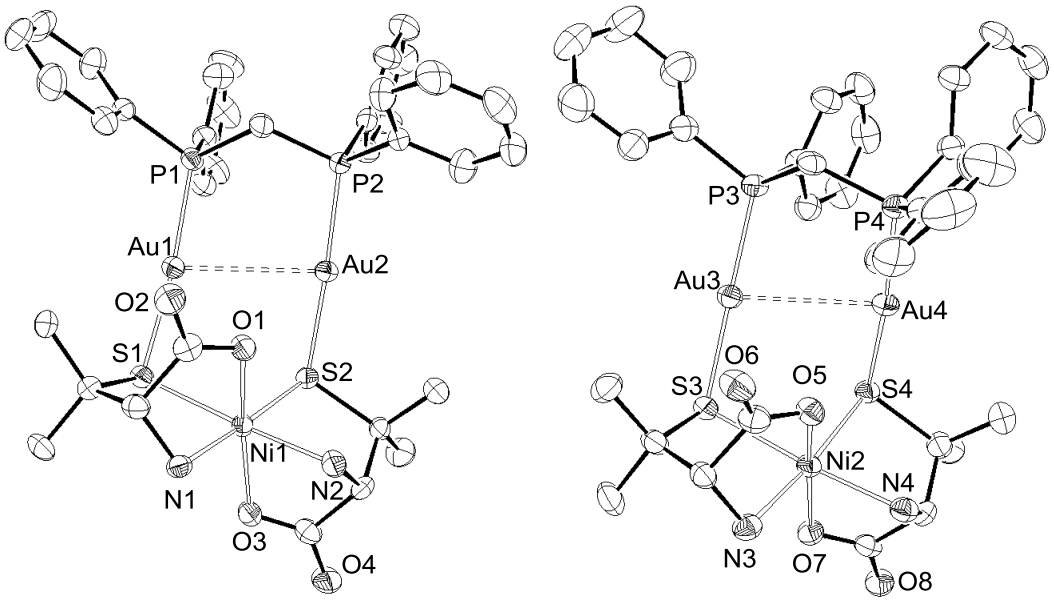

Figure II-7. ORTEP drawings of [**5a**] with 50% probability level of thermal ellipsoids. H atoms are omitted for clarity.

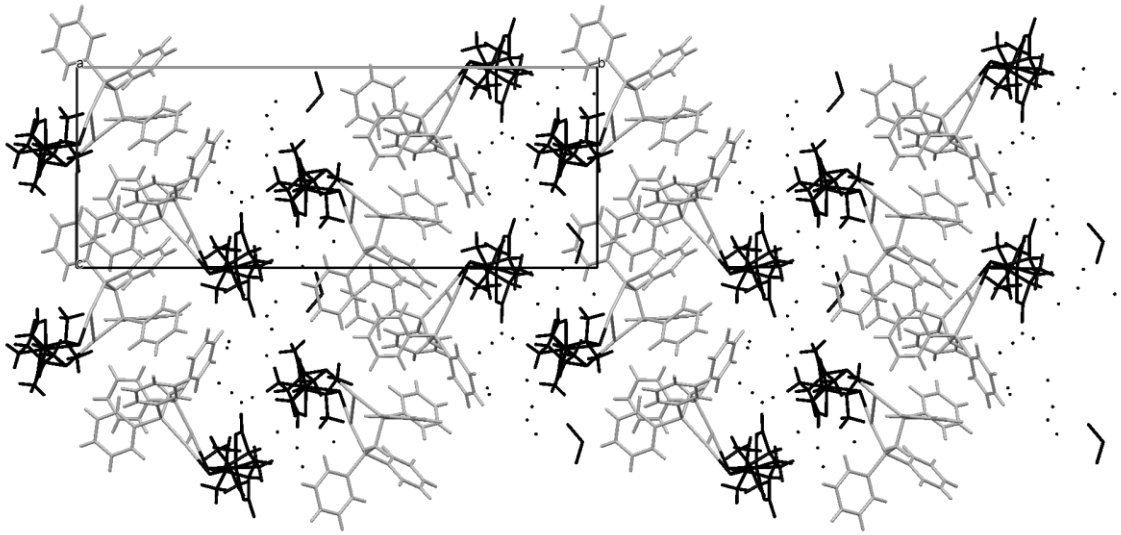

Figure II-8. Packing diagram of [**5a**] viewed along *a* axis. $\{Ni^{II}(D\text{-pen})_2\}^{2-}$ moieties, water, and ethanol molecules are shown with black sticks and $\{Au^{I}_2(dppm)\}^{2+}$ moieties are shown with gray sticks.

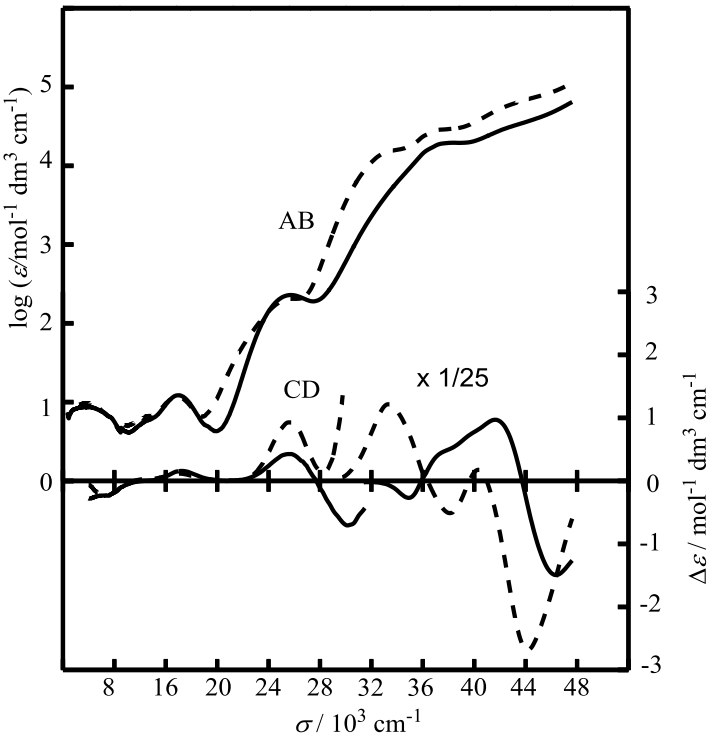

Figure II-9. Electronic absorption and CD spectra of [**5a**] (solid line) and [**6a**]Cl (dashed line) in ethanol.

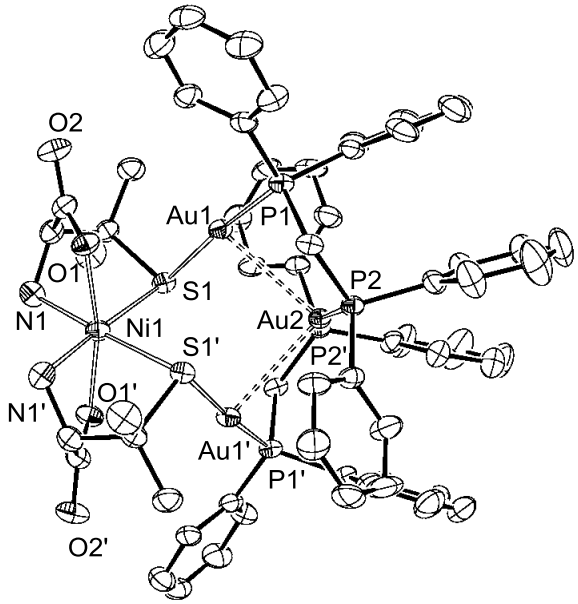

Figure II-10. ORTEP drawing of the entire complex cation in [**6a**]Cl with 50% probability level of thermal ellipsoids. H atoms are omitted for clarity. Symmetry code ('): 1–x, –y, z.

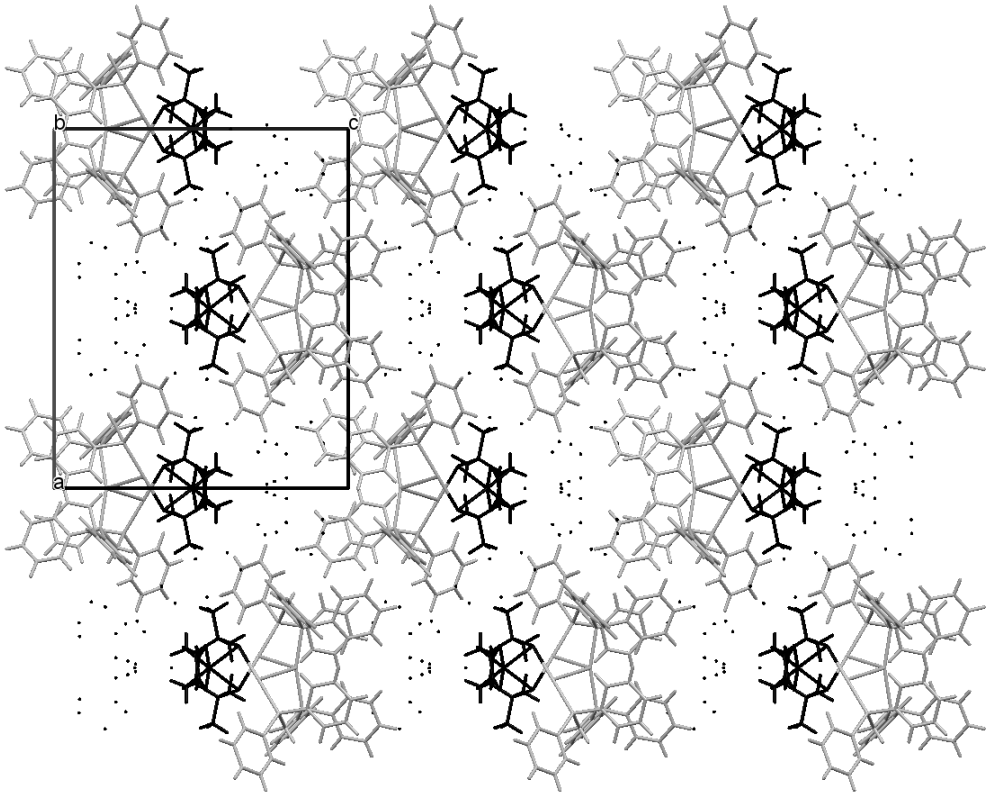

Figure II-11. Packing diagram of [**6a**]Cl viewed along *b* axis. $\{Ni^{II}(D\text{-pen})_2\}^{2-}$ moieties, Cl^- anions, and water molecules are shown with black sticks and $\{Au^{I}_3(dppm)_2\}^{3+}$ moieties are shown with gray sticks.

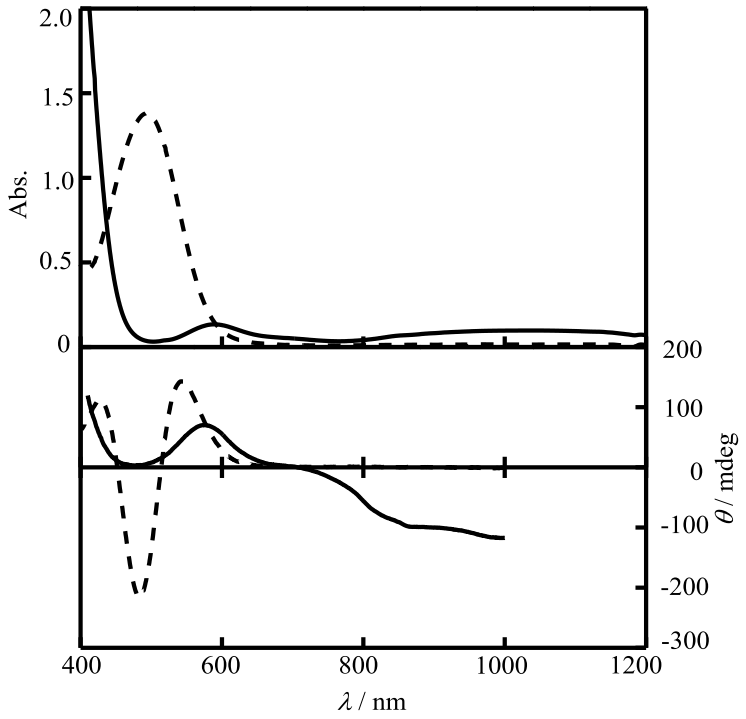

Figure II-12. Electronic absorption and CD spectra of ethanolic solution containing [**5a**] (solid line) and $[H_2\mathbf{5a'}]^{2+}$ generated from the reaction of [**5a**] with 2 molar equiv of triflic acid (dashed line).

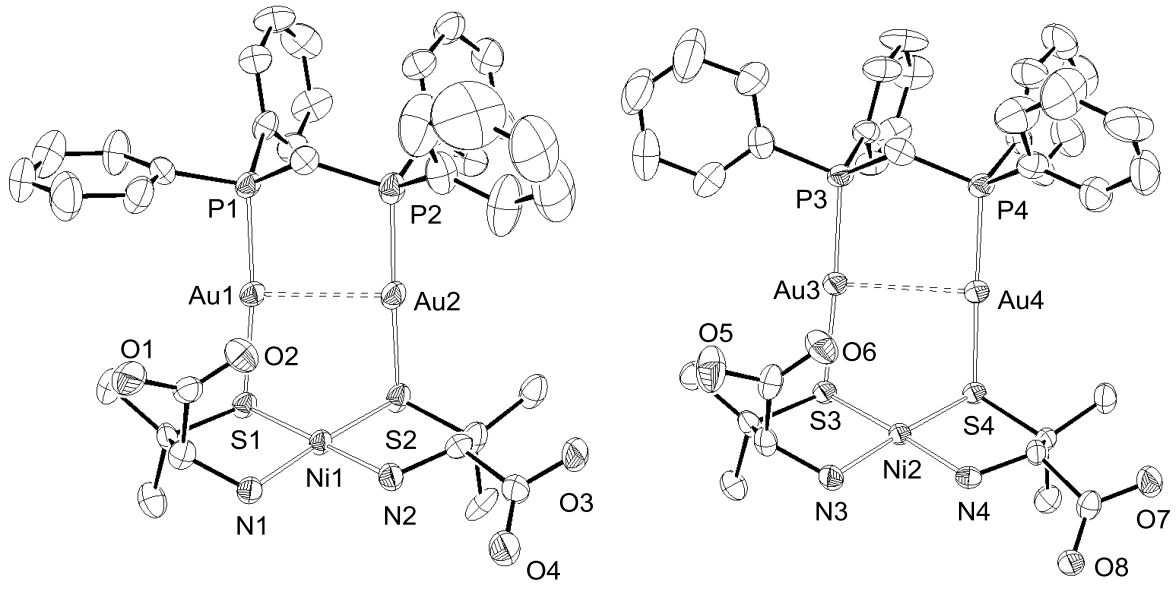

Figure II-13. ORTEP drawings of complex cations in $[H_{1.5}\mathbf{5a'}](Et_4N)_{0.5}Cl_2$ with 50% probability level of thermal ellipsoids. H atoms are omitted for clarity.

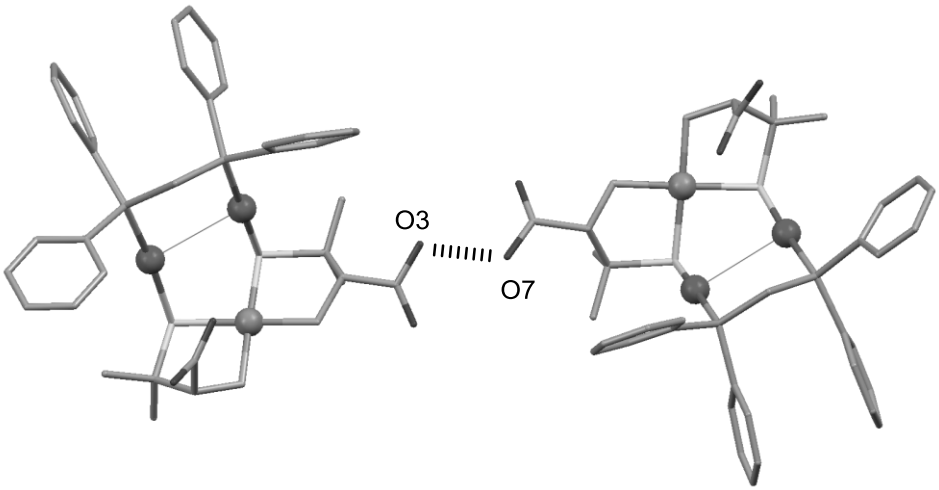

Figure II-14. Hydrogen-bonded dimer of $[H_{1.5}\mathbf{5a'}]^{1.5+}$. H atoms are omitted for clarity. Hydrogen bonds are depicted with dashed lines.

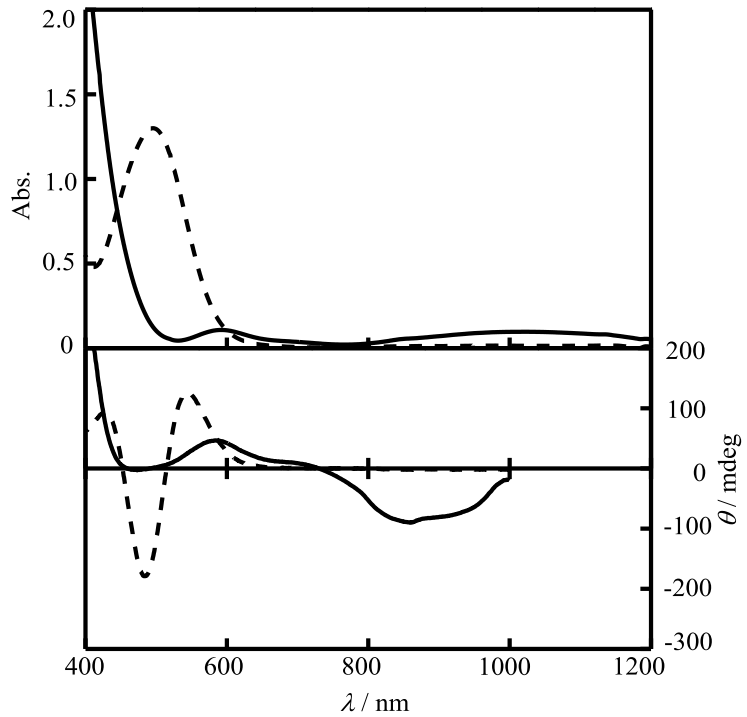

Figure II-15. Electronic absorption and CD spectra of ethanolic solution containing [**6a**]Cl (solid line) and [**6a**]Cl with 2 molar equiv of triflic acid (dashed line).

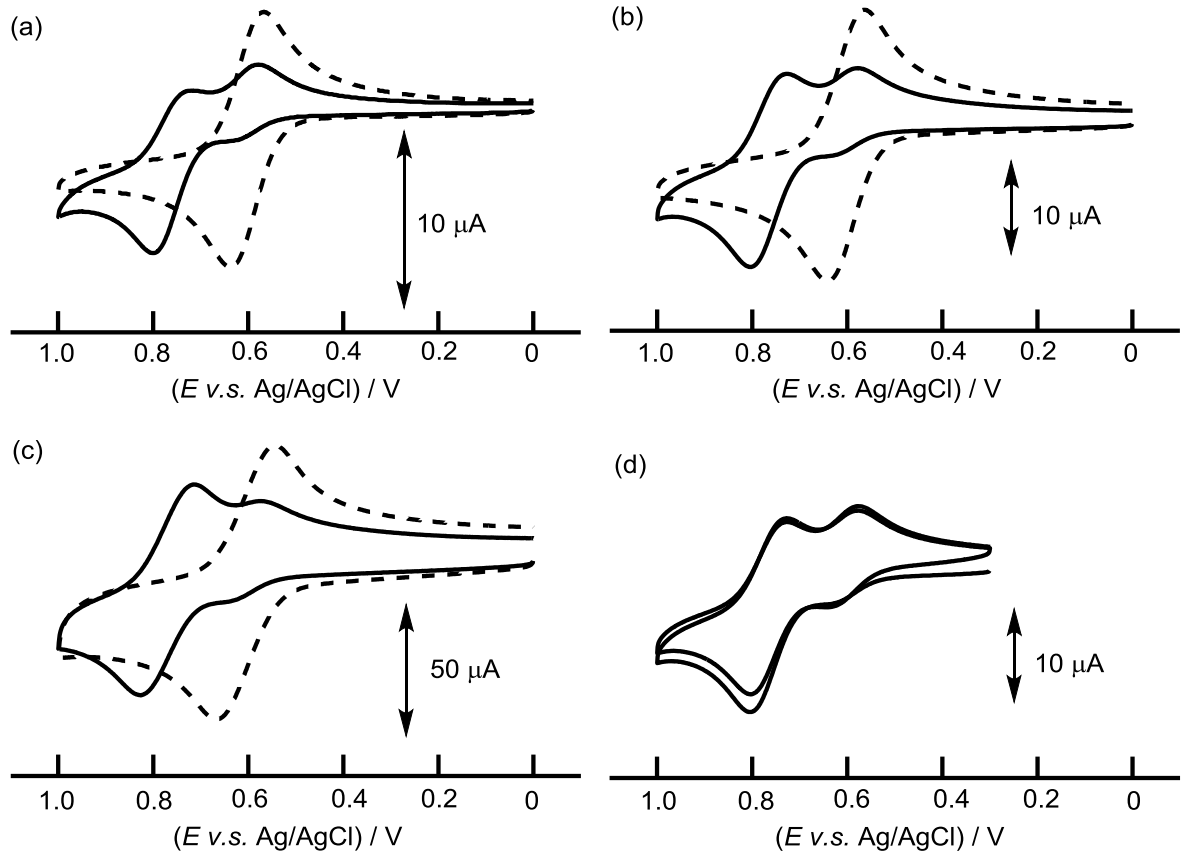

Figure II-16. Cyclic voltammogram of [**5a**] (dashed line) and [**6a**]Cl (solid line) in methanol containing 0.1 M Bu_4NPF_6 at rate of (a) 0.03 V/s, (b) 0.1 V/s, (c) 1.0 V/s, and (d) 0.1 V/s with repeating 2 cycles.

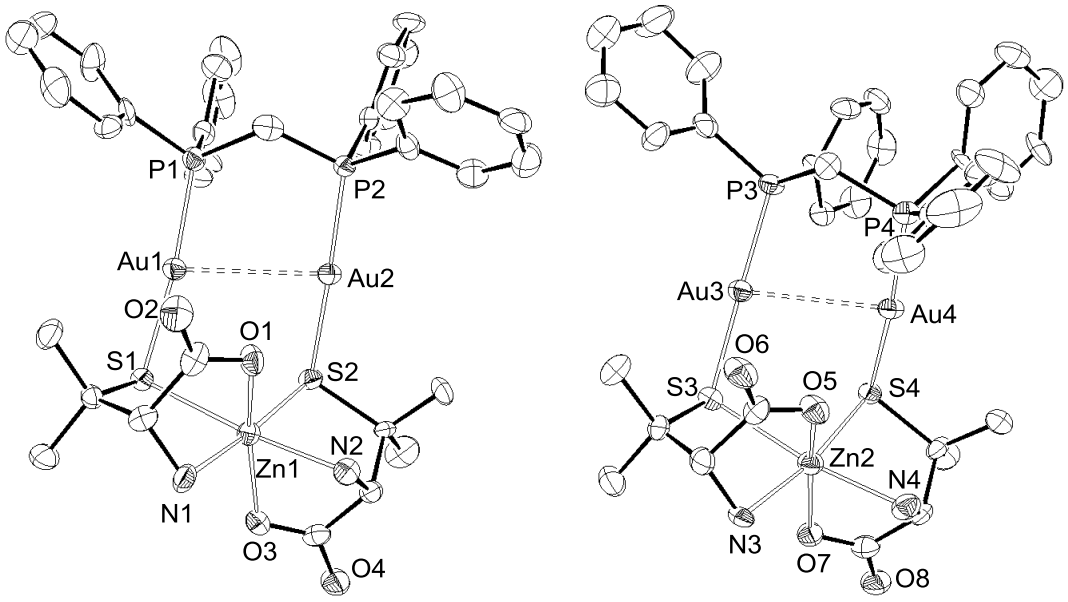

Figure II-17. ORTEP drawings of [**5b**] with 50% probability level of thermal ellipsoids. H atoms are omitted for clarity.

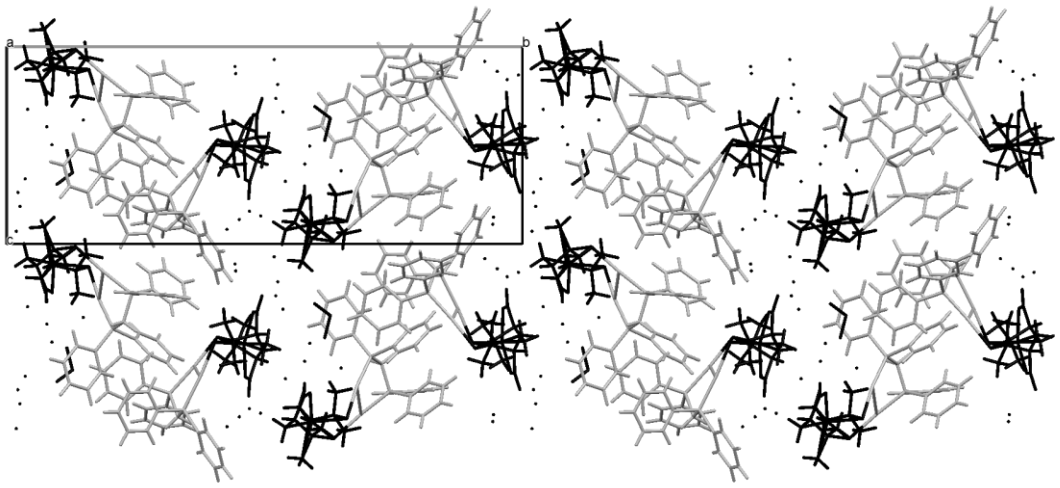

Figure II-18. Packing diagram of [**5b**] viewed along *a* axis. $\{Zn^{II}(D\text{-pen})_2\}^{2-}$ moieties, water, and ethanol molecules are shown with black sticks and $\{Au^{I}_2(dppm)\}^{2+}$ moieties are shown with gray sticks.

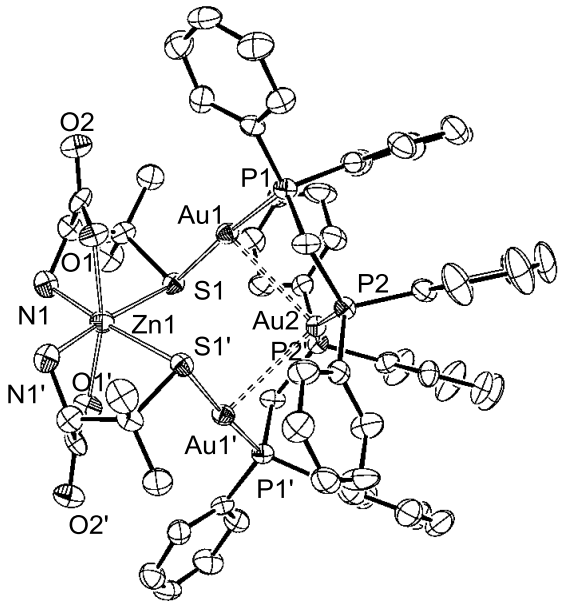

Figure II-19. ORTEP drawing of the entire complex cation in [**6b**]Cl with 50% probability level of thermal ellipsoids. H atoms are omitted for clarity. Symmetry code ('): 1–x, –y, z.

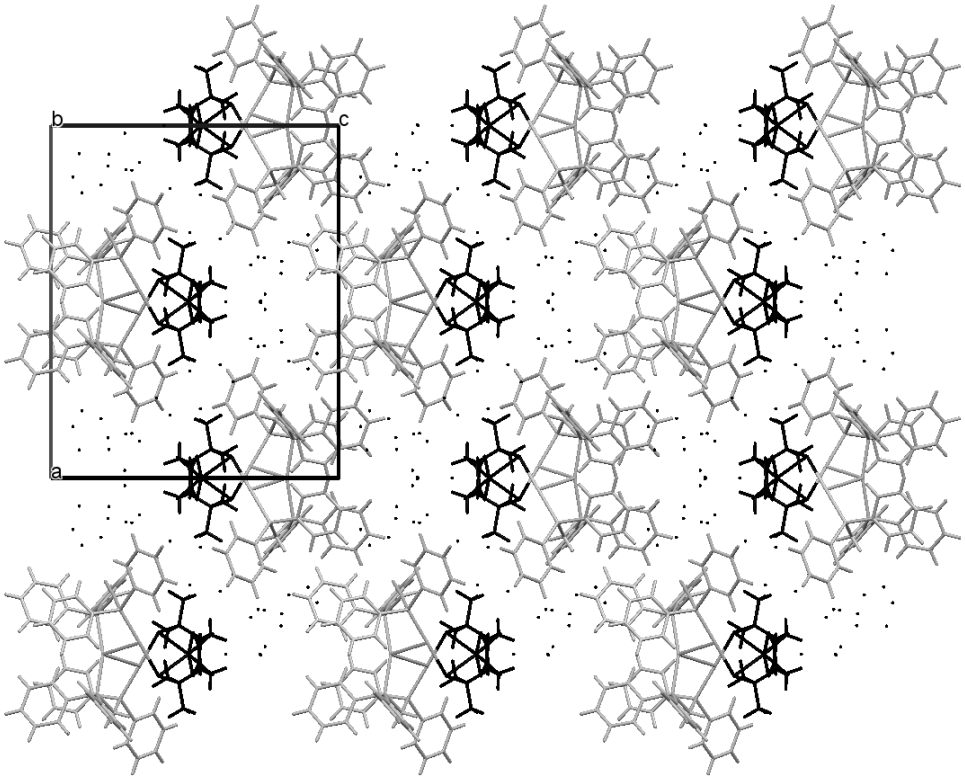

Figure II-20. Packing diagram of [**6b**]Cl viewed along *b* axis. $\{Zn^{II}(D\text{-pen})_2\}^{2-}$ moieties, Cl^- anions, and water molecules are shown with black sticks and $\{Au^{I}_3(dppm)_2\}^{3+}$ moieties are shown with gray sticks.

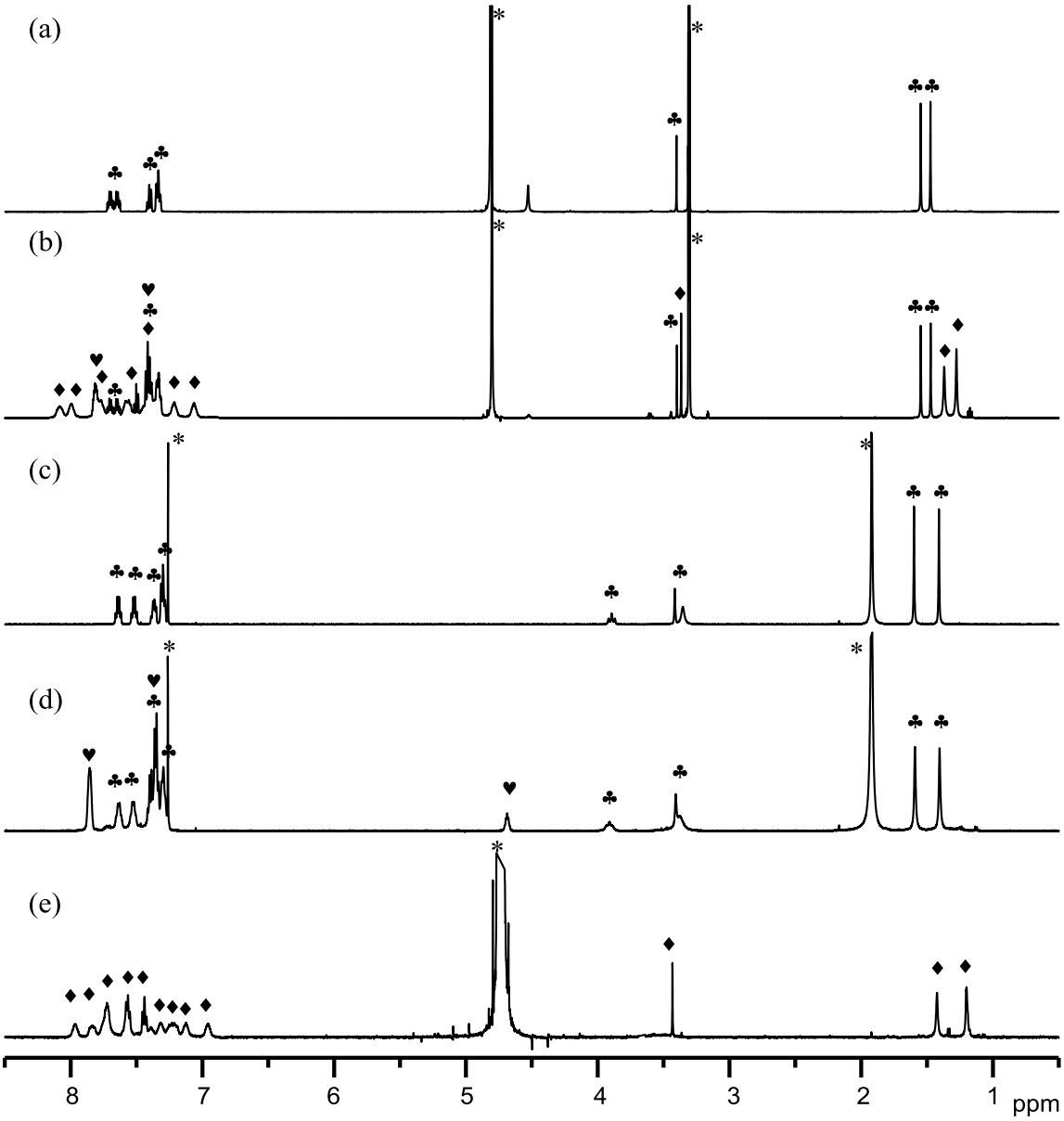

Figure II-21. ^{1}H NMR spectra of (a) [**5b**] and (b) [**6b**]Cl in methanol-d_4, (c) [**5b**] and (d) [**6b**]Cl in chloroform-*d*, and (e) [**6b**]Cl in D_2O. The symbols of club (♣), diamond (♦), and heart (♥) indicate the signals from [**5b**], [**6b**]Cl, and $[Au^{I}_{2}(dppm)_2]Cl_2$, respectively. (*) denotes the signals from solvents.

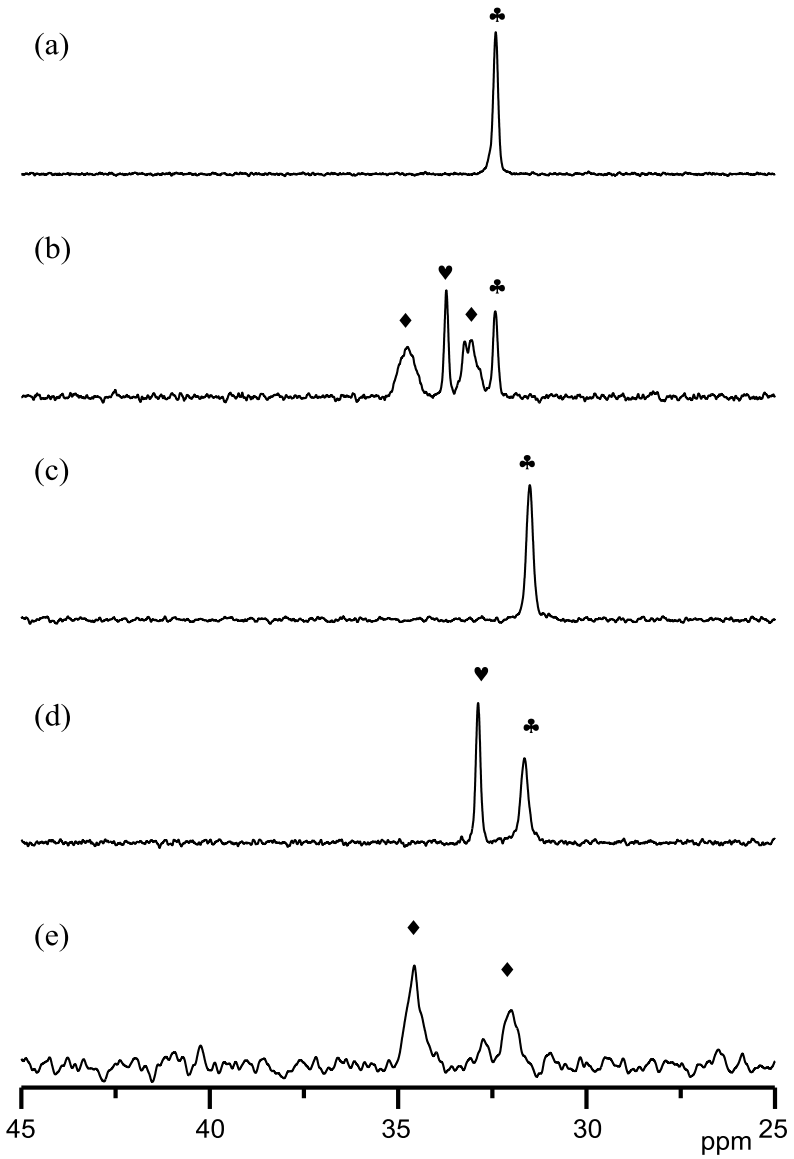

Figure II-22. ^{31}P NMR spectra of (a) [**5b**] and (b) [**6b**]Cl in methanol-d_4, (c) [**5b**] and (d) [**6b**]Cl in chloroform-*d*, and (d) [**6b**]Cl in D_2O. The symbols of club (♣), diamond (♦), and heart (♥) indicate the signals from [**5b**], [**6b**]Cl, and $[Au^{I}_{2}(dppm)_2]Cl_2$, respectively.

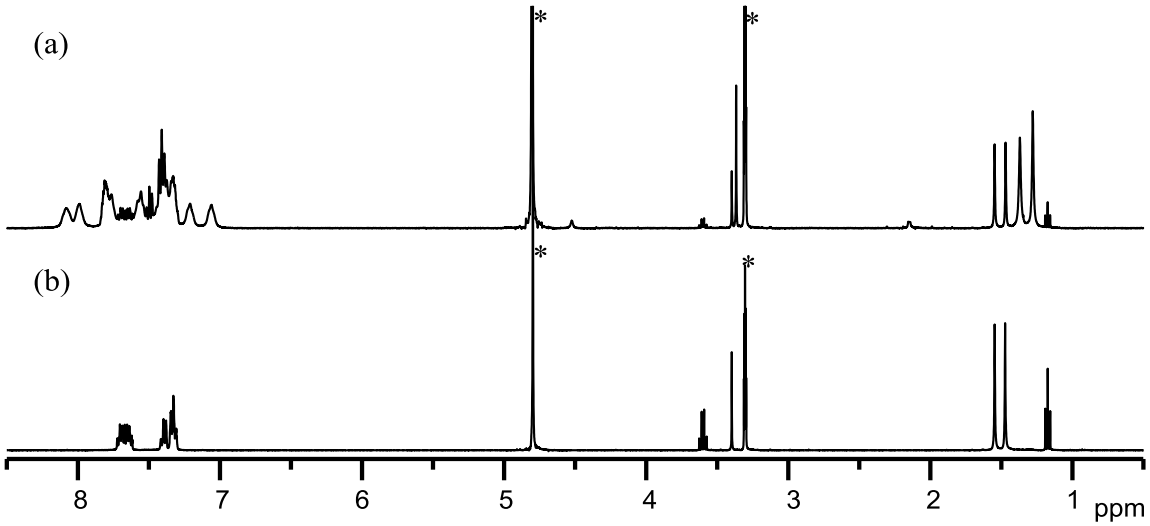

Figure II-23. ^{1}H NMR spectra of (a) reaction solution of [**5b**] with $[Au^{I}_{2}(dppm)_{2}]Cl_{2}$ and (b) reaction solution of [**5b**]Cl with $NH_{4}[Au^{I}(D\text{-}Hpen)_{2}]$ and $Zn^{II}Cl_{2}$ in methanol-d_4. (*) denotes the signals from solvents.

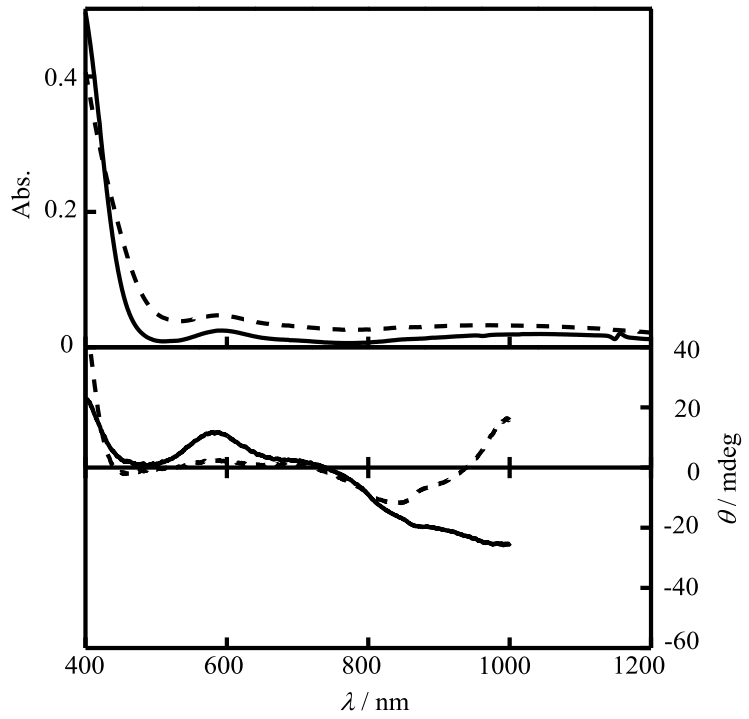

Figure II-24. Electronic absorption and CD spectra of [**6a**]Cl in chloroform (solid line) and in water (dashed line).

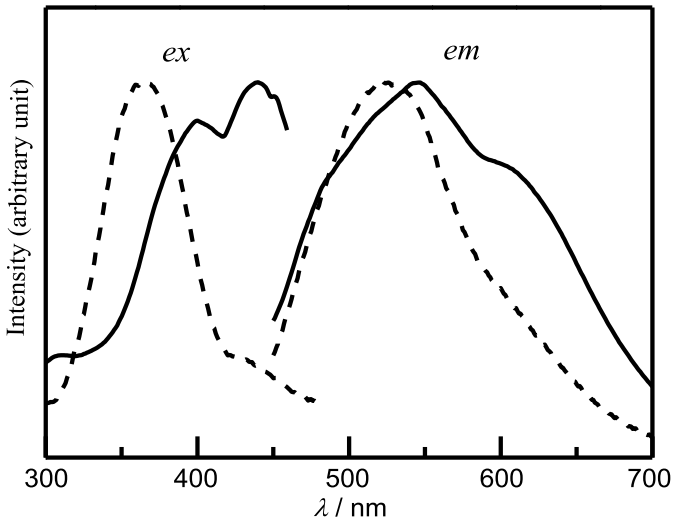

Figure II-25. Solid-state emission (*em*) and excitation (*ex*) spectra of [**5b**] (solid line) and [**6b**]Cl (dashed line) at ambient temperature.

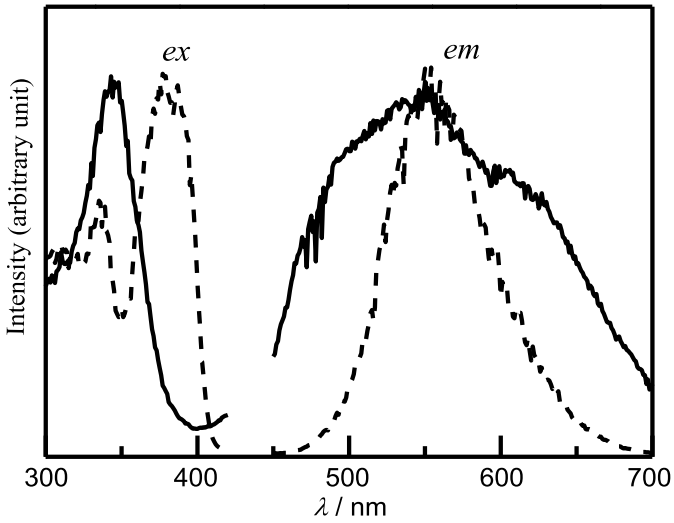

Figure II-26. Solid-state emission (*em*) and excitation (*ex*) spectra of [H_2**3**] (solid line) and [H**4**] (dashed line) at 77 K.

Table II-1. Crystallographic data for [H**4**], [**5a**], and [**6a**]Cl.

	[H**4**]·10H_2O	[**5a**]·7H_2O·0.5EtOH	[**6a**]Cl·17H_2O
empirical formula	$C_{60}H_{83}Au_3N_2O_{14}P_4S_2$	$C_{36}H_{57}Au_2N_2NiO_{11.5}P_2S_2$	$C_{60}H_{96}Au_3ClN_2NiO_{21}P_4S_2$
formula weight	1835.25	1280.54	2054.45
color, form	colorless, platelet	green, block	green, rod
crystal size /mm^3	0.20 × 0.06 × 0.03	0.15 × 0.15 × 0.02	0.10 × 0.10 × 0.10
crystal system	triclinic	monoclinic	orthorhombic
space group	*P*1	$P2_1$	$P2_12_12$
a/ Å	13.0361(7)	11.6706(4)	20.4371(6)
b/ Å	15.7152(9)	31.7998(11)	11.5371(4)
c/ Å	18.9419(11)	12.7354(5)	16.7630(6)
α (°)	66.1100(10)	90	90
β (°)	75.9380(10)	105.9110(10)	90
γ (°)	85.651(2)	90	90
V/ $Å^3$	3440.6(3)	4545.3(3)	3952.5(2)
Z	2	4	2
T/ K	200(2)	200(2)	200(2)
ρ_{calcd}/ g cm^{-3}	1.771	1.871	1.726
μ(Mo Kα)/ mm^{-1}	6.594	7.068	6.018
R_1[a] ($I>2\sigma(I)$)	0.0838	0.0385	0.0360
wR_2[b] (all data)	0.2392	0.0813	0.0695
flack parameter	0.014(12)	0.004(3)	-0.008(5)

[a] $R_1 = (\Sigma(|(|F_o| - c|F_c|)|)/(\Sigma|F_o|)$

[b] $wR_2 = [\{\Sigma w(F_o^2 - cF_c^2)^2\}/(\Sigma w|F_o^2|^2)]^{1/2}$

Table II-2. Crystallographic data for $[H_{1.5}$**5a'**$](Et_4N)_{0.5}Cl_2$, [**5b**], and [**6b**]Cl.

	$[H_{1.5}$**5a'**$](Et_4N)_{0.5}Cl_2 \cdot H_2O \cdot EtOH$	[**5b**]$\cdot 7H_2O \cdot 0.5EtOH$	[**6b**]$Cl \cdot 17H_2O$
empirical formula	$C_{41}H_{55.5}Au_2Cl_2N_{2.5}NiO_{6.5}P_2S_2$	$C_{36}H_{57}Au_2N_2O_{11.5}P_2S_2Zn$	$C_{60}H_{96}Au_3ClN_2O_{21}P_4S_2Zn$
formula weight	1336.98	2574.40	2061.11
color, form	red, platelet	colorless, block	colorless, rod
crystal size /mm^3	0.35 × 0.20 × 0.02	0.10 × 0.10 × 0.05	0.15 × 0.07 × 0.07
crystal system	monoclinic	Monoclinic	orthorhombic
space group	$P2_1$	$P2_1$	$P2_12_12$
a/ Å	11.7260(3)	11.7463(6)	20.5318(5)
b/ Å	24.3570(7)	31.863(2)	11.5885(2)
c/ Å	17.8925(5)	12.6664(9)	16.7656(4)
α (°)	90	90	90
β (°)	91.2890(10)	105.994(2)	90
γ (°)	90	90	90
V/ Å^3	5109.0(2)	4557.1(5)	3989.09(15)
Z	4	4	2
T/ K	200(2)	200(2)	200(2)
ρ_{calcd}/ g cm^{-3}	1.738	1.876	1.716
μ(Mo Kα)/ mm^{-1}	6.387	7.163	6.027
R_1[a] ($I>2\sigma(I)$)	0.0463	0.0665	0.0313
wR_2[b] (all data)	0.1009	0.1354	0.0758
flack parameter	0.005(4)	0.013(6)	0.007(6)

[a] $R_1 = (\Sigma|(|F_o| - c|F_c|)|)/(\Sigma|F_o|)$

[b] $wR_2 = [\{\Sigma w(F_o^2 - cF_c^2)^2\}/(\Sigma w|F_o^2|^2)]^{1/2}$

Table II-3. Selected bond distances (Å) and angles (°) for [H**4**].

		distances (Å)	
Au1–Au2	3.0189(4)	Au4–Au5	2.9932(4)
Au1–P1	2.281(2)	Au4–P5	2.252(2)
Au1–S1	2.288(2)	Au4–S3	2.276(2)
Au2–Au3	3.0727(3)	Au5–Au6	3.0217(3)
Au2–P2	2.325(2)	Au5–P6	2.310(2)
Au2–P3	2.312(2)	Au5–P7	2.323(2)
Au3–P4	2.278(2)	Au6–P8	2.280(2)
Au3–S2	2.292(2)	Au6–S4	2.294(2)
		angles (°)	
P1–Au1–S1	177.03(7)	P5–Au4–S3	176.51(9)
Au1–Au2–Au3	75.53(1)	Au4–Au5–Au6	75.48(1)
P2–Au2–P3	156.08(6)	P6–Au5–P7	154.52(7)
P4–Au3–S2	177.64(7)	P8–Au6–S4	176.20(7)

Table II-4. Selected bond distances (Å) and angles (°) for [**5a**].

		distances (Å)	
Au1–Au2	3.1507(3)	Au3–Au4	3.1184(3)
Au1–P1	2.2702(16)	Au3–P3	2.2715(17)
Au1–S1	2.3268(16)	Au3–S3	2.3180(16)
Au2–P2	2.2708(16)	Au4–P4	2.2600(17)
Au2-S2	2.3165(16)	Au4–S4	2.3075(16)
Ni1–N1	2.059(5)	Ni2–N3	2.086(5)
Ni1–N2	2.073(5)	Ni2–N4	2.085(5)
Ni1–O1	2.096(4)	Ni2–O5	2.089(5)
Ni1–O3	2.110(5)	Ni2–O7	2.076(4)
Ni1–S1	2.4431(17)	Ni2–S3	2.4284(17)
Ni1–S2	2.4146(16)	Ni2–S4	2.4207(17)
		angles (°)	
P1–Au1–S1	173.73(5)	P3–Au3–S3	175.30(6)
P2–Au2–S2	176.04(6)	P4–Au4–S4	173.02(6)
N1–Ni1–N2	98.1(2)	N3–Ni2–N4	101.8(2)
N1–Ni1–O1	77.70(19)	N3–Ni2–O5	76.92(19)
N1–Ni1–O3	94.75(18)	N3–Ni2–O7	94.86(19)
N1–Ni1–S1	84.74(14)	N3–Ni2–S3	84.61(15)
N1–Ni1–S2	177.36(14)	N3–Ni2–S4	174.53(15)
N2–Ni1–O1	91.31(19)	N4–Ni2–O5	94.9(2)
N2–Ni1–O3	78.5(2)	N4–Ni2–O7	78.9(2)
N2–Ni1–S1	176.81(16)	N4–Ni2–S3	173.47(16)
N2–Ni1–S2	84.48(15)	N4–Ni2–S4	83.57(16)
O1–Ni1–O3	166.46(18)	O5–Ni2–O7	168.58(19)
O1–Ni1–S1	87.97(13)	O5–Ni2–S3	87.59(13)
O1–Ni1–S2	101.97(12)	O5–Ni2–S4	101.88(13)
O3–Ni1–S1	102.66(13)	O7–Ni2–S3	99.65(13)
O3–Ni1–S2	86.08(12)	O7–Ni2–S4	87.03(13)
S1–Ni1–S2	92.63(6)	S3–Ni2–S4	90.01(6)

Table II-5. Selected bond distances (Å) and angles (°) for [**6a**]Cl.

		distances (Å)	
Au1–Au2	2.9774(3)	Ni1–N1	2.061(4)
Au1–P1	2.2737(14)	Ni1–O1	2.076(3)
Au1–S1	2.3262(13)	Ni1–S1	2.4624(15)
Au2–P2	2.3347(12)		
		angles (°)	
P1–Au1–S1	174.30(5)	N1–Ni1–S1	82.24(13)
P2–Au2–P2'	162.49(6)	N1–Ni1–S1'	177.48(13)
Au1–Au2–Au1'	88.827(10)	O1–Ni1–O1'	167.7(2)
N1–Ni1–N1'	100.1(3)	O1–Ni1–S1	87.72(11)
N1–Ni1–O1	78.42(16)	O1–Ni1–S1'	100.58(10)
N1–Ni1–O1'	93.65(16)	S1–Ni1–S1'	95.43(7)

Symmetry code('): 1–x, –y, z

Table II-6. Selected bond distances (Å) and angles (°) for $[H_{1.5}\mathbf{5a'}](Et_4N)_{0.5}Cl_2$.

		distances (Å)	
Au1–Au2	2.9275(4)	Au3–Au4	2.9963(4)
Au1–P1	2.265(2)	Au3–P3	2.2766(19)
Au1–S1	2.3254(19)	Au3–S3	2.3283(18)
Au2–P2	2.271(2)	Au4–P4	2.2749(19)
Au2–S2	2.332(2)	Au4–S4	2.3284(18)
Ni1–N1	1.925(6)	Ni2–N3	1.938(6)
Ni1–N2	1.940(6)	Ni2–N4	1.936(6)
Ni1–S1	2.192(2)	Ni2–S3	2.1911(19)
Ni1–S2	2.177(2)	Ni2–S4	2.168(2)
O1–C3	1.305(10)	O5–C38	1.321(9)
O2–C3	1.212(9)	O6–C38	1.217(10)
O3–C8	1.308(9)	O7–C43	1.281(9)
O4–C8	1.197(9)	O8–C43	1.210(9)
Ni1···O2	2.9753(58)	Ni2···O6	3.1359(60)
		angles (°)	
P1–Au1–S1	172.40(7)	P3–Au3–S3	177.06(7)
P2–Au2–S2	176.52(7)	P4–Au4–S4	174.11(7)
N1–Ni1–N2	90.9(2)	N3–Ni2–N4	90.2(2)
N1–Ni1–S1	88.25(19)	N3–Ni2–S3	88.89(18)
N1–Ni1–S2	175.5(2)	N3–Ni2–S4	176.75(19)
N2–Ni1–S1	179.0(2)	N4–Ni2–S3	176.99(19)
N2–Ni1–S2	88.53(19)	N4–Ni2–S4	88.22(17)
S1–Ni1–S2	92.36(8)	S3–Ni2–S4	92.51(7)

Table II-7. Selected bond distances (Å) and angles (°) for [**5b**].

		distances (Å)	
Au1–P1	2.269(4)	Au3–P3	2.275(4)
Au1–S1	2.322(4)	Au3–S3	2.310(4)
Au1–Au2	3.1598(7)	Au3–Au4	3.1137(6)
Au2–P2	2.271(4)	Au4–P4	2.262(4)
Au2–S2	2.316(4)	Au4–S4	2.312(4)
Zn1–N1	2.10(1)	Zn2–N3	2.152(9)
Zn1–N2	2.13(1)	Zn2–N4	2.135(9)
Zn1–O1	2.152(9)	Zn2–O5	2.14(1)
Zn1–O3	2.150(9)	Zn2–O7	2.11(1)
Zn1–S1	2.522(3)	Zn2–S3	2.514(3)
Zn1–S2	2.494(3)	Zn2–S4	2.528(3)
		angles (°)	
P1–Au1–S1	173.4(1)	P3–Au3–S3	175.7(1)
P2–Au2–S2	176.2(1)	P4–Au4–S4	172.6(1)
N1–Zn1–N2	102.0(4)	N3–Zn2–N4	108.3(4)
N1–Zn1–O1	75.6(4)	N3–Zn2–O5	75.3(4)
N1–Zn1–O3	94.8(4)	N3–Zn2–O7	94.2(4)
N1–Zn1–S1	83.3(3)	N3–Zn2–S3	82.6(3)
N1–Zn1–S2	175.0(3)	N3–Zn2–S4	169.9(3)
N2–Zn1–O1	90.8(4)	N4–Zn2–O5	94.8(4)
N2–Zn1–O3	76.2(4)	N4–Zn2–O7	77.6(4)
N2–Zn1–S1	174.1(3)	N4–Zn2–S3	169.0(3)
N2–Zn1–S2	83.0(3)	N4–Zn2–S4	81.7(3)
O1–Zn1–O3	162.1(4)	O5–Zn2–O7	164.5(4)
O1–Zn1–S1	88.0(3)	O5–Zn2–S3	88.0(3)
O1–Zn1–S2	104.4(3)	O5–Zn2–S4	105.2(3)
O3–Zn1–S1	106.2(2)	O7–Zn2–S3	102.0(3)
O3–Zn1–S2	86.5(3)	O7–Zn2–S4	87.2(3)
S1–Zn1–S2	91.8(1)	S3–Zn2–S4	87.3(1)

Table II-8. Selected bond distances (Å) and angles (°) for [**6b**]Cl.

		distances (Å)	
Au1–Au2	2.9929(3)	Zn1–N1	2.127(5)
Au1–P1	2.271(1)	Zn1–O1	2.113(4)
Au1–S1	2.318(1)	Zn1–S1	2.560(1)
Au2–P2	2.336(1)		
		angles (°)	
P1–Au1–S1	174.99(5)	N1–Zn1–S1	80.5(1)
P2–Au2–P2'	162.52(5)	N1–Zn1–S1'	174.3(1)
Au1–Au2–Au1'	89.53(1)	O1–Zn1–O1'	165.8(1)
N1–Zn1–N1'	105.2(2)	O1–Zn1–S1	87.5(1)
N1–Zn1–O1	77.2(2)	O1–Zn1–S1'	102.2(1)
N1–Zn1–O1'	94.1(2)	S1–Zn1–S1'	93.86(5)

Symmetry code('): 1–x, –y, z

Table II-9. Electronic absorption and CD spectral data of [**5a**] and [**6a**]Cl. (sh = shoulder)

absorption maxima: σ / 10^3 cm^{-1} ($\log(\varepsilon$ / mol^{-1} dm^3 cm^{-1}))		CD extrema: σ / 10^3 cm^{-1} ($\Delta\varepsilon$ / mol^{-1} dm^3 cm^{-1})	
[**5a**] in ethanol			
9.80	(0.939)	11.48	(–0.23)
16.98	(1.091)	17.36	(–0.16)
25.77	(2.364)	25.69	(+0.43)
38.31	(4.297)	30.12	(–0.70)
44.4	(4.58)sh	34.92	(–6.60)
		41.67	(+24.38)
		46.30	(–37.19)
[**6a**]Cl in ethanol			
9.80	(0.984)	11.61	(–0.22)
16.86	(1.064)	17.53	(–0.11)
25.9	(2.31)sh	25.61	(+0.92)
34.1	(4.20)sh	33.31	(+30.28)
38.3	(4.47)sh	38.11	(–12.91)
44.2	(4.85)sh	40.32	(+4.26)
		44.17	(–67.26)

Table II-10. Luminescent properties of [H_2**3**], [H**4**], [**5b**], and [**6b**]Cl in the solid state at ambient temperature.

complex	emission maxima: λ / nm [a]	lifetime: τ / μs [b]	quantum yield: Φ [c]
[H_2**3**]	546	0.024 (86%), 0.47 (11%), 3.4 (3%)	0.004
[H**4**]	554	0.023 (91%), 0.32 (7%), 3.6(2%)	< 0.001
[**5b**]	546	0.049 (76%), 0.54 (27%), 4.3 (7%)	0.033
[**6b**]Cl	522	0.61 (51%), 2.9 (36%), 12 (13%)	0.13

[a] The excitation wavelength was set to 400 nm.

[b] Determined with excitation at 355 nm. A value in parenthesis denotes the fraction of each component in triple exponential decay.

[c] Error ± 10%

Chapter III. Triphosphine System.

III-1. Introduction.

Raising again the number of phosphorus donors in a phosphine ligand from Chapter II, a coordination system with a triphosphine is demonstrated in this chapter. The use of a triphosphine permits a new class of gold(I) metalloligands possessing three SAAs functional arms, and the presence of three arms in the metalloligand is the most characteristic feature compared with the already presented metalloligands with diphosphines and the traditional non-phosphine metalloligand, $[Au^{I}(D\text{-pen})_2]^{3-}$.[1,2] Increase in the number of SAAs arms in a metalloligand is one of the straightforward improvements from non-phosphine systems in order to produce more versatile metalloligands, which can assemble more metal ions and can coordinate in a variety of possible coordination modes.[3] In addition, connecting of building blocks with three or more arms often produces closed three-dimensional structures such as a cage or extended two- or three-dimensional infinite structures,[4,5] which are potential candidates of functional materials for molecular recognition and sensing,[4b,5b,e] storage and separation of chemicals, [5b-d] template and catalyst for specific reactions,[4a,5b-d] and stabilization of highly reactive molecules,[4b] by using their internal spaces, while closed two-dimensional structures such as a ring or one-dimensional polymeric structures are derived from building blocks with two arms.[1,4b,c,5a,6]

Herein, 1,1,1-tris(diphenylphosphinomethyl)ethane (tdme) was chosen as a triphosphine ligand to achieve the metalloligand with three D-pen arms. This C_{3v}-symmetrical triphosphine has a relatively simple tripodal structure with three equivalent arms, whose phosphorus donors are separated to each other by three carbon atoms only via single bonds, providing moderate flexibility of the metalloligand to allow various coordination modes. As a part of studying on the applicative aspects of the coordination system with mixed SAAs and polyphosphines, the coordination behavior of a tripod-type trigold(I) metalloligand with tdme, $[Au^{I}_3(tdme)(D\text{-pen})_3]^{3-}$ ($[\mathbf{7}]^{3-}$), to cobalt ion was investigated.

A variety of oxidation states ranging from –I to +V, +II and +III states have been well known for cobalt,[7] and their natures are very different from each other because of the number of 3d electrons. Cobalt(III) prefers to form a low-spin complex in an octahedral coordination environment with a large ligand-field stabilization energy (LFSE) due to six 3d electrons and a higher positive charge. Therefore, the low-spin cobalt(III) complexes commonly exhibit particularly inert character on ligand substitution reactions among the first row transition metal complexes.[7,8] Because of their inertness and rich spectroscopic information for the ligand field, a huge number of cobalt(III) complexes have been synthesized through the ages. In contrast, +II state of cobalt with seven 3d electrons is commonly found in coordination compounds with a weaker ligand field, which is often

formed by a tetrahedral or distorted-octahedral geometry, and cobalt(II) ions tend to be in a high-spin state even in octahedral environments due to the weaker field. Thus, cobalt(II) complexes generally show features of lability, a smaller LFSE, and magnetism. Therefore, when a cobalt ion is in an octahedral environment with strong donors, such as amines and thiolates, a more stable oxidation state of a cobalt ion should be +III rather than +II under aerobic conditions. Actually, almost the octahedral cobalt complexes with a saturated aliphatic thiolate without neighboring electron-withdrawing groups reported in the past have low-spin cobalt(III) centers, and isolated octahedral cobalt(II) complexes with saturated aliphatic thiolates are limited to only a few structurally undetermined examples with aqua ligand occupying two or more coordination sites.[9] In addition, this trend remains in complexes with gold(I) ion binding to thiolate donors: That is, only cobalt(III) species were isolated from all the reactions of $[Au^{I}(D\text{-pen})_2]^{3-}$,[10] $[Au^{I}_2(dppe)(D\text{-pen})_2]^{2-}$,[2c,d] and $[Au^{I}(PPh_3)(D\text{-pen})]^{-}$ [11] with cobalt(II) ion under aerobic conditions.

Surprisingly, however, it was found that the reaction of $[\mathbf{7}]^{3-}$ with cobalt(II) ion produced a quite air-stable cobalt(II) complex even under aerobic conditions. Oxidation state of cobalt ion in the product was confirmed by the UV-vis and NMR spectra, the magnetic susceptibility measurement, and the crystal-structural analysis. The anomalous formation and stability of the Au^{I}-Co^{II} oxidation state is explained by the notable coordination ability of $[\mathbf{7}]^{3-}$ originated from its characteristic tripodal structure, on the basis of the structural and spectroscopic features of the Au^{I}-Co^{II} complex and its cobalt(III) derivative, together with the electrochemical measurements. In addition, the coordination versatility of $[\mathbf{7}]^{3-}$ is also discussed through the formation of another Au^{I}-Co^{III} complex from the reaction of $[H_3\mathbf{7}]$ with cobalt(III) ion.

III-2. Experimental section.

III-2-1. Materials. Complexes $[Au_3(tdme)Cl_3]$ [12] and $K_3[Co(CO_3)_3]$ [13] were prepared according to literature methods. All other chemicals were commercially available and used without further purification.

III-2-2. Synthesis of Au^{I} metalloligand with tdme: $[Au^{I}_3(tdme)(D\text{-Hpen})_3]$ ($[H_3\mathbf{7}]$).

To a white suspension containing 2.00 g (1.51 mmol) of $[Au_3(tdme)Cl_3]$ in 100 mL of ethanol was added 0.68 g (4.6 mmol) of D-H_2pen. The mixture was stirred at room temperature for 1 h, which gave a colorless solution with a small amount of white solid of unreacted D-H_2pen, which was removed by filtration. After addition of 45 mL (4.5 mmol) of an aqueous NaOH solution (0.10 M), the colorless solution was concentrated, giving a white powder. The white powder was washed with 40 mL of water three times and dried *in vacuo*. Yield: 2.37 g (90%). Anal. Found: C, 38.34; H, 4.49; N, 2.38%. Calcd for

$[Au_3(tdme)(D\text{-}Hpen)_3]\cdot 5H_2O$ = $C_{56}H_{79}N_3O_{11}P_3S_3Au_3$: C, 38.43; H, 4.55; N, 2.40%. IR spectrum (cm^{-1}, KBr disk): 1627 (ν_{COO}). ^1H NMR spectrum (ppm from TMS, methanol-d_4): δ 0.99 (s, 3H), 1.33 (s, 9H), 1.67 (s, 9H), 3.47 (s, 3H), 3.18-3.28 (m, 6H), 7.53-7.54 (m, 18H), 7.65-7.70 (m, 6H), 7.76-7.80 (m, 6H). ^{31}P NMR spectrum (ppm from H_3PO_4, methanol-d_4): δ 22.1 (s).

III-2-3. Reactions of Au^I metalloligand with cobalt ion.

(a) Synthesis of $[Co^{II}_3\{Au^I_3(tdme)(D\text{-}pen)_3\}_2]$ ([8]). A white suspension containing 0.50 g (0.29 mmol) of $[H_3\mathbf{7}]\cdot 5H_2O$ in 50 mL of ethanol turned to a colorless clear solution on the addition of 8.6 mL (0.86 mmol) of an aqueous NaOH solution (0.10 M). To the resulting colorless solution was added 0.11 g (0.44 mmol) of $Co(CH_3COO)_2\cdot 4H_2O$, which gave an orange solution. Diethyl ether vapor was diffused into the orange-brown solution over 2 weeks, and brown crystals appeared. After the removal of the supernatant by decantation, the crystals were washed with a small amount of acetone and collected by filtration. Yield 0.33 g (60%). Anal. Found: C, 34.56; H, 4.45; N, 2.18%. Calcd for $[Co_3\{Au_3(tdme)(D\text{-}pen)_3\}_2]\cdot 22H_2O$ = $C_{112}H_{176}N_6O_{34}P_6S_6Co_3Au_6$: C, 34.60; H, 4.56; N, 2.16%. IR spectrum (cm^{-1}, KBr disk): 1594 (ν_{COO}). ^1H NMR spectrum (ppm from TMS, methanol-d_4/D_2O = 1/1): δ –50.9 (s, 3H), –30.6 (s, 3H), –17.6 (s, 3H), 2.2 (s, 3H), 5.0 (s, 9H), 10.9 (s, 3H), 11.4 (s, 6H), 11.8 (s, 6H), 46.0 (s, 9H). ^{31}P NMR spectrum (ppm from H_3PO_4, methanol-d_4/D_2O = 1/1): δ –100.9 (s).

(b) Synthesis of $[Co^{III}\{Au^I_3(tdme)(D\text{-}pen)_3\}]$ ([9]). To a colorless solution containing 0.50 g (0.29 mmol) of $[H_3\mathbf{1}]\cdot 5H_2O$ in mixture of 50 mL of methanol and 50 mL of H_2O was added 0.38 mL (*ca.* 0.29 mmol) of a freshly prepared aqueous solution of $K_3[Co(CO_3)_3]$ (*ca.* 0.75 M), which gave a green suspension. The mixture was stirred at 60°C for 2 days, and gave a purple suspension with a small amount of brown precipitate. The purple suspension was concentrated *in vacuo* to give a purple residue. The residue was suspended in 25 mL of methanol, and a deep purple solution was obtained by filtering off the insoluble pale purple powder, and 20 ml of water was added to the solution. After standing for 3 weeks with slow evaporation, purple needle crystals appeared with a purple-brown powder. The crystals were isolated from the mixture by decantation. Yield: 0.14 g (26%). Anal. Found: C, 35.40; H, 4.42; N, 2.28%. Calcd for $[Co\{Au_3(tdme)(D\text{-}pen)_3\}]\cdot 10H_2O$ = $C_{56}H_{86}N_3O_{16}P_3S_3Co_1Au_3$: C, 35.47; H, 4.57; N, 2.22%. IR spectrum (cm^{-1}, KBr disk): 1600 (ν_{COO}). ^1H NMR spectrum (ppm from TMS, methanol-d_4): δ 1.44 (s, 9H), 1.75 (s, 9H), 1.78 (s, 3H), 2.54 (dd, 3H), 3.33 (s, 3H), 3.53 (t, 3H), 6.51 (dd, 6H), 7.30 (t, 6H), 7.45 (t, 3H), 7.86 (t, 6H), 7.99 (t, 3H), 8.37 (dd, 6H). ^{31}P NMR spectrum (ppm from H_3PO_4, methanol-d_4): δ 22.7 (s).

III-2-4. Synthesis of $[Co^{III}_3\{Au^I_3(tdme)(D\text{-}pen)_3\}_2](NO_3)_3$ ([8'](NO$_3$)$_3$).

To a pale brown solution containing 0.20 g (0.052 mmol) of [**8**]·22H_2O in 30 mL of

methanol was added an orange solution containing 0.088 g (0.16 mmol) of $Ce(NH_4)_2(NO_3)_6$ and 0.25 g (3.1 mmol) of NH_4NO_3 in 30 mL of methanol, which gave a greenish-blue solution, and blue microcrystals began to appear within 5 minutes. The mother liquor was removed by decantation next day. The remaining blue crystals were dissolved in 100 mL of water to give greenish-blue solution. After addition of 13 mL (13 mmol) of an aqueous NH_4NO_3 solution (1.0 M), the solution was kept at room temperature for 1 week, which gave blue block crystals of [**2'**]$(NO_3)_3$. Yield: 0.13 g (59%). Anal. Found: C, 32.16; H, 4.32; N, 3.03%. Calcd for $[Co_3\{Au_3(tdme)(D\text{-}pen)_3\}_2](NO_3)_3\cdot 28H_2O = C_{112}H_{188}N_9O_{49}P_6S_6Co_3Au_6$: C, 32.17; H, 4.53; N, 3.01%. IR spectrum (cm^{-1}, KBr disk): 1647 (ν_{COO}), 1355 (ν_{NO3}). ^1H NMR spectrum (ppm from TMS, methanol-d_4): δ 0.83 (s, 9H), 1.31 (s, 9H), 2.39 (dt, 3H), 3.00 (t, 3H), 3.09 (s, 3H), 3.90 (s, 3H), 6.83 (dd, 6H), 7.43 (td, 6H), 7.58 (dd, 3H), 7.71 (td, 6H), 7.92 (dd, 3H), 8.09 (br, 6H). ^{31}P NMR spectrum (ppm from H_3PO_4, methanol-d_4): δ 13.9 (s).

III-2-5. Physical measurements. The electronic absorption spectra were recorded on a JASCO V-660 spectrophotometer at room temperature. The CD spectra were recorded on a JASCO J-820 spectropolarimeter at room temperature. The IR spectra were recorded on a JASCO FT/IR-4100 spectrometer using KBr disks at room temperature. The ^1H and ^{31}P NMR spectra were measured on a JEOL ECA-500 NMR spectrometer at room temperature using tetramethylsilane (TMS, δ 0.0 ppm) as the internal standard for ^1H NMR and triphenyl phosphate (δ –17.6 ppm) as the external standard for ^{31}P NMR. The X-ray fluorescence spectrometries were performed on a HORIBA MESA-500 or SHIMADZU EDX-720 spectrometer. The elemental analyses (C, H, N) were performed using YANACO CHN coder MT-5 or MT-6. Cyclic voltammetric studies were performed with a BAS CV-600A apparatus by using a glassy-carbon working electrode (3 mmϕ), an Ag/AgCl (3 M NaCl aq.) reference electrode with a salt bridge (0.1 M Bu_4NPF_6 in methanol), and a Pt wire auxiliary electrode. Electrochemical experiments were conducted at room temperature in a methanolic solution of 0.1 M Bu_4NPF_6. The potential of ferrocenium/ferrocene (Fc^+/Fc) couple was + 0.40 V (*v.s.* Ag/AgCl) under this condition. Magnetic susceptibility data was collected on powdered samples on a Quantum Design MPMS SQUID magnetometer at temperatures ranging from 3 to 300 K.

III-2-6. X-ray structural determinations. Single-crystal X-ray diffraction measurements for [**8**]$\cdot 22H_2O\cdot$EtOH, [**8'**]$(NO_3)_3\cdot nH_2O$, and [**9**]$\cdot 16.5H_2O$ were made on a Rigaku RAXIS-RAPID or R-AXIS VII imaging plate diffractometer with graphite-monochromated Mo-Kα radiation at –73°C. The intensity data were collected by the ω scan mode, and were corrected for Lorentz and polarization. Empirical absorption corrections were also applied.

The structure was solved by the direct method with SHELXS-97 [14] All calculations were performed using the Yadokari-XG software package [15] except for refinement, which was

performed using SHELXL-97.[14] For [**8'**]$(NO_3)_3$, since the nitrate anions and solvation molecules could not be modeled, their contribution was excluded using SQUEEZE the subroutine of PLATON program.[16] Hydrogen atoms except those of water molecules were placed at calculated positions but were not refined. All non-hydrogen atoms except those in solvation molecules and a disordered complex cation in [**8'**]$(NO_3)_3$ were refined anisotropically for [**8**]·$22H_2O$·EtOH and [**8'**]$(NO_3)_3$, and Au, Co, P, and S atoms were refined anisotropically and the other atoms were refined isotropically for [**9**]·$16.5H_2O$. Crystal data and selected bond distances and angles are summarized in Tables III-1 – III-4.

III-3. Results and discussion.

III-3-1. Synthesis and characterization of complexes.

(a) Au^I complex ([$H_3$7**]).** The trigold(I) metalloligand with tdme, [H_3**7**] was prepared from its corresponding chlorido precursor, in analogy to the other metalloligands presented in the previous chapters. The reaction of [Au^I_3(tdme)Cl_3] [12] with 3 molar equiv of D-H_2pen in ethanol, followed by the addition of NaOH, gave a colorless solution, from which [H_3**7**] was isolated as a white powder (Scheme III-1). The elemental analytical data of [H_3**7**] were in agreement with the formula of [Au^I_3(tdme)(D-Hpen)$_3$]·$5H_2O$, and the presence of Au atom was confirmed by X-ray fluorescence spectrometry. As shown in Figure III-1, the IR spectrum of [H_3**7**] exhibited a strong absorption band assignable to asymmetric COO^- stretching at 1627 cm^{-1},[17] which indicates that [H_3**7**] has D-$Hpen^-$ in a zwitter ionic form like the other D-penicillaminato gold(I) metalloligands [1,2,11] and free D-H_2pen.[18] The ^{1}H NMR spectrum of [H_3**7**] in methanol-d_4 gave four singlet signals at δ 0.99, 1.33, 1.67 and 3.47 ppm attributed to methyl groups in tdme, and two diastereotopic methyl groups and methine group in D-pen, respectively, and signals from methylene groups in tdme in the region of δ 3.18 - 3.28 ppm and phenyl groups in 7.50 - 7.80 ppm, which are intricately split by spin couplings of ^{1}H-^{1}H and ^{1}H-^{31}P nuclei (Figure III-2). In addition to the single set of D-pen signals in the ^{1}H spectrum, only one resonance observed in the ^{31}P NMR spectrum (δ 22.1 ppm) corresponds to the C_3-symmetrical structure expected for [H_3**7**] (Figure III-3).

(b) Au^I-Co^{II} nonanuclear complex ([8]). In order to investigate the coordination ability of the new tripodal metalloligand [H_3**7**], 2 molar equiv of $Co^{II}(CH_3COO)_2$·$4H_2O$ was reacted in ethanol/water under a normal aerobic condition. In contrast to the case of [**2a**]ClO_4 where the color of the reaction solution changed to dark brown in 2 h, the reaction mixture of [H_3**7**] and $Co^{II}(CH_3COO)_2$ remained pale orange color during crystallization by vapor diffusion of diethyl ether into the mixture, and then brown platelet crystals ([**8**]·$22H_2O$) were obtained from it (Scheme III-1). The elemental analytical data of the crystals indicated the formula of [Co_3{Au_3(tdme)(D-pen)$_3$}$_2$]·$22H_2O$, which means that the complex [**8**] does not contain cobalt(III) ions but cobalt(II) ions, contrary to an expectation of a Au^I-Co^{III} complex

analogized from the related systems.[2b,c,11] To figure out the structure of [**8**], X-ray diffraction measurement was carried out for a single crystal of [**8**].

Single-crystal X-ray structural analysis revealed the existence of a nonanuclear complex of [**8**] together with some solvation molecules in the asymmetric unit, as well as the absence of any anions in agreement with the elemental analysis. As shown in Figure III-4, the complex molecule has a ball-shaped Au_6Co_3 nonanuclear structure, $[Co_3\{Au_3(tdme)(D\text{-pen})_3\}_2]$, in which two $[Au^I_3(tdme)(D\text{-pen})_3]^{3-}$ ([**7**]$^{3-}$) metalloligands (av. Au–P = 2.269 Å, Au–S = 2.329 Å, P–Au–S = 177.4°) sandwich three Co ions. The top and bottom parts of the complex "ball" are covered with hydrophobic phenyl groups of tdme ligands, and the D-pen ligands form a hydrophilic belt in the middle part. Inside of the "ball" is filled mainly with six Au ions and two methyl groups of tdme ligands, which face each other with a C···C distance of 3.24 Å that is shorter than the twice the van der Waals radius of carbon atom (3.40 Å).[19] In [**8**], each cobalt ion is coordinated by two D-pen with a *trans*(*O*)-$N_2O_2S_2$ octahedral geometry, which is very similar to that in [**2a**]$^+$ and $[Co^{III}_2\{Au_2(dppe)(D\text{-pen})_2\}_2]^{2+}$, nevertheless there are definite differences in coordination bond lengths of Co centers. The significant elongations of the coordination bond distances around cobalt centers in [**8**] (av. Co–N = 2.15 Å, Co–O = 2.12 Å, Co–S = 2.486 Å) was observed compared with those in [**2a**]ClO_4 and $[Co^{III}_2\{Au_2(dppe)(D\text{-pen})_2\}_2](ClO_4)_2$. The distances around cobalt centers in [**8**] are within the range of typical cobalt(II) complexes, which indicate cobalt(II) oxidation state with a high-spin configuration of 3d electrons in an octahedral field (S = 3/2).

In order to obtain more reliable evidence for the oxidation and spin state of cobalt ion in [**8**], the magnetic measurement was carried out. The magnetic susceptibility for the solid sample of [**8**] at room temperature was given as $\chi_M T$ = 7.14 cm^3 K mol^{-1} for three cobalt centers. The magnetic moment value that calculated from $\chi_M T$ value as magnetically independent three cobalt ions is μ_{eff} = 4.37 μ_B at 300 K. This value is typical for an octahedral cobalt(II) center with $^4T_{1g}$ ground state and located between the spin-only value of high-spin cobalt(II) (3.87 μ_B; $\mu_{so} = [4S(S + 1)]^{1/2}$; S = 3/2) and the value expected when the spin momentum and orbital momentum exist independently [5.20 μ_B; $\mu_{ls} = [L(L + 1) + 4S(S + 1)]^{1/2}$; L = 3, S = 3/2].[20] In addition, the paramagnetic character of [**8**] was also supported by the ^{1}H and ^{31}P NMR spectra of [**8**] in a 1:1 mixture of methanol-d_4 and D_2O, which exhibited broadened signals in the abnormally wide range of δ –50.9 - +46 ppm for ^{1}H signals and at δ –100.9 ppm for ^{31}P signal (Figures III-5 and III-6). The electronic absorption and CD spectra of [**8**] in a 1:1 mixture of methanol and water exhibited two weak d-d transition bands corresponding to an octahedral high-spin cobalt(II) complex in the visible region (Figure III-7). All spectral features of [**8**] in solution were retained under ambient conditions for several days, therefore, it is indicated that cobalt(II) complex [**8**] is highly air-stable even in solution.

The oxidative resistance of [**8**] was also confirmed by the electrochemical measurements.

The cyclic voltammogram recorded for [**8**] in methanol with Bu_4NPF_6 as a supporting electrolyte showed a weak oxidation signal at E_{pa} = +0.57 V (*v.s.* Ag/AgCl) assignable to the oxidation from Co^{II} to Co^{III} (Figure III-8). The indistinct wave may be attributed to adsorption of the oxidation product onto the electrode due to the poor solubility in methanol. A reduction signal which seems to couple with that oxidation was shown at –0.33 V, and the large separation ΔE_p = 0.9 V indicates an electrochemically irreversible process in this redox cycle, which makes the reaction difficult to interpret. However, the cyclic voltammogram recorded for $[Co^{II}\{Au^{I}(PPh_3)(\text{D-pen})\}_2]$ ([**2a'**]), which was *in situ* prepared from the 2:1 reaction of [H**1**] with $Co(CH_3COO)_2$ under an inert atmosphere, showed a corresponding oxidation signal at much lower potential (E_{pa} = +0.20 V). Thus these observations demonstrate the remarkable oxidative resistance of [**8**].

(c) Au^{I}-Co^{III} nonanuclear complex ([8'](NO$_3$)$_3$). On the other hand, when [**8**] was treated with ceric ammonium nitrate (CAN), which is a well-known strong oxidant,[21] apparent color change of the reaction solution from pale brown to greenish-blue and following precipitation of blue crystalline materials occurred. In contrast, while no significant change was observed in the reaction employing several hours air-bubbling or PbO_2, which were used as oxidants for the purpose of the yield improvement in dppe system.[2d] The oxidation product was obtained as blue crystals ([**8'**]$(NO_3)_3$) from the recrystallization of the blue crystalline materials (Scheme III-1). The aqueous solution of the blue crystals gave much intense signals in the electronic absorption and CD spectra as compared to those of [**8**] (Figure III-9). The IR spectrum of [**8'**]$(NO_3)_3$ is largely similar to that of [**8**] except for appearance of strong absorption of nitrate anion at 1355 cm^{-1},[17] that indicates cationic complex, and a small but considerable higher-frequency shift of asymmetric COO^- stretching band (1647 cm^{-1} in [**8'**]$(NO_3)_3$, 1594 cm^{-1} in [**8**]), probably suggesting the increasing of the bond order of uncoordinated O–C bond associated with the enhancement of Co–O coordination bond (Figure III-1). The ^{1}H and ^{31}P NMR spectra of complex [**8'**]$(NO_3)_3$ in D_2O exhibited a set of sharp signals attributable to 1/3 of the metalloligand $[\mathbf{7}]^{3-}$, which consists of signals due to methyl (δ 0.83 and 1.31 ppm) and methine (δ 3.90 ppm) groups in D-pen, and methyl (δ 3.09 ppm), methylene (δ 2.39 and 3.00 ppm), and phenyl (δ 6.83, 7.43, 7.58, 7.71, 7.92, and 8.09 ppm) groups in tdme, indicative of a highly symmetric structure and diamagnetic character of [**8'**]$(NO_3)_3$ (Figures III-2 and III-3). From these results, together with the elemental analytical data, it was strongly suggested that [**8'**]$(NO_3)_3$ is also a nonanuclear complex with a quite similar structure to [**8**] but containing low-spin cobalt(III) ions (S = 0) instead of high-spin cobalt(II) ions, $[Co^{III}_3\{Au^{I}_3(\text{tdme})(\text{D-pen})_3\}_2](NO_3)_3$.

The expected nonanuclear structure of $[\mathbf{8'}]^{3+}$ was confirmed by the single-crystal X-ray structural analysis, which shows the complex cations occupying two crystallographically different sites in the crystal (Figure III-10). One of two complex cations provides low-reliable structural parameters due to severe disorder resulting from misalignment between molecular

and crystallographic 3-fold axes. Moreover, nitrate anions and solvation molecules could not be included in the model due to their severe disorder. On the other hand, the molecular structure of the other complex cation, which is located at crystallographically D_3-symmetrical point to make only the 1/6 of the cation crystallographically independent, was successfully solved with enough precisions to discuss. Significant decreases in coordination-bond lengths of Co center in [**8'**]$^{3+}$ (Co–N = 1.96 Å, Co–O = 1.93 Å, Co–S = 2.309 Å), as compared with [**8**], strongly support the oxidation from cobalt(II) to cobalt(III) accompanied with the change of spin state. On the other hand, coordination bonds of Au center in [**8'**]$^{3+}$ (av. Au–P = 2.273 Å, Au–S = 2.354 Å) are a little longer than those of [**8**], and it may show the distortion from compensation of contraction in Co–S bond lengths as discussed below. The characteristic methyl-methyl contact of C···C = 3.18 Å inside the nonanuclear structure of [**8'**]$^{3+}$, which seems to be ascribed to the significant large down-field shift of the methyl signal in the ^{1}H NMR spectrum of [**8'**]$(NO_3)_3$ as compared to that of [H_3**7**], is shorter than that in [**8**].

(d) Au^{I}-Co^{III} tetranuclear complex ([9]). Since the oxidation of the Au^{I}-Co^{II} complex [**8**] gave the cobalt(III) derivative [**8'**]$(NO_3)_3$, a direct reaction of [H_3**7**] with cobalt(III) ion was carried out by way of an experiment. As a result, the reaction mixture of [H_3**7**] and $K_3[Co^{III}(CO_3)_3]$ gave not the blue solution containing [**8'**]$^{3+}$ but a deep purple solution, from which purple crystals of [**9**] were isolated (Scheme III-1). The elemental analytical data and fluorescent X-ray spectrometry for the crystalline sample of [**9**] indicated a 1:1 adduct of [**7**]$^{3-}$:Co, namely a formula of [Co{Au_3(tdme)(D-pen)$_3$}]. As shown in Figures III-2 and III-3, the ^{1}H and ^{31}P NMR spectra of [**9**] also showed signals attributable to 1/3 of [**7**]$^{3-}$ like [**8'**]$(NO_3)_3$, which indicates diamagnetic character of [**9**] with a low-spin cobalt(III) ion, although their chemical shifts are quite different from those of [**8'**]$(NO_3)_3$. While well-split ^{1}H resonances of phenyl and methylene groups of tdme over wide ranges indicates that the metalloligand is fixed to a rigid conformation on coordination to cobalt ion, the ^{1}H signals from D-pen and methyl group of tdme in addition to the ^{31}P signal show similar trends to those of the free metalloligand ([H_3**7**]) rather than [**8'**]$(NO_3)_3$. Especially, the methyl signal of tdme (δ 1.78 ppm) appeared in a typical chemical shift for alkyl groups, which implies the absence of the inside methyl-methyl contact of the ball-like nonanuclear structure. In addition, the electronic absorption and CD spectra of [**9**] in methanol also exhibited quite different feature from those of [**8'**]$(NO_3)_3$ (Figure III-11).

X-ray crystallography revealed the molecular structure of [**9**], which is a tetranuclear complex molecule with one cobalt ion coordinated by one metalloligand [**7**]$^{3-}$ with a hexadentate-N_3,S_3 chelating mode (Figure III-12). Uncoordinated carboxylate groups in [**9**] are consistent with the appearance of a ν_{COO} band with relatively lower wavenumber (1600 cm^{-1}) in the IR spectrum (Figure III-1). Relatively short coordination bonds around the cobalt center suggest a low-spin Co^{III} ion (av. Co–N = 2.02 Å, Co–S = 2.287 Å), together with the absence of any counter ion in the crystal. The Λ chiral configuration of {Co(D-pen-*N*,*S*)$_3$}$^{3-}$

unit seems to be induced by the chirality of D-pen, which prefers the δ conformation of 5-membered N,S-chelate ring with a carboxylate group in an equatorial position, as observed for $[Au^{I}_{3}\{M(D\text{-pen-}N,S)_3\}_2]^{3-}$ (M = Ni^{II} or Co^{III}).[2b,10,22] Note that no evidence for other isomer was found in the ^1H NMR spectrum of the reaction solution of [H_3**7**] with $K_3[Co^{III}(CO_3)_3]$ (Figure III-13). Three Au^{I} ions in a molecule approach to each other by aurophilic interactions to bend P–Au–S lines inward (av. Au–P = 2.272 Å, Au–S = 2.342 Å, P–Au–S = 169.4°), which are in a right-handed helical arrangement arising from the combination of the chiralities of Λ(δ_3) around the Co center and *R* configurations on bridging sulfur atoms (averaged torsion angle of S–A···Au–S = –38.8°).

III-3-2. Control of $Co^{II/III}$ oxidation states by tripodal Au^{I} metalloligand.

The most remarkable result in this tdme system is that the complex [**8**] contains very rare octahedral cobalt(II) center coordinated by aliphatic thiolates in spite of its coordination environment of cobalt ion that is essentially the same as those in $[Co^{III}\{Au^{I}(PPh_3)(D\text{-pen})\}_2]^{+}$ ([**2a**]$^{+}$) and $[Co^{III}_{2}\{Au^{I}(dppe)(D\text{-pen})_2\}_2]^{2+}$ (Scheme I-1 in Chapter I and Chart 2 in General Introduction, respectively). Although it is no wonder that there is a striking difference in their phosphine ligands, a significant difference hardly seems to exist in their electronic properties, because, in particular, dppe and tdme both belong in a family of diphenylphosphinoalkanes. Thus, the determinant factor for the oxidation number of their cobalt centers should be mainly attributed to the shape of the backbone. The cobalt(III) derivative [**8'**]$(NO_3)_3$ is of help to discuss their structural features in detail. Although the cobalt ions in [**8'**]$(NO_3)_3$ are certainly assigned to cobalt(III) in the low-spin state on the basis of the much shorter coordination bond lengths in the crystal structure together with the spectral data, the Co–S bond is considerably longer than other related D-penicillaminato cobalt(III) complexes.[1,2c,d,10,23] Among the Au^{I}-Co^{III} complexes with mixed D-pen and phosphines, there is a trend of the Co–S distances increasing in order of [**2a**]$^{+}$ (2.259(2) Å) < $[Co^{III}_{2}\{Au^{I}(dppe)(D\text{-pen})_2\}_2]^{2+}$ (2.286(3) Å) < [**8'**]$^{3+}$ (2.309(4) Å) with increasing the number of P donor in the phosphine ligands, while no significant difference is found in the Co–N and Co–O distances (Table III-6). In addition, a distinct structural feature of the nonanuclear complexes is also found in their μ_2-thiolato bridging angles, which are extraordinary small as compared to those of the analogues (av. Au–S–Co = 90.9(2)° for [**8**], 96.9(2)° for [**8'**]$^{3+}$, 102.4(7)° for [**2a**]$^{+}$, 102.1(1)° for $[Co^{III}_{2}\{Au^{I}(dppe)(D\text{-pen})_2\}_2]^{2+}$). The monophosphine analogue [**2a**]$^{+}$ should adopt the intrinsically most preferable bond lengths and angles for this class of compounds among them because of its unrestricted backbone. Thus, these trends indicate that the sterically more fettered backbone in the nonanuclear complexes with tdme distorts the Co–S coordination bonds from a proper state, which can weaken the orbital interaction between Co and S. If the sulfur atoms were pushed outward of the molecule by laying P-Au-S lines, the Au–S–Co bridging angle and Co–S distance should adopt more proper value like those in [**2a**]$^{+}$, but it is

hardly permitted due to a steric limitation by the tripodal backbone of tdme as well as the inside methyl-methyl repulsion. The larger and more distorted coordination sphere forms a weaker ligand field, which seems to be suitable for high-spin cobalt(II) state with a larger ionic radius rather than low-spin cobalt(III) state.

From the structural features described above, a smaller splitting of the cobalt 3d orbitals in the nonanuclear structure is expected. The smaller energy gap was evidenced by the electronic absorption spectrum of [**8'**]$(NO_3)_3$ in water showing a band peaked at 610 nm assignable to $^1T_{1g} \leftarrow {}^1A_{1g}$ d-d transition derived from a low-spin octahedral cobalt(III) center, whose transition energy is smaller than the corresponding transition of [**2a**]ClO_4 observed as a shoulder around 580 nm (Figure III-9).

As described above, all the spectroscopic data of [**8'**]$(NO_3)_3$ in solution were collected in water solvent, since [**8'**]$(NO_3)_3$ was soluble in water but hardly soluble in organic solvents unlike the other complexes with mixed D-pen and phosphines presented in this thesis, probably due to its tricationic character and hydrophilic nitrate anions. Moreover, when methanol-d_4 was added into the D_2O solution of [**8'**]$(NO_3)_3$, broadening of the signals derived from [**8'**]$^{3+}$ and appearance of new intricate signals were observed within 1 day in ^{1}H NMR monitoring, indicative of decomposition of [**8'**]$^{3+}$ (Figure III-14). The nonanuclear structure of [**8'**]$^{3+}$ that is not so preferable for short coordination bonds of cobalt(III) ion seems not to retain the structure in a less-polar solvent, while no detectable change was observed in the NMR spectrum of [**8'**]$(NO_3)_3$ in D_2O at least for 1 weak.

On the other hand, the tetranuclear complex [**9**] obtained from the direct reaction of [H_3**7**] with cobalt(III) ion seems to be much stable cobalt(III) species in contrast to [**8'**]$(NO_3)_3$, because no indication of the decomposition were observed in the spectra of [**9**] in solution. The formation of a pair of the Au^I-Co^{III} complexes, [**8'**]$^{3+}$ and [**9**], is reminiscent of another pair of Au^I-Co^{III} complexes composed of $[Au^I(D\text{-pen})_2]^{3-}$ and cobalt(III) ion, $[Au^I_3\{Co^{III}(D\text{-pen-}N,O,S)_2\}_3]$ and $(\Lambda)_2$-$[Au^I_3\{Co^{III}(D\text{-pen-}N,S)_3\}_2]^{3-}$, in point of their D-penicillaminato cobalt(III) units, $\{Co^{III}(D\text{-pen-}N,O,S)_2\}^-$ and (Λ)-$\{Co^{III}(D\text{-pen-}N,S)_3\}^{3-}$ (Chart I-1 in Chapter I).[10] While the previously reported complexes were concurrently formed by the reaction of $NH_4[Au^I(D\text{-Hpen})_2]$ with cobalt(II) ion under aerobic conditions, the separate synthesis of [**8**] and [**9**] can be explained by extremely different natures of cobalt ions depending on their oxidation state, which can make a critical influence on the complexation process of [**7**]$^{3-}$ with cobalt ions in their solution. It is simply expected that the tripodal metalloligand [**7**]$^{3-}$ can adopt endo and exo conformations, whose methyl group of tdme exist inside and outside the fence consisting of three arms as found in [**8**] and [**9**], respectively (Chart III-1). On the one hand, the exo conformer of [**7**]$^{3-}$, which may be more stable in solution because of the multiple intramolecular aurophilic interactions, can provide a cobalt ion with a relatively tight space surrounded by three D-pen ligands to generate a [**9**] via the rapid bimolecular reaction. In addition, the N_3S_3 environment gives a stronger ligand field

to be suitable for a low-spin cobalt(III) center. On the other hand, the reaction involving two metalloligands and three cobalt ions may slowly proceed finally to generate the nonanuclear structure ([**8**]) as a thermodynamic product, through turning the conformation of [**7**]$^{3-}$ inside out. The resulting relatively loose coordination space for cobalt ion should be comfortable for high-spin cobalt(II) centers in [**8**], while the conversion to low-spin cobalt(III) species with keeping the nonanuclear structure was achieved by using a strong oxidant of CAN. Furthermore, once cobalt(III) complexes are formed, they are kinetically stabilized due to the inert character of low-spin cobalt(III) ion in general.

III-4. Conclusion.

In order to reveal the effects of the introduction of multidentate phosphine ligand into the thiolato coordination system, the coordination behavior of tris(D-penicillaminato) trigold(I) metalloligand with a triphosphine (tdme) toward cobalt ion was investigated in this chapter. The trigold(I) complex [H_3**7**], which was synthesized in a similar manner to other D-penicillaminato gold(I) metalloligands with phosphines, acted as a multidentate metalloligand with a total of nine donor groups consisting of three amines, three carboxylates, and three thiolates. When the metalloligand [**7**]$^{3-}$ coordinated to cobalt ion by using all of N,O,S donors, which is the standard coordination mode of this class of the metalloligands toward octahedral metal ions,[1,2c,d,11] the nonanuclear complex [**8**] was formed as a complex with the highest nuclearity in this thesis, according to the expectation that more coordination arms assemble more metal ions. On the other hand, [**7**]$^{3-}$ also functioned as a hexadentate-N_3,S_3 chelating metalloligand to form the tetranuclear complex [**9**], which confirms the coordination versatility of the multidentate metalloligand. Thus, it is demonstrated that the coordination ability of this class of metalloligands can be extended by designing polyphosphine ligands as the backbone. The two coordination modes of [**7**]$^{3-}$ were determined by the conformational conversion of [**7**]$^{3-}$ involving formation/cleavage of the intramolecular aurophilic interactions in addition to the characters of metal ions such as ionic radii and substitution reactivity. Therefore the utility of the aurophilic interactions for construction of heterometallic multinuclear complexes is emphasized again here.

Moreover, it was revealed that the tris(tridentate-N,O,S) coordination of [**7**]$^{3-}$ unexpectedly stabilized rare octahedral cobalt(II) centers coordinated by aliphatic thiolates. The presence of high-spin cobalt(II) in [**8**] was confirmed by the electronic absorption and NMR spectra, the crystal structure, and the magnetic susceptibility data, and in addition, its oxidative resistance was established by the stationary spectra in solution even under aerobic conditions together with the electrochemical measurements. The structural and spectral comparison of the cobalt(III) derivative [**8'**]$(NO_3)_3$ with the other Au^I-Co^{III} complexes with mixed D-pen and phosphines ([**2a**]ClO_4 and $[Co^{III}{}_2\{Au^I(dppe)(D\text{-}pen)_2\}_2](ClO_4)_2$) indicated

that the steric limitations raising from tripodal backbone provide weaker ligand fields and longer coordination bonds suitable for high-spin cobalt(II) centers. The strategy for the ligand-field modulation by adjustment of distances between metal ions and donor atoms is interesting yet still challenging, in particular, it is quite rare to be achieved by supporting ligands on another metal ion, while direct modifications of the donor ligands such as introduction of electron-donating or -withdrawing groups are commonly employed for this purpose.[24] The successful control of oxidation state presented here indicates a possibility that the strategy to use the phosphines for the regulation of the coordination ability of SAA functional groups will provide an approach for the functional system inspired by metalloproteins, where polypeptide backbones regulate the functionality of active centers containing metal ions.[25] Proper design of phosphine ligands should promote the achievement of such coordination systems.

III-5. References.

[1] See Chapter II in this thesis.

[2] (a) D. J. LeBlanc, J. F. Britten, Z. Wang, H. E. Howard-Lock, C. J. L. Lock, *Acta Crystallogr. Sect. C Cryst. Struct. Commun.* **1997**, *53*, 1763. (b) A. Igashira-Kamiyama, T. Konno, *Dalton Trans.* **2011**, *40*, 7249. (c) R. Lee, A. Igashira-Kamiyama, H. Motoyoshi, T. Konno, *CrystEngComm* **2012**, *14*, 1936. (d) R. Lee, PhD thesis, Osaka University, Toyonaka, Japan, **2012**.

[3] (a) J.-C. Hierso, R. Amardeil, E. Bentabet, R. Broussier, B. Gautheron, P. Meunier, P. Kalck, *Coord. Chem. Rev.* **2003**, *236*, 143. (b) S. Maggini, *Coord. Chem. Rev.* **2009**, *253*, 1793. (c) S. Maggini, *Coord. Chem. Rev.* **2009**, *253*, 1793. (d) M.-C. Dul, E. Pardo, R. Lescouëzec, Y. Journaux, J. Ferrando-Soria, R. Ruiz-Carcía, J. Cano, M. Julve, F. Lloret, D. Cangussu, C. L. M. Pereira, H. O. Stumpf, J. Pasán, C. Ruiz-Pérez, *Coord. Chem. Rev.* **2010**, *254*, 2281.

[4] (a) M. Yoshizawa, J. K. Klosterman, M. Fujita, *Angew. Chem. Int. Ed.* **2009**, *48*, 3418. (b) R. Chakrabarty, P. S. Mukherjee, P. J. Stang, *Chem. Rev.* **2011**, *111*, 6810. (c) N. B. Debata, D. Triphaty, D. K. Chand, *Coord. Chem. Rev.* **2012**, *256*, 1831.

[5] (a) A. J. Blake, N. R. Champness, P. Hubberstey, W.-S. Li, M. A. Withersby, M. Schröder, *Coord. Chem. Rev.* **1999**, *183*, 117. (b) S. L. James, *Chem. Soc. Rev.* **2003**, *32*, 276. (c) S. Kitagawa, R. Kitaura, S. Noro, *Angew. Chem. Int. Ed.* **2004**, *43*, 2344. (d) A. U. Czaja, N. Trukhan, U. Müller, *Chem. Soc. Rev.* **2009**, *38*, 1284. (e) M. D. Allendorf, C. A. Bauer, R. K. Bhakta, R. J. T. Houk, *Chem. Soc. Rev.* **2009**, *38*, 1330.

[6] A. N. Khlobystov, A. J. Blake, N. R. Champness, D. A. Lemenovskii, A. G. Majouga, N. V. Zyk, M. Schröder, *Coord. Chem. Rev.* **2001**, *222*, 155.

[7] (a) N. N. Greenwood, A. Earnshaw, *Chemistry of the Elements*, 2nd ed.,

Butterworth-Heinemann, pp. 1117–1119 (1997). (b) P. V. Bernhardt, G. A. Lawrance, in *Comprehensive Coordination Chemistry II*, J. A. McCleverty, T. J. Meyer, Eds.; Elsevier Inc., vol. 6, pp. 1–145 (2003).

[8] (a) D. F. Shriver, P. W. Atkins, *Inorganic Chemistry*, 3rd ed., Oxford University Press (1999). (b) J. R. Gispert, *Coordination Chemistry*, Wiley VCH (2008).

[9] (a) N. R. Rao, P. V. Rao, G. V. Reddy, M. C. Ganorkar, *Indian J. Chem., Sect. A*, **1987**, *26*, 887. (b) L. F. Larkworthy, D. Sattari, *J. Inorg. Nucl. Chem.* **1980**, *42*, 551. (c) B. Aswar, *J. Indian Chem. Soc.* **1997**, *74*, 679. (d) A. Z. El-Sonbati, A. S. Al-Shihri, A. A. El-Bindary, *Spectrochim. Acta, Part A*, **2004**, *60*, 1763.

[10] T. Konno, A. Toyota, A. Igashira-Kamiyama, *J. Chin. Chem. Soc.* **2009**, *56*, 26.

[11] See Chapter I in this thesis.

[12] P. Sevillano, M. E. García-Fernández, A. Habtemariam, S. Parsons, P. J. Sadler, *Met. Based. Drugs* **1999**, *6*, 211.

[13] (a) M. Mori, M. Shibata, E. Kyuno, T. Adachi, *Bull. Chem. Soc. Jpn.* **1956**, *29*, 883. (b) *Modern Syntheses of Cobalt (III) Complexes*, M. Shibata, Eds., Springer Berlin Heidelberg, pp. 26–45 (1983).

[14] G. M. Sheldrick, *Acta Crystallogr., Sect. A* **2008**, *64*, 112.

[15] C. Kabuto, S. Akine, E. Kwon, *J. Cryst. Soc. Jpn.* **2009**, *51*, 218.

[16] A. L. Spek, *Acta Crystallogr., Sect. D* **2009**, *65*, 148.

[17] K. Nakamoto, *Infrared and Raman Spectra of Inorganic and Coordination Compounds*, 5th ed., Wiley, Chichester (1997).

[18] H. E. Howard-Lock, C. J. L. Lock, P. S. Smalley, *J. Chem. Crystallogr.* **1983**, *13*, 333.

[19] A. Bondi, *J. Phys. Chem.* **1964**, *68*, 441.

[20] (a) M. Gerloch, P. N. Quested, *J. Chem. Soc. A* **1971**, 3729. (b) M. Gerloch, P. N. Quested, R. C. Slade, *J. Chem. Soc. A* **1971**, 3741. (c) Md. J. Hossain, M. Yamasaki, M. Mikuriya, A. Kuribayashi, H. Sakiyama, *Inorg. Chem.* **2002**, *41*, 4058.

[21] (a) N. G. Connelly, W. E. Geiger, *Chem. Rev.* **1996**, *96*, 877. (b) N. A. Piro, J. R. Robinson, P. J. Walsh, E. J. Schelter, *Coord. Chem. Rev.* **2014**, *260*, 21.

[22] (a)M. Taguchi, A. Igashira-Kamiyama, T. Kajiwara, T. Konno, *Angew. Chem. Int. Ed.* **2007**, *46*, 2422. (b) Y. Sameshima, N. Yoshinari, K. Tsuge, A. Igashira-Kamiyama, T. Konno, *Angew. Chem. Int. Ed.* **2009**, *48*, 8469.

[23] (a) P. de Meester, D. J. Hodgson, *Chem. Commun.* **1976**, 280. (b) P. de Meester, D. J. Hodgson, *J. Am. Chem. Soc.* **1977**, *99*, 101. (c) H. M. Helis, P. de Meester, D. J. Hodgson, *J. Am. Chem. Soc.* **1977**, *99*, 3309. (d) K.-I. Okamoto, K. Wakayama, M. Ohmasa, J. Hidaka, *Chem. Lett.* **1981**, 453. (e) K.-I. Okamoto, K. Wakayama, H. Einaga, M. Ohmasa, J. Hidaka, *Bull. Chem. Soc. Jpn.* **1982**, *55*, 3473. (f) T. Konno, N. Matsuno, K. Okamoto, M. Hirotsu, *Chem. Lett.* **1999**, 1243. (g) T. Konno, M. Hattori, T. Yoshimura, M. Hirotsu, *Chem. Lett.* **2000**, 852. (h) Y. Yamada, M. Tsumita, A. Hirano, Y.

Miyashita, K. Fujisawa, K. Okamoto, *Inorg. Chim. Acta* **2002**, *332*, 108. (i) H. Honda, T. Yoshimura, M. Hirotsu, T. Kawamoto, T. Konno, *Inorg. Chem.* **2002**, *41*, 2229. (j) Y. Yamada, M. Uchida, M. Fujita, Y. Miyashita, K. Okamoto, *Polyhedron* **2003**, *22*, 1507. (k) Y. Yamada, A. Hirano, M. Fujita, N. Amir, Y. Miyashita, K. Okamoto, *Inorg. Chim. Acta* **2005**, *358*, 667. (l) Y. Yamada, K. Okamoto, *Inorg. Chim. Acta* **2006**, *359*, 3963. (m) A. Igashira-Kamiyama, J. Fujioka, T. Kodama, T. Kawamoto, T. Konno, *Chem. Lett.* **2006**, *35*, 522. (n) Y. Yamada, M. Inoue, Y. Miyashita, K. Okamoto, M. Koikawa, T. Tokii, *Polyhedron* **2007**, *26*, 2749. (o) S. Mitsunaga, M. Tamura, A. Igashira-Kamiyama, T. Konno, *Chem. Lett.* **2007**, *36*, 790. (p) Y. Yamada, M. Inoue, K. Okamoto, *J. Coord. Chem.* **2008**, *61*, 1385. (q) Y. Yamada, M. Kono, Y. Miyoshi, T. Nagasaki, M. Koikawa, T. Tokii, *J. Coord. Chem.* **2010**, *63*, 742.

[24] (a) A. M. Allgeier, C. A. Mirkin, *Angew. Chem. Int. Ed.* **1998**, *37*, 894. (b) T. Ren, *Coord. Chem. Rev.* **1998**, *175*, 43. (c) S. P. Flanagan, P. J. Guiry, *J. Organomet. Chem.* **2006**, *691*, 2125. (d) S. Hayami, Y. Komatsu, T. Shimizu, H. Kamihata, Y. H. Lee, *Coord. Chem. Rev.* **2011**, *255*, 1981.

[25] (a) S. J. Lippard, J. M. Berg, *Principles of Bioinorganic Chemistry*, Univ Science Books (1994). (b) *Handbook of Metalloproteins*, A. Messerschmidt, Eds.; Wiley (2001).

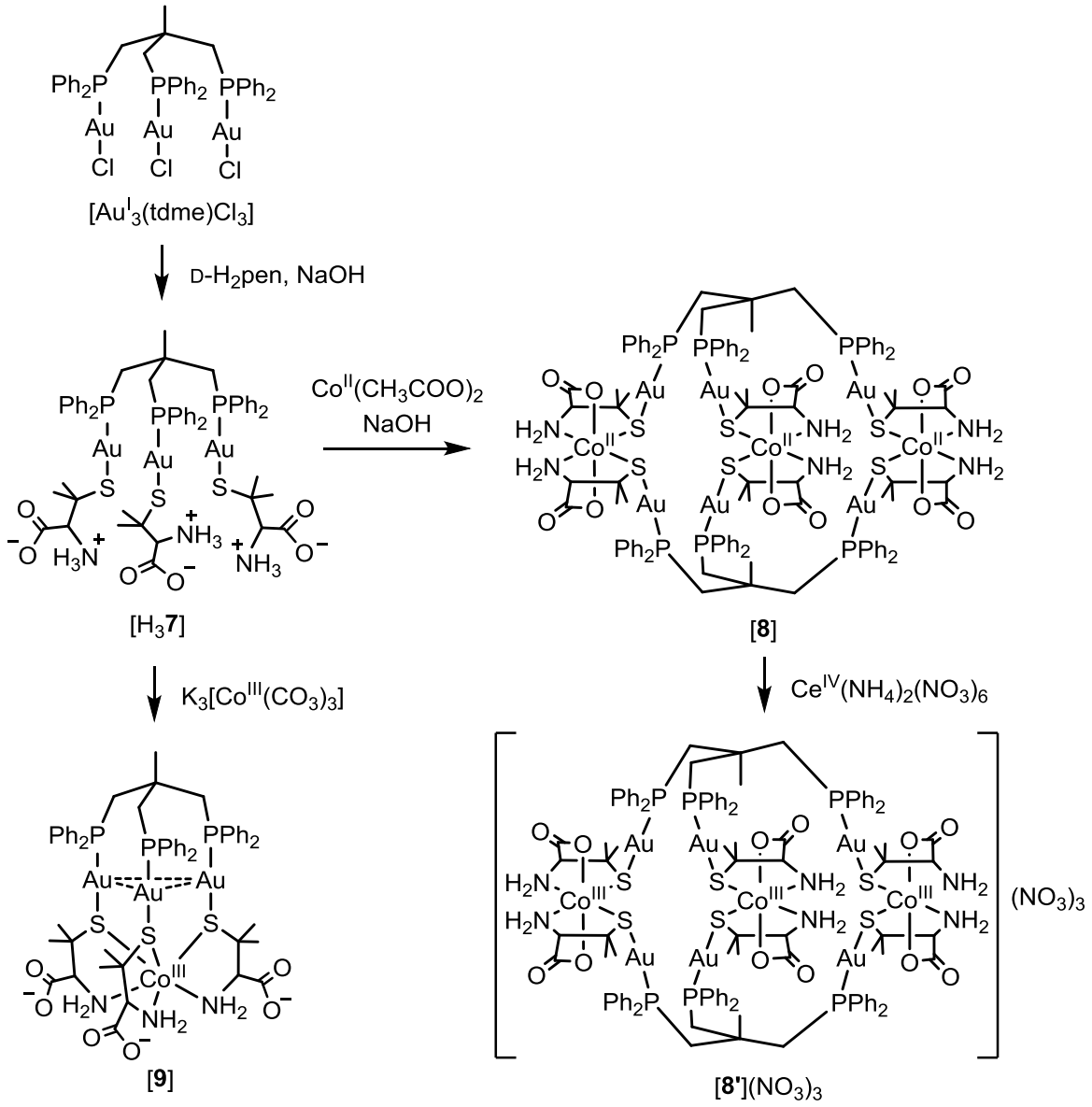

Scheme III-1. Synthesis of complexes [H_3**7**], [**8**], [**8'**]$(NO_3)_3$, and [**9**].

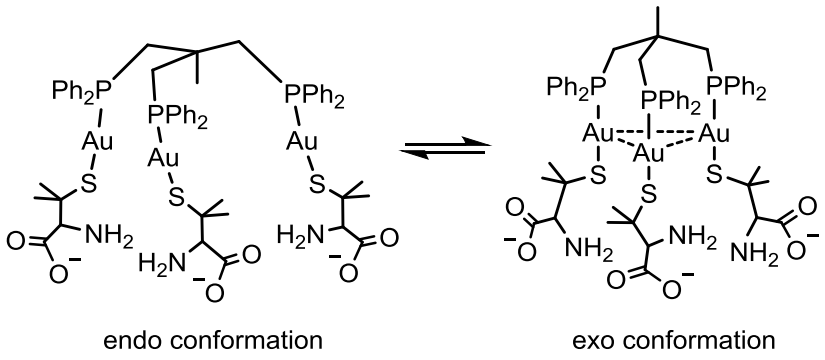

Chart III-1. Conformational conversion of $[\mathbf{7}]^{3-}$.

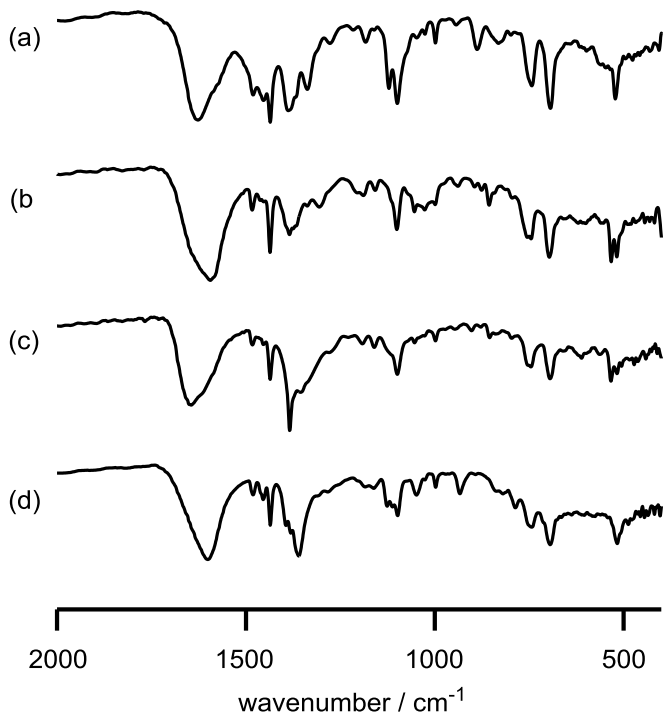

Figure III-1. IR spectra of (a) [H_3**7**], (b) [**8**], (c) [**8'**]$(NO_3)_3$, and (d) [**9**] (KBr disk).

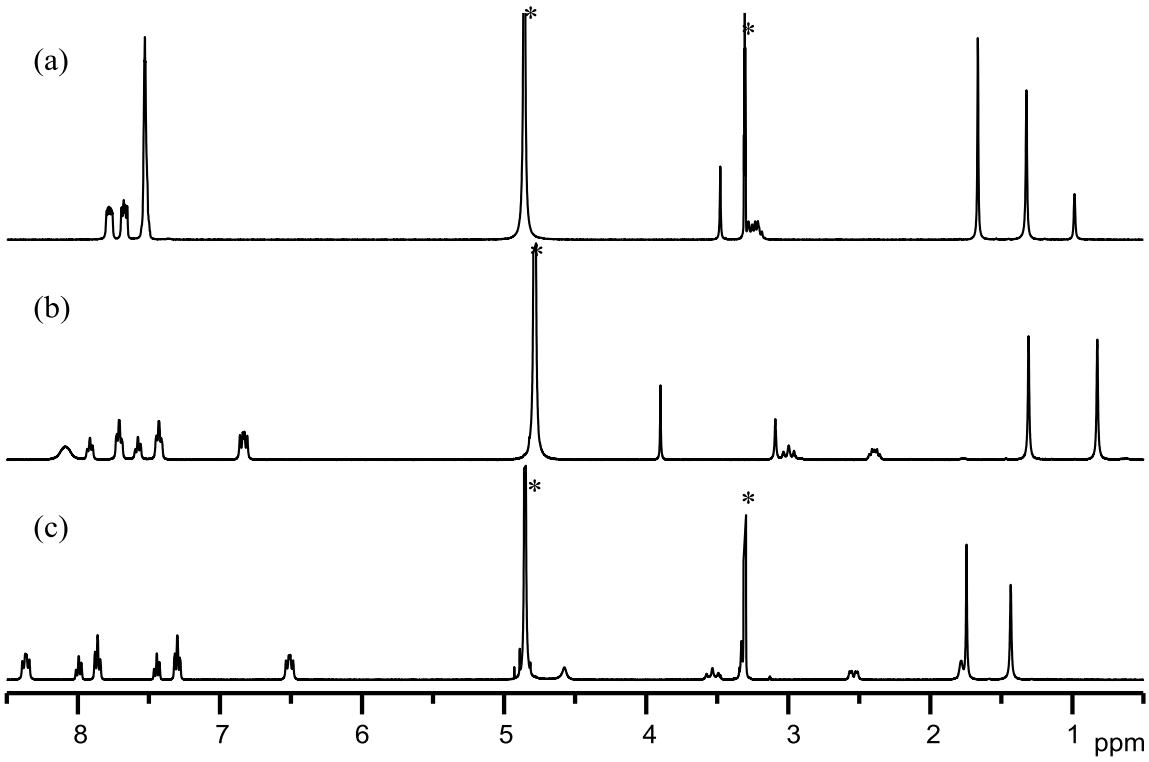

Figure III-2. ^{1}H NMR spectra of (a) [H_3**7**] in methanol-d_4, (b) [**8'**]$(NO_3)_3$ in D_2O, and (c) [**9**] in methanol-d_4. (*) denotes the signals from solvents.

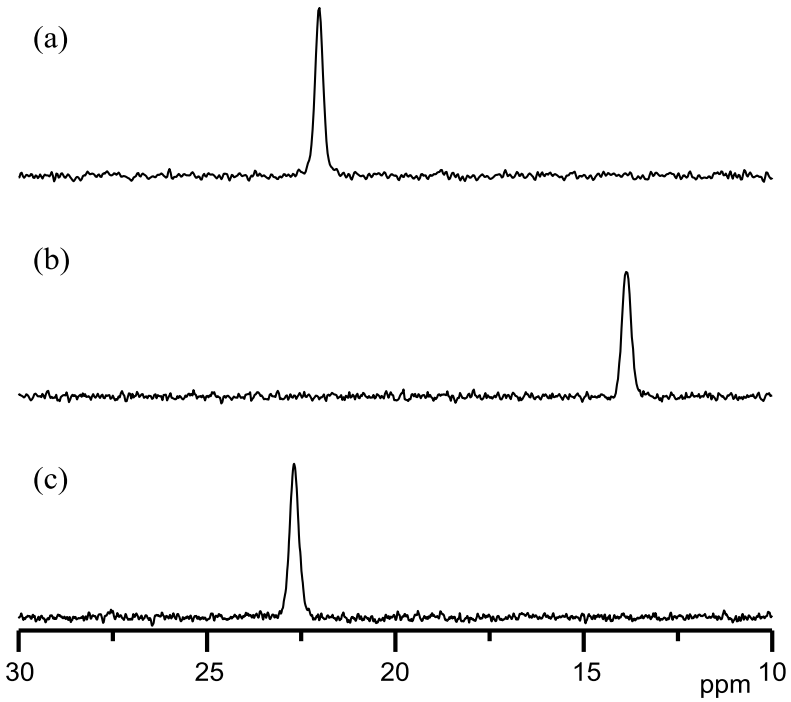

Figure III-3. ^{31}P NMR spectra of (a) [H_3**7**] in methanol-d_4, (b) [**8'**]$(NO_3)_3$ in D_2O, and (c) [**9**] in methanol-d_4.

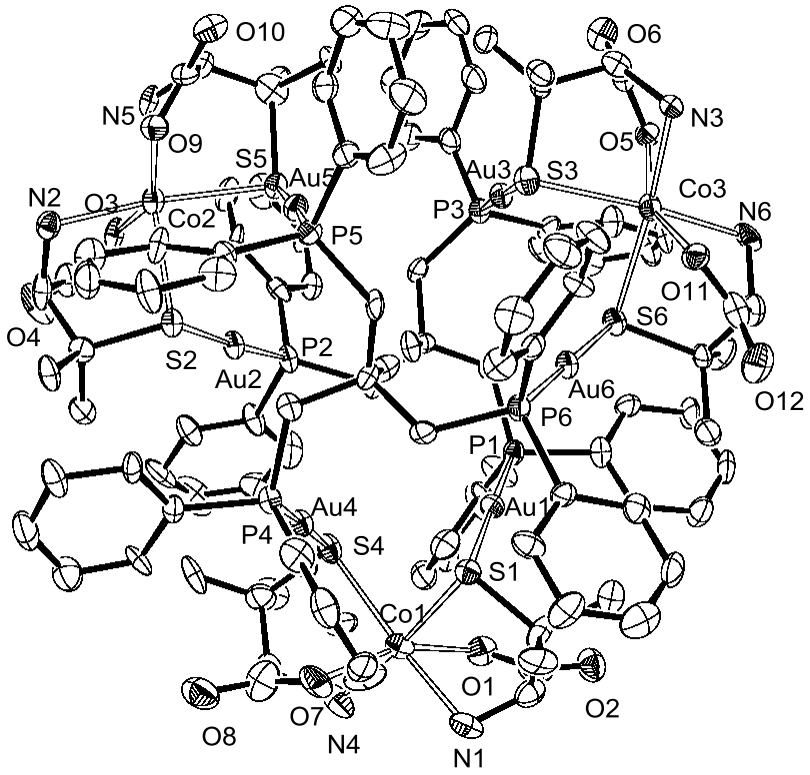

Figure III-4. ORTEP drawing of [**8**] with 30% probability level of thermal ellipsoids. H atoms are omitted for clarity.

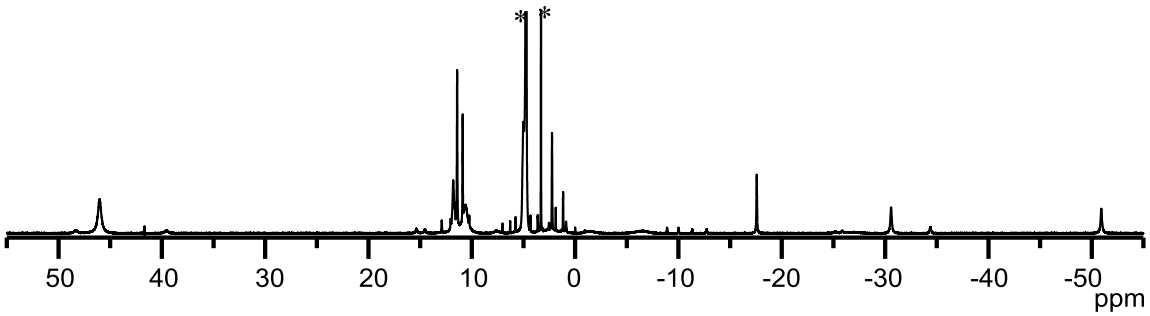

Figure III-5. ^{1}H NMR spectra of [**8**] in a 1:1 mixture of methanol-d_4 and D_2O. (*) denotes the signals from solvents.

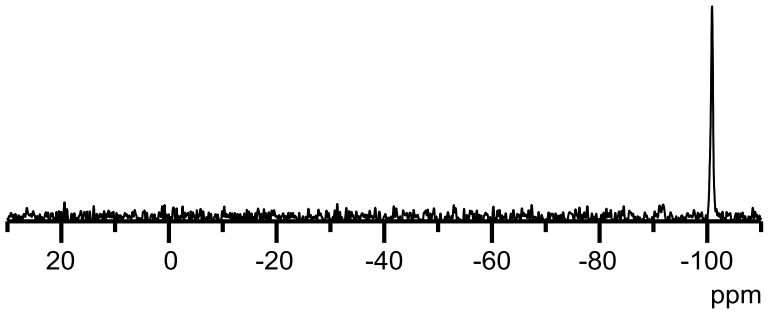

Figure III-6. ^{31}P NMR spectra of [**8**] in a 1:1 mixture of methanol-d_4 and D_2O.

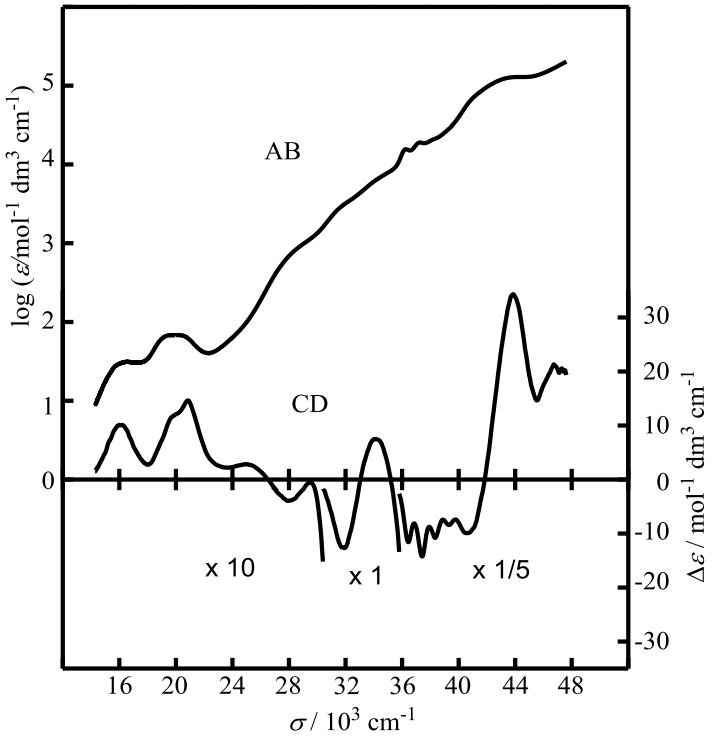

Figure III-7. Electronic absorption and CD spectra of [**8**] in a 1:1 mixture of methanol and water.

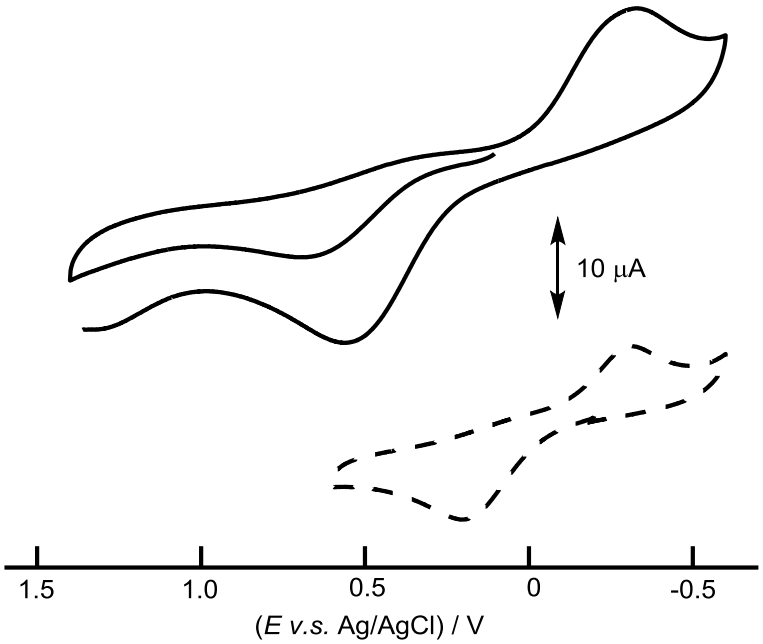

Figure III-8. Cyclic voltammograms of [**8**] (solid line) and [**2a'**] (dashed line) in methanol containing 0.1 M Bu_4NPF_6 at rate of 0.1 V/s.

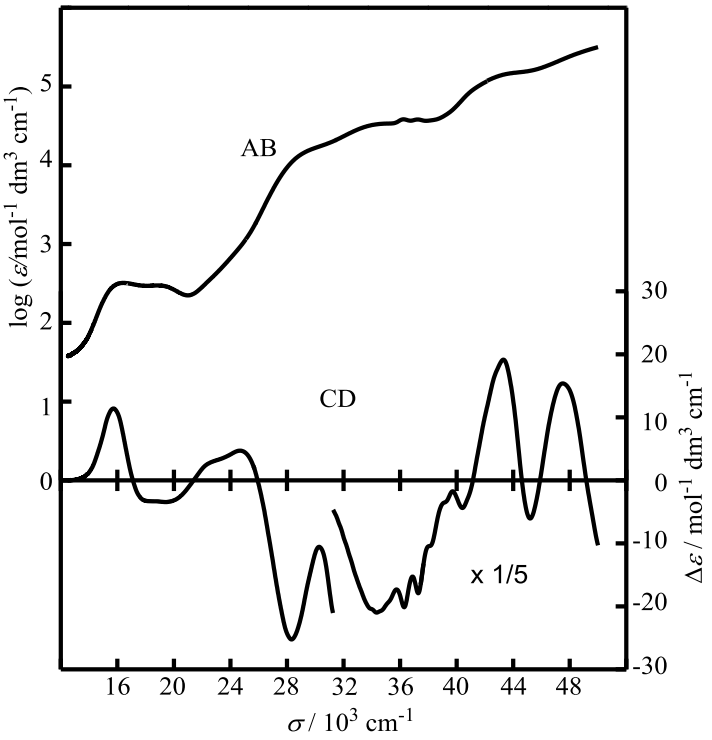

Figure III-9. Electronic absorption and CD spectra of [**8'**]$(NO_3)_3$ in water.

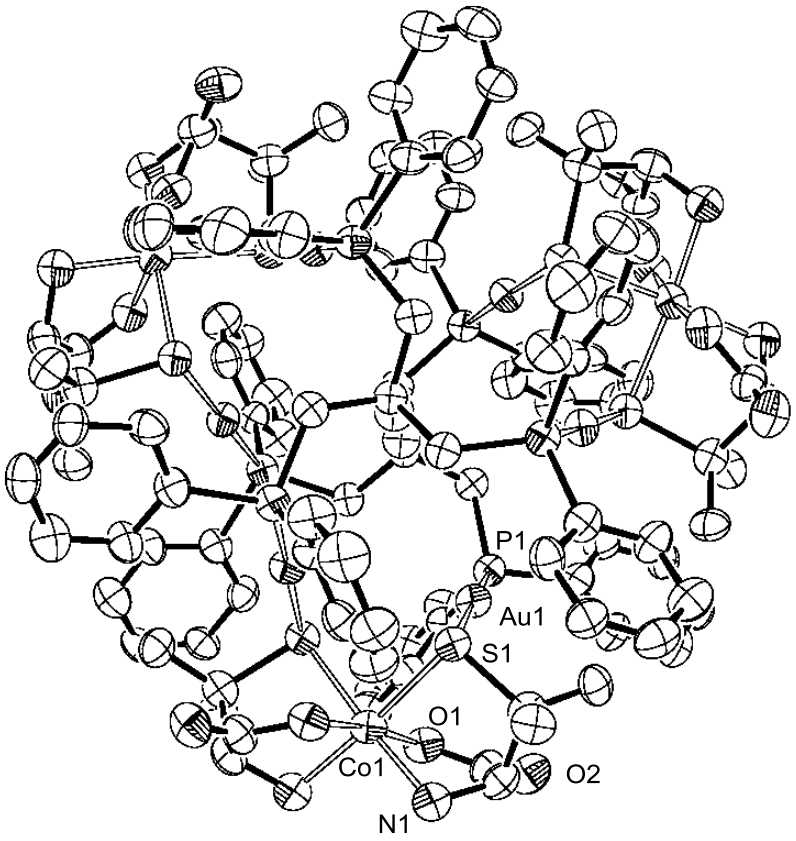

Figure III-10. ORTEP drawing of non-disordered one of the complex cations in [**8'**]$(NO_3)_3$ with 30% probability level of thermal ellipsoids. H atoms are omitted for clarity.

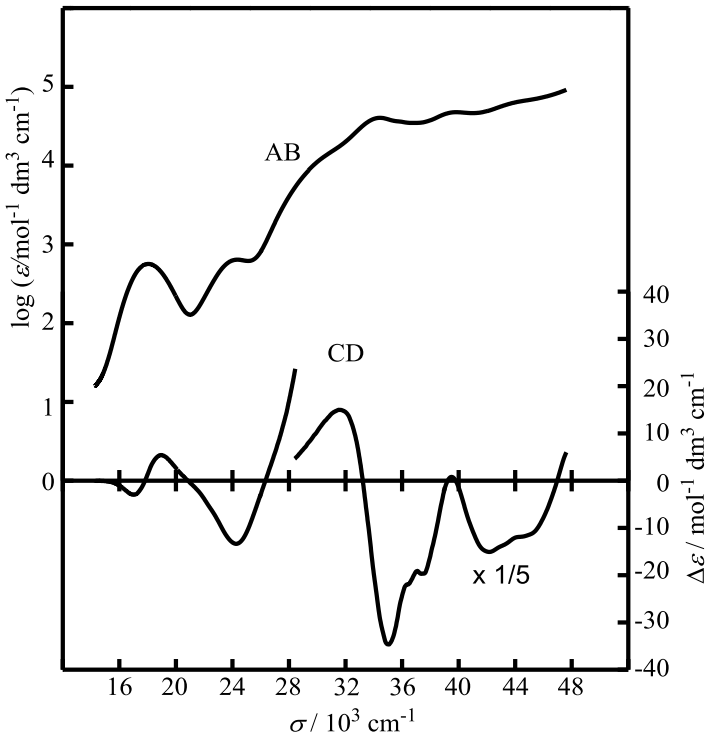

Figure III-11. Electronic absorption and CD spectra of [**9**] in methanol.

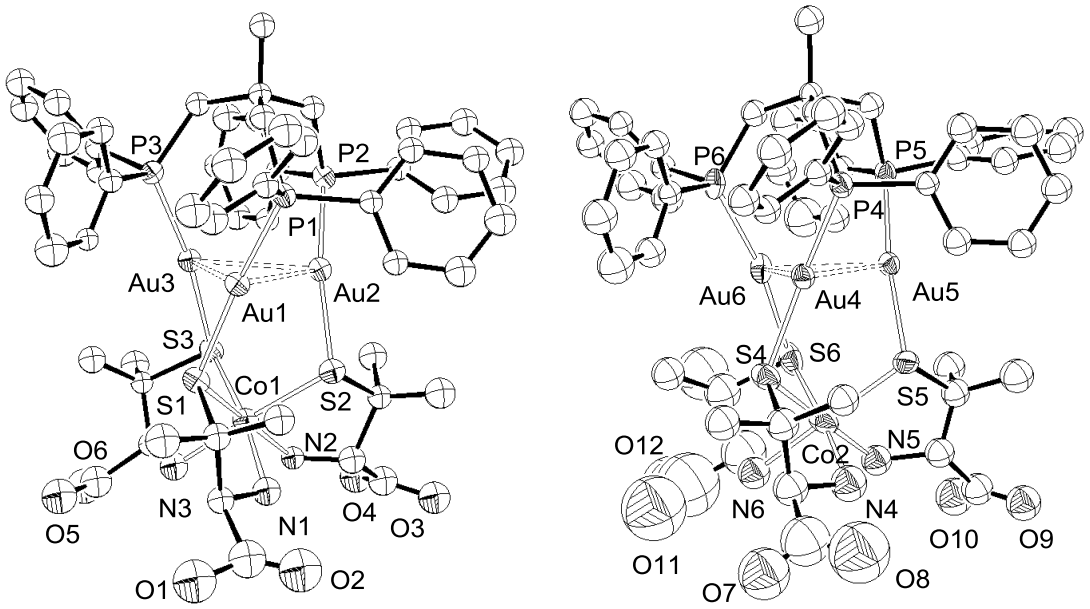

Figure III-12. ORTEP drawings of [**9**] with 30% probability level of thermal ellipsoids. H atoms are omitted for clarity.

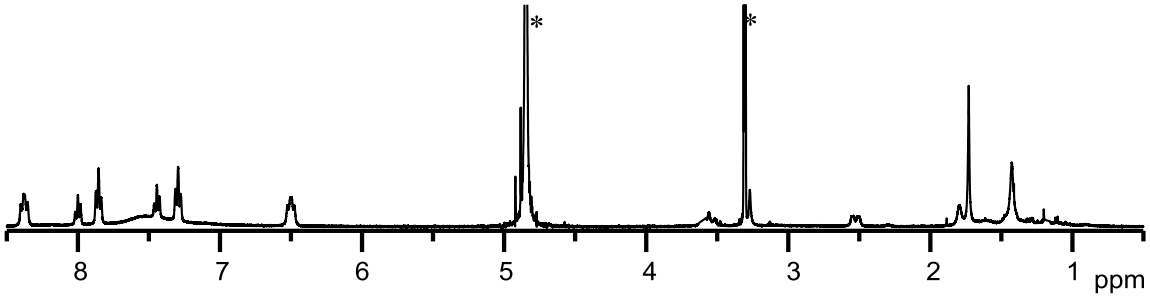

Figure III-13. ^{1}H NMR spectrum of the reaction mixture of [H_3**7**] with $K_3[Co^{III}(CO_3)_3]$ in methanol-d_4. (*) denotes the signals from solvents.

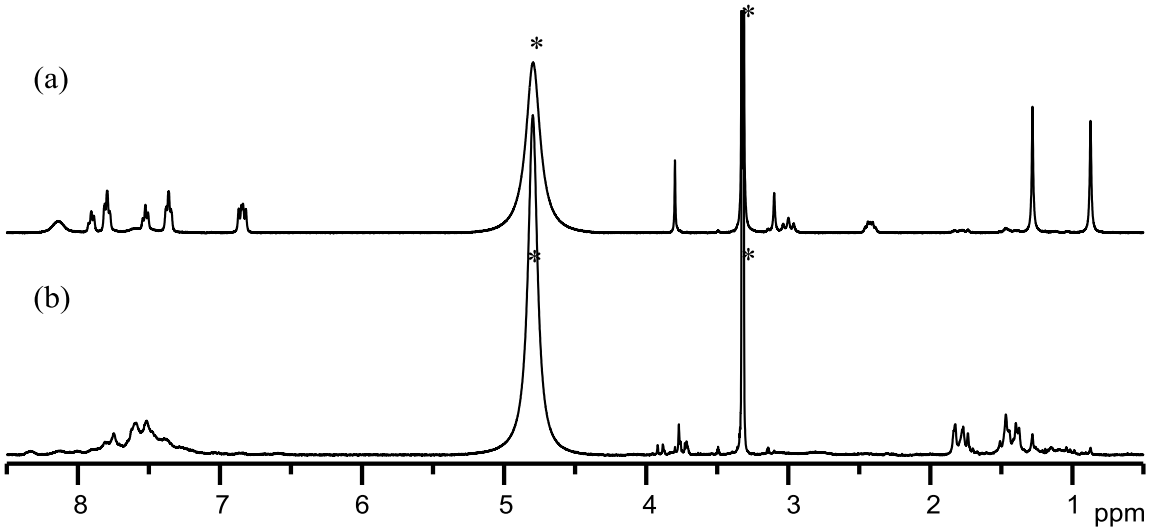

Figure III-14. ^{1}H NMR spectrum of [**8'**]$(NO_3)_3$ in a 1:1 mixture of methanol-d_4 and D_2O recorded (a) immediately and (b) 21 hours after dissolving. (*) denotes the signals from solvents.

Table III-1. Crystallographic data for [**8**], [**8'**]$(NO_3)_3$, and [**9**].

	[**8**]·22H_2O·EtOH	[**8'**]$(NO_3)_3$·$n$$H_2O$	[**9**]·16.5H_2O
empirical formula	$C_{114}H_{182}Au_6Co_3N_6O_{35}P_6S_6$	$C_{112}H_{132}Au_6Co_3N_6O_{12}P_6S_6$ [c]	$C_{56}H_{99}Au_3CoN_3O_{22.50}P_3S_3$
formula weight	3933.43	3491.01 [c]	2013.30
color, form	brown, platelet	blue, block	purple, rod
crystal size /mm^3	0.15 × 0.15 × 0.10	0.20 × 0.20 × 0.15	0.15 × 0.05 × 0.03
crystal system	monoclinic	hexagonal	orthorhombic
space group	*C*2	*P*6$_3$22	*P*2$_1$2$_1$2$_1$
a/ Å	33.652(5)	18.2469(5)	13.2998(3)
b/ Å	27.637(4)	18.2469(5)	35.1784(9)
c/ Å	16.973(2)	52.5358(14)	36.4733(9)
α (°)	90	90	90
β (°)	97.635(6)°	90	90
γ (°)	90	120	90
V/ Å^3	15646(4)	15148.3(7)	17064.6(7)
Z	4	4	8
T/ K	200(2)	200(2)	200(2)
ρ_{calcd}/ g cm^{-3}	1.670	1.531 [c]	1.567
μ(Mo Kα)/ mm^{-1}	6.119	6.299	5.524
R_1[a] (I>2σ(I))	0.0623	0.0870	0.0799
wR_2[b] (all data)	0.1544	0.2249	0.2003
flack parameter	0.001(6)	0.081(14)	0.055(7)

[a] $R_1 = (\Sigma(|(|F_o| - c|F_c|)|)/(\Sigma|F_o|)$

[b] $wR_2 = [\{\Sigma w(F_o^2 - cF_c^2)^2\}/(\Sigma w|F_o^2|^2)]^{1/2}$

[c] Contributions of NO_3^- and H_2O are not included.

Table III-2. Selected bond distances (Å) and angles (°) for [**8**].

		distances (Å)	
Au1–P1	2.269(4)	Co1–O7	2.12(1)
Au1–S1	2.328(4)	Co1–S1	2.457(4)
Au2–P2	2.265(4)	Co1–S4	2.513(4)
Au2–S2	2.333(3)	Co2–N2	2.16(1)
Au3–P3	2.268(4)	Co2–N5	2.17(1)
Au3–S3	2.329(4)	Co2–O3	2.083(9)
Au4–P4	2.265(3)	Co2–O9	2.172(9)
Au4–S4	2.330(4)	Co2–S2	2.521(4)
Au5–P5	2.272(3)	Co2–S5	2.463(4)
Au5–S5	2.334(3)	Co3–N3	2.13(1)
Au6–P6	2.271(4)	Co3–N6	2.10(1)
Au6–S6	2.321(4)	Co3–O5	2.13(1)
Co1–N1	2.15(1)	Co3–O11	2.08(1)
Co1–N4	2.15(2)	Co3–S3	2.459(4)
Co1–O1	2.14(1)	Co3–S6	2.513(5)
		angles (°)	
P1–Au1–S1	176.1(1)	N5–Co2–O3	87.4(4)
P2–Au2–S2	176.3(1)	N5–Co2–O9	72.7(4)
P3–Au3–S3	178.8(1)	N5–Co2–S2	171.7(3)
P4–Au4–S4	178.1(1)	N5–Co2–S5	83.0(3)
P5–Au5–S5	176.6(1)	O3–Co2–O9	151.6(4)
P6–Au6–S6	178.6(1)	O3–Co2–S2	89.9(3)
N1–Co1–N4	102.0(6)	O3–Co2–S5	108.7(3)
N1–Co1–O1	73.1(5)	O9–Co2–S2	112.5(3)
N1–Co1–O7	92.0(5)	O9–Co2–S5	89.2(3)
N1–Co1–S1	83.4(4)	S2–Co2–S5	90.5(1)
N1–Co1–S4	174.6(4)	N3–Co3–N6	102.2(5)
N4–Co1–O1	92.2(5)	N3–Co3–O5	73.2(4)
N4–Co1–O7	75.2(5)	N3–Co3–O11	89.4(4)
N4–Co1–S1	174.6(4)	N3–Co3–S3	84.1(3)
N4–Co1–S7	83.3(4)	N3–Co3–S6	174.2(3)
O1–Co1–O7	158.3(5)	N6–Co3–O5	88.2(5)

Table III-2. (continued)

		angles (°)	
O1–Co1–S1	89.3(3)	N6–Co3–O11	76.1(5)
O1–Co1–S4	107.2(3)	N6–Co3–S3	172.8(4)
O7–Co1–S1	105.0(3)	N6–Co3–S6	83.2(4)
O7–Co1–S4	89.1(3)	O5–Co3–O11	153.6(4)
S1–Co1–S4	91.3(1)	O5–Co3–S3	90.4(3)
N2–Co2–N5	15.7(4)	O5–Co3–S6	109.3(3)
N2–Co2–O3	77.6(4)	O11–Co3–S3	107.7(3)
N2–Co2–O9	88.3(4)	O11–Co3–S6	90.1(3)
N2–Co2–S2	81.4(3)	S3–Co3–S6	90.6(1)
N2–Co2–S5	169.8(3)		

Table III-3. Selected bond distances (Å) and angles (°) for [**8'**]$(NO_3)_3$.

		distances (Å)	
Au1–P1	2.273(3)	Co1–O1	1.93(1)
Au1–S1	2.354(3)	Co1–S1	2.309(5)
Co1–N1	1.96(1)		
		angles (°)	
P1–Au1–S1	175.3(1)	N1–Co1–S1'	175.9(4)
N1–Co1–N1'	96.0(6)	O1–Co1–O1'	172.7(5)
N1–Co1–O1	80.7(5)	O1–Co1–S1	88.6(3)
N1–Co1–O1'	94.4(5)	O1–Co1–S1'	96.6(4)
N1–Co1–S1	87.2(4)	S1–Co1–S1'	89.7(2)

Symmetry code('): –x, x+y, –z

Table III-4. Selected bond distances (Å) and angles (°) for [**9**].

		distances (Å)	
Au1–Au2	2.9826(9)	Au4–Au5	3.0250(8)
Au1–Au3	3.0036(8)	Au4–Au6	2.995(1)
Au1–P1	2.281(4)	Au4–P4	2.262(4)
Au1–S1	2.334(4)	Au4–S4	2.373(4)
Au2–Au3	2.9777(9)	Au5–Au6	2.955(1)
Au2–P2	2.263(4)	Au5–P5	2.260(5)
Au2–S2	2.332(4)	Au5–S5	2.323(5)
Au3–P3	2.272(4)	Au6–P6	2.275(5)
Au3–S3	2.349(4)	Au6–S6	2.347(5)
Co1–N1	2.04(1)	Co2–N4	2.06(2)
Co1–N2	1.99(1)	Co2–N5	1.98(1)
Co1–N3	2.03(1)	Co2–N6	2.06(2)
Co1–S1	2.268(4)	Co2–S4	2.293(5)
Co1–S2	2.269(5)	Co2–S5	2.304(5)
Co1–S3	2.262(4)	Co2–S6	2.299(7)
		angles (°)	
Au2–Au1–Au3	59.66(2)	Au5–Au4–Au6	58.78(2)
P1–Au1–S1	170.4(1)	P4–Au4–S4	169.6(2)
Au1–Au2–Au3	60.52(2)	Au4–Au5–Au6	60.11(2)
P2–Au2–S2	167.0(1)	P5–Au5–S5	170.9(2)
Au1–Au3–Au2	59.82(2)	Au4–Au6–Au5	61.11(2)
P3–Au3–S3	170.1(1)	P6–Au6–S6	168.6(2)
N1–Co1–N2	88.3(5)	N4–Co2–N5	89.6(7)
N1–Co1–N3	88.1(6)	N4–Co2–N6	92.4(8)
N1–Co1–S1	85.4(4)	N4–Co2–S4	85.1(6)
N1–Co1–S2	92.6(4)	N4–Co2–S5	91.6(6)
N1–Co1–S3	172.4(4)	N4–Co2–S6	175.8(6)
N2–Co1–N3	89.9(5)	N5–Co2–N6	91.3(7)
N2–Co1–S1	172.7(4)	N5–Co2–S4	173.9(5)
N2–Co1–S2	83.8(4)	N5–Co2–S5	83.5(5)
N2–Co1–S3	93.7(4)	N5–Co2–S6	92.5(5)
N3–Co1–S1	93.5(4)	N6–Co2–S4	91.9(5)

Table III-4. (continued)

		angles (°)	
N3–Co1–S2	173.6(4)	N6–Co2–S5	173.4(5)
N3–Co1–S3	84.6(4)	N6–Co2–S6	83.9(5)
S1–Co1–S2	92.9(2)	S4–Co2–S5	93.7(2)
S1–Co1–S3	93.0(2)	S4–Co2–S6	93.0(2)
S2–Co1–S3	94.8(2)	S5–Co2–S6	92.3(2)

Table III-5. Electronic absorption and CD spectral data of [**8**], [**8'**]$(NO_3)_3$, and [**9**]. (sh = shoulder)

absorption maxima: σ / 10^3 cm^{-1} ($\log(\varepsilon$ / mol^{-1} dm^3 cm^{-1}))		CD extrema: σ / 10^3 cm^{-1} ($\Delta\varepsilon$ / mol^{-1} dm^3 cm^{-1})	
[**8**] in methanol/water (1:1)			
16.58	(1.495)	15.96	(+1.01)
20.09	(1.835)	20.80	(+1.46)
29.2	(3.03)sh	24.94	(+0.28)
32.9	(3.62)sh	27.95	(–0.39)
36.26	(4.205)	31.87	(–12.59)
37.26	(4.287)	34.18	(+7.48)
44.21	(5.111)	36.44	(–57.95)
		37.43	(–71.22)
		38.34	(–54.08)
		39.34	(–42.15)
		40.65	(49.61)
		43.86	(+171.55)

Table III-5. (continued)

absorption maxima: σ / 10^3 cm^{-1} (log (ε / mol^{-1} dm^3 cm^{-1}))		CD extrema: σ / 10^3 cm^{-1} ($\Delta\varepsilon$ / mol^{-1} dm^3 cm^{-1})	
[**8'**]$(NO_3)_3$ in water			
16.40	(2.507)	15.74	(+11.40)
18.91	(2.475)	19.43	(–3.44)
29.4	(4.18)sh	24.73	(+4.71)
34.5	(4.53)sh	28.36	(–25.23)
36.23	(4.595)	34.36	(–20.49)
37.23	(4.594)	36.31	(–19.69)
43.5	(5.16)sh	37.23	(–17.46)
		43.29	(+19.16)
		45.17	(–6.04)
		47.53	(+15.38)
[**9**] in methanol			
18.03	(2.752)	17.01	(–2.97)
24.41	(2.803)	18.95	(+5.43)
30.8	(4.16)sh	24.27	(–13.36)
34.44	(4.609)	31.67	(+74.90)
39.84	(4.679)	34.97	(–173.04)
44.9	(4.83)sh	37.43	(–98.47)
		39.49	(+4.03)
		42.16	(–75.34)

Table III-6. Specific averaged bond parameters for [**2a**]ClO_4,[11] [**8'**]$(NO_3)_3$, and $[Co^{III}\{Au^{I}_2(dppe)(D\text{-}pen)_2\}_2](ClO_4)_2$.[2c]

	[**2a**]ClO_4	$[Co^{III}\{Au^{I}_2(dppe)(D\text{-}pen)_2\}_2](ClO_4)_2$	[**8'**]$(NO_3)_3$
		distances (Å)	
Au–P	2.258(2)	2.268(2)	2.273(3)
Au–S	2.323(2)	2.319(2)	2.354(3)
Co–N	1.95(1)	1.95(1)	1.96(1)
Co–O	1.90(1)	1.91(1)	1.93(1)
Co–S	2.259(2)	2.286(3)	2.309(4)
		angles (°)	
P–Au–S	174.9(7)	177.8(1)	175.3(1)
N–Co–S	173.8(2)	174.3(4)	175.9(4)
O–Co–O	176.0(2)	176.2(3)	172.7(5)
Co–S–Au	102.4(7)	102.1(1)	96.9(2)

Concluding Remarks.

This research has established a series of new thiolato-bridged heterometallic multinuclear coordination systems constructed by coordination of the gold(I) metalloligands with mixed sulfur-containing amino acids (SAAs) and various phosphines toward the secondary metal ions (M), aimed to achieve new functionalities that have not achieved in traditional thiolato-bridged systems without phosphines. In the Au^{I}-M-SAAs-phosphines coordination systems, each component plays specific roles for the aim; hydrophilic SAAs as pH-responsive multi-functional donors, hydrophobic arylphosphines as structural-controlling backbones, gold(I) ions as connectors of SAAs and phosphines, and secondary metal ions as sources that exert different properties and reactivity depending on the combination of their inherent characters and coordination environments (Chart 3 in General Introduction). In addition, aurophilic interactions are available for the structural control. Actually, a variety of heterometallic Au^{I}-M complexes were constructed from the coordination of gold(I) complexes with mixed D-pen and various phosphines toward several 3d metal ions according to the strategy for the rational construction of heterometallic structures based on thiolato metalloligands. Then, the basic features and the functionalities that can lead to future applications of the Au^{I}-M-SAAs-phosphines coordination systems was presented through the syntheses, structures, properties, and reactivities of the Au^{I}-M complexes with mixed D-pen and mono-, di-, or triphosphine described in Chapters I, II, or III, respectively.

In Chapter I, the coordination behavior of the monogold(I) metalloligand with PPh_3, $[Au^{I}(PPh_3)(D\text{-pen})]^{-}$ ($[\mathbf{1}]^{-}$), to three 3d metal ions (Co^{II}, Ni^{II}, Zn^{II}) was investigated. Since the monophosphine occupies one of two coordination sites on gold(I) ion, the nuclearity of the product is limited to the small number. This is disadvantageous to show cooperative effects in multinuclear coordination systems. Conversely, however, the coordination system based on $[\mathbf{1}]^{-}$, which is one of the simplest metalloligand in this class, provided essential knowledge for understanding the Au^{I}-M-SAAs-phosphines coordination systems.

Expressly, the Au^{I}-Co^{III} complex [**2a**]ClO_4, which was synthesized via air-oxidation of cobalt(II) ion, was fully characterized by spectroscopic, crystallographic, and elemental analytical data, which gave rich information for fundamental coordination chemistry of Au^{I}-M-SAAs-phosphines systems. Besides, Au^{I}-Ni^{II} complex [**2b**] achieved the pH-induced geometrical conversion of nickel(II) center accompanied with drastic changes in color and magnetism, and Au^{I}-Zn^{II} complex [**2c**] exhibited a solid-state photo-luminescent property raising from the P–Au–S luminophore and its enhancement on zinc(II) binding, in addition to their basic spectroscopic and analytical data.

Moreover, the additional features that are specific for the Au^{I}-M-SAAs-phosphines systems were demonstrated by comparing with the previous Au^{I}-M-SAAs systems including

the dppe system as follows: (i) the preference of the coordination mode forming *trans*(*O*)-{M(D-pen-*N*,*O*,*S*)$_2$} unit on the coordination to the octahedral metal ions (M = Co^{III}, Ni^{II}, Zn^{II}), (ii) the presence of the intermolecular hydrophobic interactions in the crystal packing, and (iii) the good solubility in organic solvents. The knowledge about these fundamental features of Au^{I}-M-SAAs-phosphines coordination systems will be helpful of understanding not only the systems with multidentate phosphines mentioned in the other chapters in this thesis but also more complicated systems developing in the future.

In Chapter II, the coordination behavior of the two gold(I) metalloligands with dppm, $[Au^{I}_2(dppm)(D\text{-pen})_2]^{2-}$ ([**3**]$^{2-}$) and $[Au^{I}_3(dppm)_2(D\text{-pen})_2]^{-}$ ([**4**]$^{-}$), to nickel(II) and zinc(II) ions were investigated. Initially, dppm was selected on the purpose of effective utilization of aurophilic interactions for control of the coordination mode of the metalloligand and the structure of resulting heterometallic Au^{I}-M complexes. This intention was attained as the hexadentate-N_2,O_2,S_2 coordination mode of the digold(I) metalloligand [**3**]$^{2-}$ to produce the heterometallic Au^{I}-Ni^{II} and Au^{I}-Zn^{II} complexes with 8-membered metallorings ([**5a**] and [**5b**]). Not only the digold(I) products, the structural stabilization effect by the effective intramolecular aurophilic interactions also allowed the isolation of the trigold(I) metalloligand [**4**]$^{-}$ and the heterometallic Au^{I}-Ni^{II} and Au^{I}-Zn^{II} complexes with 12-membered metallorings derived from [H**4**] ([**6a**]Cl and [**6b**]Cl).

Moreover, it was demonstrated that these pairs of digold(I)/trigold(I) structures ([H_2**3**]/[H**4**], [**5a**]/[**6a**]$^{+}$, and [**5b**]/[**6b**]$^{+}$) are interconvertible by the insertion/removal of a $\{Au^{I}(dppm)\}^{+}$ extension agent generated from $[Au_2(dppm)_2]^{2+}$. Therefore, the interesting switching systems involving metalloring expansion/contraction were achieved for the pairs of the cyclic complexes. Note that all these structural conversions were very quickly completed owing to the substitution-active character of coordinatively unsaturated linear Au^{I} center, which is facilitated in the presence of phosphine donors. In addition, it is noteworthy that the interconversions between the 8-membered and 12-membered rings were also triggered by the external stimuli of solvent polarities, solution pH, and electronic potentials, to exert the significant changes in chromogenic, chiroptical, magnetic, and luminescent properties of the materials. This is indicative of potential applications of this class of compounds for smart nano-materials such as chiral molecular sensors.

Ultimately, the intramolecular aurophilic interactions supported by dppm play critical roles for all specific features in this system, therefore indicating that the use of the aurophilicity is very helpful to design the molecular structures and conformations, and supramolecular arrangements together with the well-known hydrogen-bonding and hydrophobic interactions.

In Chapter III, the coordination behavior of the trigold(I) metalloligand with tdme,

$[Au^{I}_{3}(tdme)(D\text{-}pen)_3]^{3-}$ ($[\mathbf{7}]^{3-}$), to cobalt ions in different oxidation states was investigated. The use of the triphosphine expanded the capability of the D-penicillaminato gold(I) metalloligands family by increasing the number of the D-pen moieties in them. Indeed, the formation of the complex [**8**] containing totally six gold(I) and three cobalt(II) ions in the structure clearly shows the effectiveness of the usage of multidentate phosphines for construction of heterometallic complexes with a higher nuclearity. Besides, the tetranuclear complex [**9**] formed via another coordination mode of $[\mathbf{7}]^{3-}$ is a proof of the coordination versatility of this multidentate and multi-topic metalloligand. It is interesting that intramolecular aurophilic interactions are involved in the change of coordination modes, emphasizing again the importance of this attractive force on molecular design.

Moreover, the most notable result in this system is the isolation of the air-stable complex with octahedral cobalt(II) centers coordinated by aliphatic thiolates ([**8**]). The anomalous oxidative resistance of [**8**] both in the solid and solution states was evinced by the treatment with some oxidants, the spectral monitoring, and the electrochemical measurements. In addition, the origin of the rare stability of the high-spin cobalt(II) state was discussed on the basis of the crystal structure and the electronic absorption spectrum of the cobalt(III) derivative, [**8'**]$(NO_3)_3$, obtained from the treatment of [**8**] with a strong oxidant, by comparing with those of the analogues ([**2a**]ClO_4 and $[Co^{III}\{Au^{I}_{2}(dppe)(D\text{-}pen)_2\}_2](ClO_4)_2$). These data provided information about strength of the coordination bonds and the ligand fields in them. As a result, it was revealed that steric limitations originated from the tripodal tdme backbone disturb the strong interaction between cobalt ion and thiolates to provide the more spacious environment and the weaker field suitable for high-spin cobalt(II) ions rather than low-spin cobalt(III) ions. The approach to control the coordination ability of donor groups by remote supporting ligands linked through “supporting” metal ions may open new avenues for the regulation of ligand fields, which seems to be most important to bring out the functionalities arising from metal centers.

As demonstrated above, the coordination systems developed in this study have achieved the various properties and reactivities that are difficult to be attained by the traditional thiolato-bridged multinuclear coordination systems without phosphines. This fact implies that the additional introduction of phosphines extensively allows further functionalization for a large number of gold(I)-thiolate coordination systems well-established before.

Meanwhile, although this study has revealed the fundamental and essential knowledge, as well as some potential applications of these systems, these are presumably only part of the vast chemistry of this kind of coordination systems, considering a wide variety of available phosphine ligands. Therefore, there is room for further improvement to achieve more desirable functionalities. More applied systems will be developed by employing a variety of phosphines and SAAs in the future.

Acknowledgement.

I would like to expresses his sincere gratitude to Professor Takumi Konno for expert guidance, suggestions, and warm encouragement throughout this study. I am grateful to Professor Yasuhiro Funahashi and Professor Kazuya Yamaguchi for valuable advices from diverse and expert perspectives. I am also grateful to Professor Kiyoshi Tsuge in University of Toyama, Associate Professor Toshiaki Tsukuda in University of Yamanashi, Assistant Professor Asako Igashira-Kamiyama, Assistant Professor Nobuto Yoshinari, and Assistant Professor Naoto Kuwamura for their helpful suggestions and warm encouragement. I thank Professor Koichi Nozaki and Mr. Daisuke Naruse in University of Toyama for the measurement of emission quantum yields and lifetimes described in Chapter II. I also extend my thanks to my all collaborators of Konno Laboratory for their supports and friendships.

I am grateful for the financial support from the Global COE (center of excellence) Program “Global Education and Research Center for Bio-Environmental Chemistry” of Osaka University.

Finally, I would like to thank my family for their constant supports and encouragement.

February 2014

Yuji Hashimoto